TUTORIAL REVIEW

Biomass-derived carbons and their modification techniques in electrochemical capacitive deionization desalination

Jin-Jing Jiang, Xue-Jing Ma, [ID] * Juan Zhou, Ashkar Batol, Huan Gou and Wei-Bin Zhang [ID] *

Capacitive deionization (CDI), a new electrochemical technique, exhibits excellent desalting performance for removing salt from seawater. The desalting performance mainly depends on the electrode adsorption and desorption processes in CDI devices, which are inseparable from the structure of the electrode material. Traditional porous electrode materials are typically carbon-based, and among these materials, biomass-derived carbon has emerged as a promising candidate owing to its abundant raw material sources, structural tunability, and environmental benignity. In this study, the desalination mechanism and process of CDI are comprehensively expounded, and the advantages and disadvantages of each unit structure of CDI are summarized. This study completely analyzes the entire process of biomass-derived carbon materials from raw material selection, pretreatment of precursors, and preparation of bio-derived carbon to modification, providing a complete technical route. By selecting the appropriate CDI unit structure and combining the preparation and modification technologies of biomass materials, it is expected that electrode materials with economical, environmentally friendly and excellent desalination performance can be designed. In addition, this study focuses on the desalination performance of different biomass-derived carbons under various modification technologies, providing scholars with a comprehensive research perspective on modification technologies.

Sustainability spotlight

Desalination of seawater is a sustainable technology. Carbon materials are one of the most fundamental materials. The modification technology of carbon materials is key to the development of capacitive deionization desalination technology for sustainability.

1 Introduction

Due to the rapid growth of population, people's demand for freshwater has increased significantly in daily life and industrial water use.[1,2] Most of the world's water resources are saline water, and freshwater accounts for only 3% of the world's water resources. There is an urgent need for a technology that can convert brine to freshwater.[1,3]

At present, many technologies for desalination have been developed. One is the pressure-driven process of membranes, such as reverse osmosis (RO) and nanofiltration (NF). Electrochemically driven processes, such as forward osmosis (FO), electrodialysis (ED), and capacitive deionization (CDI), are by far the most dominant technologies for producing fresh water from various water sources.[4] However, conventional membrane pressure-driven processes have certain limitations, such as high

energy consumption and insufficient generation of secondary chemicals or waste. In contrast, emerging electrochemically driven processes are favored by researchers because of their lower energy consumption and lower environmental impact.[5,6] Among them, capacitive deionization technology, which is a technology based on electrochemical methods to generate fresh water, has attracted much attention owing to its advantages of high energy efficiency, high cost-effectiveness and environmental friendliness.[5,7,8] The principle is based on a mechanism similar to that of double capacitance and pseudo-capacitance.[9] When the capacitor electrode,[10] or Faraday electrode[11] is energized by an external power supply, an electric double layer is formed at the interface between the electrode and the solution. This electric double layer is able to adsorb excess ions in the salt solution, thus achieving desalting.[12]

CDI technology's unique working principle enables it to regulate the salinity of the produced freshwater. Its energy consumption is proportional to the required reduction in the salt concentration. This proves that CDI is more energy efficient than traditional technologies.[13,14] CDI covers a variety of

College of Materials and Chemistry and Chemical Engineering, Chengdu University of Technology, Chengdu 610059, China. E-mail: maxuejing17@cdut.edu.cn; zhangweibin17@cdut.edu.cn

structural forms, including static electrode CDI, hybrid capacitive deionization (HCDI), membrane capacitive deionization (MCDI) and flow electrode capacitive deionization (FCDI).[15] Each of these structures has its characteristics and is suitable for different application scenarios and needs.[16] The desalination capacity of capacitive deionization technology mainly depends on the electrode material in its structure, and when the salt adsorption capacity of the CDI electrode material reaches the upper limit, we need to optimize the electrode material to significantly improve the adsorption performance of the CDI technology.[17]

At present, various materials have been applied in the research and development of CDI electrode materials. There are two main types: carbon-based materials and Faraday materials, including activated carbon, high-performance biochar, graphene, carbon aerogel, carbon-based composites, metal–organic framework derivatives, and carbon nanotubes.[18] Faradaic materials, however, encompass transition metal oxides (TMOs), transition metal sulfides (TMSs), transition metal carbides (TMCs), layered double hydroxides (LDHs), Ag, and organic-based electrode materials.[19] These materials not only exhibit unique physical and chemical properties but can also effectively improve the performance and desalination efficiency of electrodes through different mechanisms, showing good application prospects.[18,20]

A common configuration of faradaic materials in CDI involves the use of Na^+ insertion materials, including sodium transition metal oxides, polyanionic conversion compounds, and metal hexacyanometallates. Their mechanism relies on trapping/releasing Na^+ through insertion/extraction. Meanwhile, Cl^- capture is achieved via conversion-type materials, such as Ag/AgCl or $Bi/BiOCl_2$.[21]

These materials not only possess unique physicochemical properties but can also effectively enhance electrode performance and seawater desalination efficiency through diverse mechanisms, demonstrating promising application prospects.[18,20]

Compared with other materials, activated carbon features simple preparation, high cost-effectiveness, a porous structure, and a high specific surface area. However, it still has drawbacks, such as certain environmental impacts.[22] Porous carbon materials with high specific surface areas and excellent conductivities exhibit significant advantages for adsorbing large amounts of salt ions for seawater desalination. Nevertheless, carbon materials have a limited charge storage capacity because they can only adsorb ions on their surface. Owing to the presence of ions with the same charge in the material, repulsive effects occur, significantly reducing the charging efficiency. Moreover, as the solution concentration increases, the charging efficiency decreases noticeably, thereby impairing desalination performance. Faradaic electrodes, however, can significantly overcome these limitations. They provide a larger charge storage capacity by reacting with ions at the electrode–electrolyte interface or within the material. Additionally, faradaic materials exhibit selectivity, reacting only with ions carrying specific charges, which avoids co-ion effects and notably improves the desalination efficiency of CDI in high-concentration solutions. Nevertheless, the types of faradaic cathode materials are

relatively fewer compared to carbon-based materials, and faradaic anode materials (often silver based) are expensive, leading to higher application costs.[23]

To integrate the advantages and mitigate the drawbacks of both material types, biomass-derived carbon has emerged as an ideal alternative to electrode materials.[24] From the perspective of cost and environmental sustainability, biomass-derived carbon materials are considered promising electrode materials owing to their unique characteristics, such as low cost and low environmental pollution.[25] Biomass-derived carbon materials are activated carbon derived from biological waste, and their preparation methods include high-temperature carbonization,[26] activation method[27] and template method.[28,29] Biochar has attracted much attention owing to its porous structure, high surface area and abundant functional groups; in addition, it has the advantages of good biodegradability and environmental friendliness.[30,31] Researchers have been working on the preparation of bio-derived carbon electrode materials with excellent properties, and the modification technology aims to improve the adsorption and electrochemical properties of carbon materials, such as structural modification and elemental doping.[32] A common doping modification method is to change the electronic structure of bio-derived carbon materials by doping with N, P, and S, thereby increasing their porosity and adsorption area.[33,34] One of the structural modification methods is composite modification. Biomass-derived carbon materials are eco-friendly and have various sources. When developed as the main carbon matrix, they can be modified by combining them with other materials. This helps improve their poor wettability and insufficient physical and chemical stability.[35]

Based on this, the purpose of this review is to systematically review the previous research progress of the CDI technology and to explain the working mechanism of CDI and its application in the field of desalination. By analyzing the unique advantages of biomass-derived carbon as a CDI electrode material, the key links of its preparation process are elaborated, multiple strategies for biochar modification technology are comprehensively summarized, and the application performance of modified biochar in desalination practice is discussed in detail.

2 Capacitive deionization technology for desalination

2.1 History of capacitive deionization

Over the past two decades, a total of 4109 articles were identified in the field of CDI according to the search criteria, with an average of 8432 citations per year. Publication and citation data from 2004 to 2024 are shown. As illustrated in Fig. 1, the number of papers in the field of CDI in the Web of Science database is increasing yearly, indicating that the research and development of CDI systems are on the increase.

Throughout the evolution of CDI theory over half a century, its development trajectory has profoundly confirmed the rigor and innovative vitality of the discipline system. In the early 1960s, Blair, Murphy and colleagues first proposed electrochemical desalination of water, which systematically
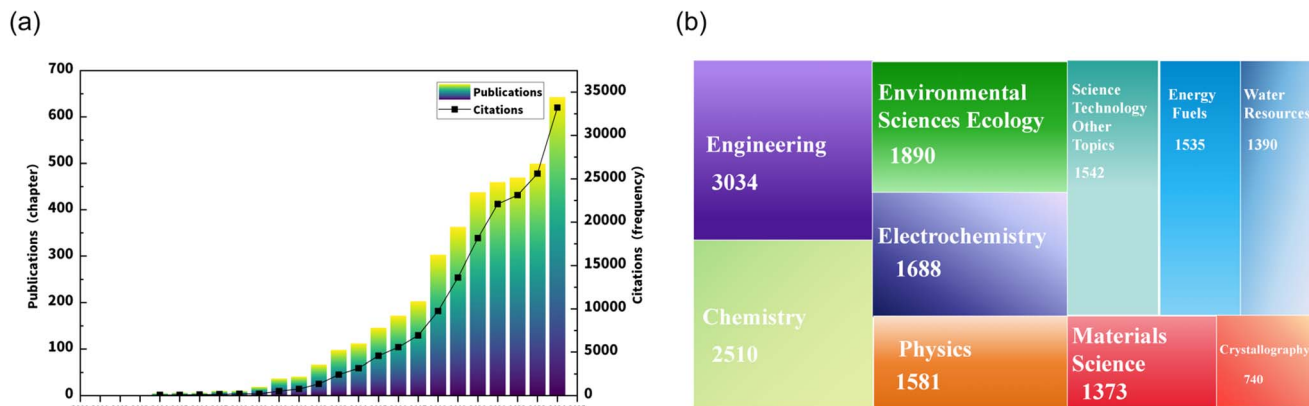
(a)

(b)

Fig. 1 Images of (a) Web of Science over the past 20 years and (b) literature map of each discipline.

demonstrated the adsorption effect of electrode polarization on salt ions, creating a new model of electrochemical desalination, and focused on the distinction between cations and anions, which evolved into the distinction of electrodes.[36] Soon after, Murphy and Caudle *et al.* successfully simulated the process of electrochemical desalination and successfully completed the experiment under different variable conditions, completing the leap from the theory to the practice of electrochemical desalination.[37] Further, Evans and Hamilton *et al.* discovered the Faraday reaction and explored the principle of the original electrochemical desalination, which was to adsorb hydrogen ions through the cathode to produce a Faraday reaction, thereby generating OH^-. In the regeneration process, the alkaline solution composed of OH^- makes the weakly acidic groups on the electrode surface exchange with the ions in the brine, and the cations enter the aqueous solution, thereby achieving desalination. However, at that time, the electrode material was mainly carbon, and later, scholars gradually discovered that the Faraday effect was not the core reaction of electrochemical desalination.[38] Therefore, in 1970, Johnson *et al.* proposed the "potential-modulated ion sorption" theory, which is the EDL theory, stating that the electroadsorption capacity (SAC) is determined by the capacitance of EDLs, and this has remained the driving mechanism of electrochemical desalination until now.[39] In 1986, Reid *et al.* innovatively discovered a new application strategy for electrochemical desalination, which could not only remove salt ions but also achieve Ca^{2+}, Mg^{2+}, SO_4^{2-} and other ions, which provides a theoretical framework for the subsequent capacitive deionization in sewage and the removal of heavy metal ions.[40] Electrochemical desalination continued to be studied until the 90 s of the 20th century, when Farmer *et al.* first named electrochemical desalination capacitive deionization (CDI).[41] With the rapid development of CDI in the past 20 years, various scholars have created various unit structures of CDI, such as FCDI and iCDI, which are elaborated below.[42]

2.2 Capacitor deionization mechanism

The ions in capacitive deionization are separated by electro-adsorption and desorption by capacitive or Faraday ion storage

mechanisms. When the electrode is charged, the electro-adsorption process is completed by the electric double-layer effect or Faraday reaction, while the desorption process is achieved by a short circuit or reversal of the power supply. Therefore, we next introduce in detail the two principles of ion storage and adsorption in the adsorption process: the EDL ion storage principle and the Faraday reaction.[43]

2.2.1 EDL ion storage. The ability of CDI to adsorb and desorb salt ions mainly depends on the capacitive characteristics of EDL.[44] The EDL refers to the area between the electrode and the electrolyte solution. Its principle is that when the electrode is charged, ion adsorption occurs—specifically, ions accumulate at the interface between the electrode and the electrolyte. At the end of the 19th century, Helmholtz proposed a theoretical model of this principle, pointing out that the phenomenon of charge separation occurs at the interface between the electrode and the electrolyte on the surface of the planar electrode. This is due to the accumulation of charges on the electrode surface, while the opposite charges accumulate on the other side of the electrolyte solution, as depicted in Fig. 2a.[44] However, the Helmholtz EDL model does not consider the fact that the ions do not aggregate by completely attaching to the electrode surface owing to the thermal motion in the electrolyte solution. Therefore, Gouy and Chapman further modified the Helmholtz EDL model, proposing that the ions in the electrolyte solution move and continuously distribute in the solution to form a diffusion layer, and proposed the Gouy-Chapman model (Fig. 2b).[45] At higher potentials, it was found that the instability of the EDL capacitance limits the desalination performance of CDI. Therefore, based on the Helmholtz model, Gouy–Chapman–Stern proposed a new hypothesis by combining the previous models and pointed out that the double layer can be divided into the Helmholtz layer and Gouy–Chapman layer, also known as the inner layer region and the diffusion region. The regions are distinguished mainly by the position of the ion, which is the inner region on the surface of the electrode, and the area where the ion is far away from the surface of the electrode is the diffusion region, as shown in Fig. 2c.[46] In response to electrodynamic force, ions migrate to electrodes of opposite polarity and form EDLs on accessible surfaces.[47] The GCS model
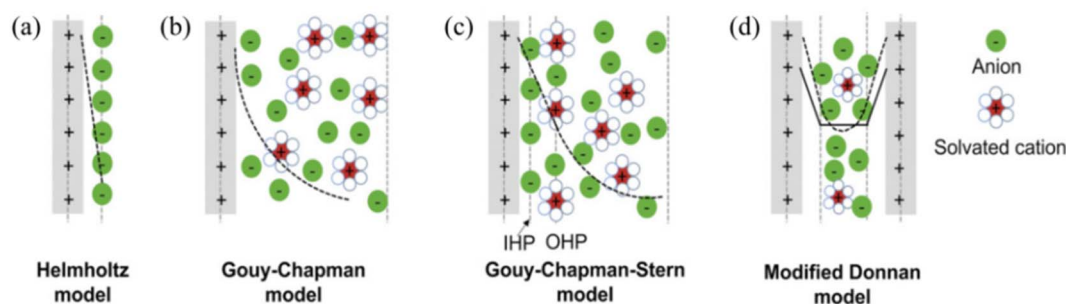
Fig. 2 Models for describing the structure of an electrical double layer at a positively charged surface:[45] (a) the Helmholtz model, (b) Gouy–Chapman model, (c) Stern model, and (d) modified Donna model.

is suitable only when the EDL does not overlap; when the Debye length is equal to or greater than the pore size of the micropores, it is adjusted and improved by considering that ions will produce additional non-electrostatic attraction when entering the pores. As shown in Fig. 2d, the Donnan model was proposed, which can accurately describe the charge and salt adsorption capacity simultaneously and meet the needs of the desalination performance of CDI.[47]

2.2.2 **Faraday ion storage.** Faraday reactions typically use a pseudo-capacitance/intercalation effect to store ions through a reversible redox reaction.[48] In contrast, FPCs store energy through surface redox processes and have a higher energy density than EDL but have poor power density and cycling stability.[49] Among them, the Faraday reaction is at the positively charged electrode in the electrodesorption process, that is, the anode, and oxidation reactions, such as carbon electrode oxidation, water oxidation and chloride oxidation, may occur; the reduction reaction, such as oxygen reduction, occurs at the cathode.[47] However, the reduction reaction occurring at the cathode in the Faraday electrode automatically drives the anode potential to the value of the subsequent anodic oxidation, resulting in a significant decrease in the long-term stability and desalination performance of the electrode.[50] Charge storage in pseudo-capacitive materials involves electron transfer reactions, but not all Faraday processes result in pseudo-capacitive behavior.[51]

The intercalation process achieves pseudo-capacitance by ions that occupy tunnels or vacancies inside most materials, accompanied by rapid Faraday charge transfer without changing the crystal phase.[52] This is shown in Fig. 3a. Commonly used intercalation electrode materials are sodium transition metal oxides (NaTMO, TM = Mn, Ti, Fe, Ni, Co, etc.), sodium ferrophosphate, Prussian blue analogues for cation trapping, and conductive polymers (polypyrrole or polyaniline), along with Ag/AgCl and BiOCl for anionic bonding[53]. In addition, there are differences in the ions of different dimensions of materials, such as the rapid diffusion and storage of ions through tunnels in one-dimensional materials. A two-dimensional material with a layered space can accommodate the original ion insertion. Simultaneously, three-dimensional materials provide three-dimensional ion transport channels.[54] Rapid and reversible oxidation/reduction reactions occur in electrode-based two- and quasi-two-dimensional planes compared to electric double-layer mechanisms, resulting in higher specific capacitance and energy density.[55] Faraday ion storage is mostly driven by electric field forces that undergo redox reactions.[56] As shown in Fig. 3b, redox reactions can occur on the electrode surface to form higher densities of pseudo-capacitance. The most commonly used pseudocapacitance materials are transition metal oxides (e.g., RuO_2 and MnO_2), including manganese dioxide (MnO_2), sodium manganese oxide, and nickel hexacyanoferrate.[57] Compared to cations,
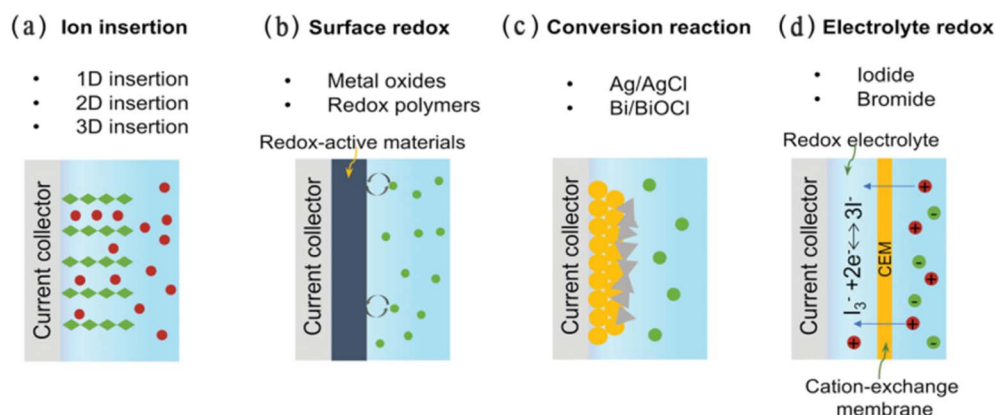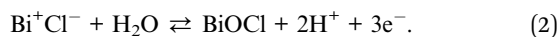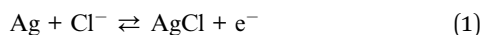

Fig. 3 faradaic ion capture mechanisms:[45] (a) ion insertion, (b) surface redox, (c) conversion reaction, and (d) electrolyte redox.

anions in aqueous solutions are stable and difficult to react with other electrode materials. As shown in Fig. 3c, desorption anions can only be desorbed by binding to specific Faraday electrode materials within a limited potential range (between H_2 and O_2 release), including silver, bismuth, conductive polymers, MXenes, and TMDs. Ag and AgCl as well as Bi and BiOCl are the most common materials for Cl^- removal, and the principle is shown in eqn (1) and (2):[58]

$$Ag + Cl^- \rightleftarrows AgCl + e^- \tag{1}$$

$$Bi^+Cl^- + H_2O \rightleftarrows BiOCl + 2H^+ + 3e^-. \tag{2}$$

The CDI can also compensate for the charge through the Faraday transformation reaction, as shown in Fig. 3d, by gaining or losing electrons at the solid/liquid interface to change its oxidation state, showing that the cation is adsorbed by the oxidation reaction; the reduction reaction is completed after being released into the solution, and the ion selection or desorption can be achieved, as shown in eqn (3):[54]

$$I^{3-} + 2e^- \rightleftarrows 3I^-. \tag{3}$$

2.2.3 Desalination performance test for CDI. Salt adsorption capacity (SAC) and desalination efficiency (DE) were used to evaluate desalination performance.

Salt adsorption capacity (SAC) is expressed as a function of the weight of the adsorbed electrode, expressed in the mass of the adsorbed salt, and calculated according to eqn (4) in milligrams of adsorbed salt per gram of electrode material:

$$\tau = \frac{(C_t - C_0)\ V}{m}, \tag{4}$$

where SAC is the salt absorption capacity ($mg\ g^{-1}$); C_0 and C_t are the conductivity of the salt solution in the initial and saturation stages, respectively ($mg\ L^{-1}$); V is the volume of the salt solution (L), and m is the effective mass of the active material (g).[59]

Desalination efficiency (DE) is calculated using eqn (5):

$$DE = \frac{(C_t - C_0)\ V}{m\ \Delta t}, \tag{5}$$

where DE is the desalting rate ($mg\ g^{-1}\ h^{-1}$); G_0 and G_t are the conductivity of the salt solution in the initial and saturation stages, respectively ($\mu S\ cm^{-1}$); m is the effective mass of the active material (g), and Δt is the charging time (h).[60]

The average adsorption rate is calculated using the following eqn (6):

$$ASAR = \frac{\tau}{t}, \tag{6}$$

where t is the adsorption time.[61]

2.2.4 Various capacitive deionization unit structures

2.2.4.1 Traditional capacitive deionization. Traditional capacitive deionization (CDI) technology has the advantages of a relatively simple structure and low operating cost. The desalination process mainly relies on two basic mechanisms to drive

ion removal, each of which impacts desalination performance. Among them, the Faraday process is driven by a pseudo-capacitive intercalation effect, which is usually combined with a redox reaction on the surface of the electrode or inside the matrix, and can achieve a charging efficiency of 92.2% at low running voltages. However, owing to the complexity of the redox reaction, the process can produce chemical by-products that can shorten the electrode's lifespan. Simultaneously, the ion removal efficiency is relatively low; there is room for improvement in charging efficiency, and the treatment time of seawater is longer. In addition, the Faraday process has poor selectivity for some special ions, and there is an ionization effect, leading to problems such as ion residue and poor desorption effect, which affects the overall desalination efficiency.[62]

Based on the electric double layer theory, the electrode becomes polarized owing to the charge, ions in the solution are adsorbed onto the corresponding electrode *via* the electric double layer, and the salt ions in the feed solution are adsorbed to the electrode that has the opposite charge to the ions, that is, the electrode adsorbs the counterion and remains in the electric double layer in the electrostatic form, thus removing the ions. When electroadsorption reaches saturation, reverse polarization is formed by removing or reversing the voltage, and the adsorbed ions on the electrode are discharged and thus unbound, allowing the electrode to be regenerated and reused.[63,64] The mechanism of the electrode reaction during the desorption process was studied by measuring the conductivity, effluent, pH, and current through the battery at different electrode potentials. The results showed that within the potential range of 0.8–1.5 V, the amounts of NaCl adsorbed within 10 minutes were 5.64, 8.24, 12.22, and 15.42 mg at electrode potentials of 0.8, 1.0, 1.2, and 1.5 V, respectively. This confirms that the NaCl adsorption capacity increases linearly with increasing potential. Additionally, the desalination efficiency (η_t) at each potential, calculated as a function of adsorption time using Formula (7), is presented in Fig. 3:

$$\eta_t = \left(1 - \frac{\int_0^t C_{eff} dt}{t C_0}\right) \times 100\%, \tag{7}$$

where C_0 is the initial concentration of the feed solution, C_{eff} is the effluent concentration, and t is the adsorption time. As shown in Fig. 5, desalination efficiency increases as the cell potential increases, reaching a maximum of 83.4% at 1.5 V. However, the removal efficiency decreases over time because the electrode gradually becomes saturated with adsorbed salt ions.

As shown in Fig. 4, the seawater desalination efficiency increases with an increase in potential. In addition, as shown in Fig. 5, the pH value of the solution changes significantly with the change in potential. When the potential is less than 1.0 V, the pH value increases owing to the decrease in dissolved oxygen. At potentials above 1.2 V, the pH decreases owing to the oxidation reaction of the anode. The change in current indicates that the adsorbed ions are not completely desorbed and that a small fraction of the ions remain on the carbon electrode. When the potential is reapplied, these accumulated ions are
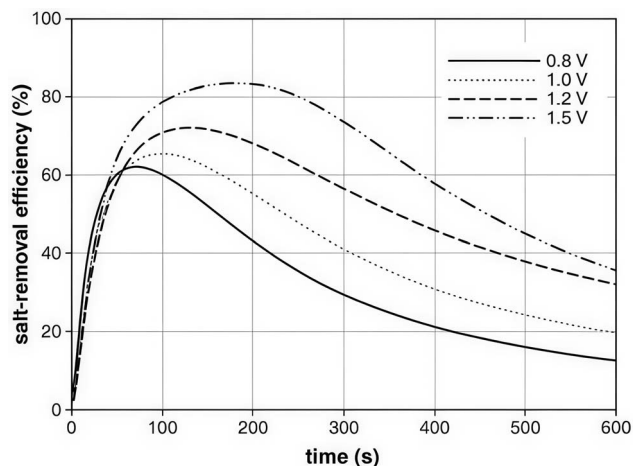
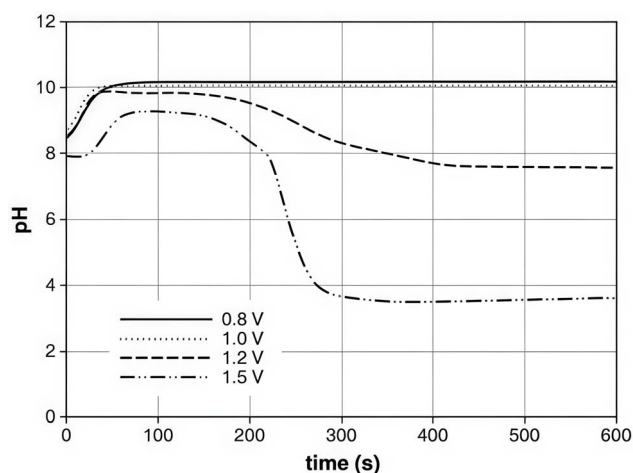**Fig. 4** Changes in desalination efficiency with adsorption time under different applied potentials.[65]

Fig. 5 Changes in the effluent pH during adsorption at different potentials.[65]

Fig. 6 Schematic of the (a) FCDI components and (b) experimental procedure used for the FCDI device.

readsorbed on the electrode surface, resulting in a decrease in the desalination efficiency of CDI.[65]

Therefore, based on the original CDI, various scholars have made different adjustments to each part. To adapt to the desalination scenarios of different salt concentrations, desalination efficiency is improved.

2.2.4.2 Flow-electrode capacitive deionization. Flow electrode capacitive deionization (FCDI) enables continuous operation by combining ion-selective membranes with flow electrodes, making up for the shortcomings of intermittent operation of traditional CDI and improving desalination efficiency.[66,67] As shown in Fig. 6, it is the components and usage program of FCDI.[68]

Although FCDI has moved beyond the traditional CDI cell structure, there are still shortcomings of a high carbon load (20.0–35.0 wt%), which leads to the blockage of the flow electrode material and shortens its service life. In addition, cleaning and maintenance caused by blockages further increase costs.[68]
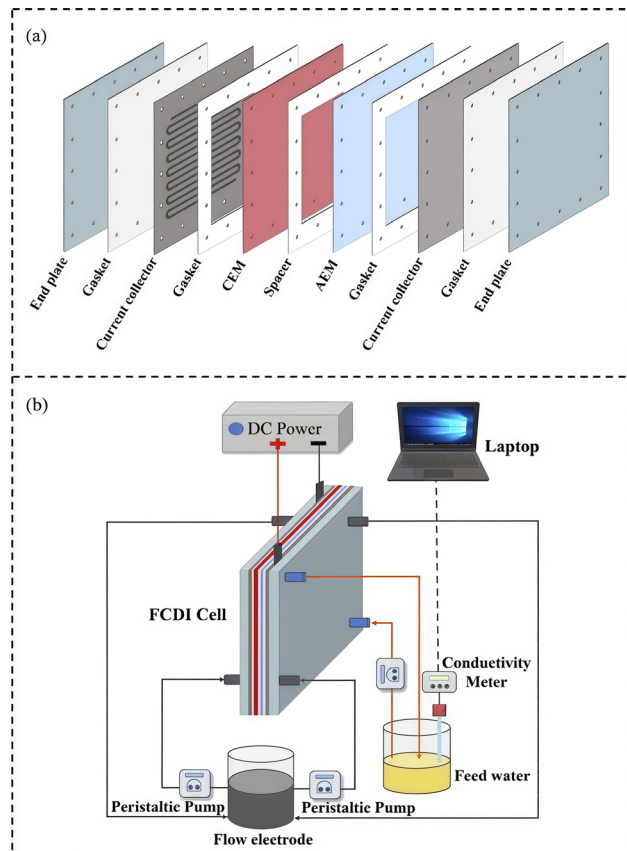
To optimize the desalination performance of FCDI, researchers focus on the preparation of electrode materials, which can improve the adsorption capacity and reduce the electrode resistance, thereby reducing the energy consumption of desalination.[69]

2.2.4.3 Membrane capacitive deionization. In the CDI process, ions cannot be fully removed, which significantly reduces desalination efficiency. To overcome this challenge, researchers have developed membrane capacitive deionization (MCDI), which introduces selective cation removal and anion exchange membranes to the traditional CDI to improve desalination performance. The diagram illustrates the composition of an MCDI system that controls the conventional and cyclic flow of desalination *via* the flow rate of the concentrator tank, as shown in Fig. 7.[70,71] In the MCDI process, the MCDI temporarily stores the detached electrons in the electric double layer of the porous electrode, and ions with a high ionic charge and hydration radius are preferentially adsorbed to the porous electrode.[72] Furthermore, based on the relationship between the amount of adsorbed ions and the strength and duration of the applied current, the ion concentration of the effluent can be adjusted by controlling the applied current.[73] In addition, based on the characteristics of its ion exchange membrane, researchers have conducted studies on the selective separation and recovery of various ion species.[74] It is widely used in soft tap
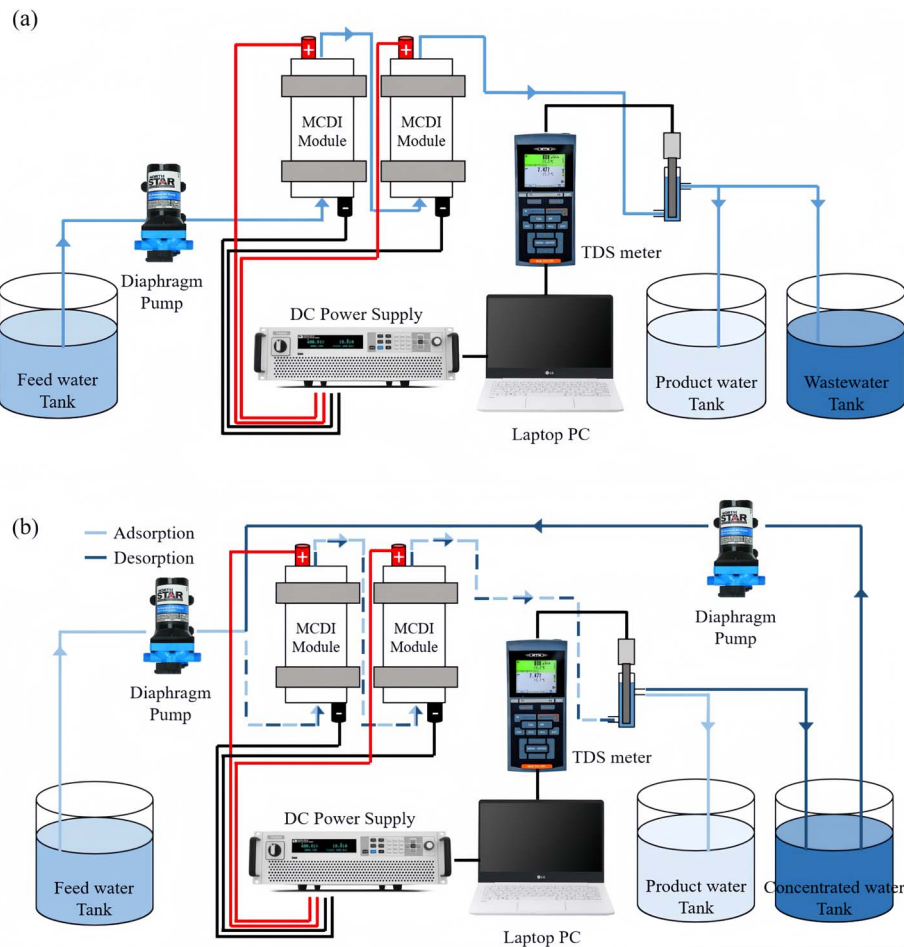
Fig. 7 Configuration of the MCDI system:[70,71] (a) the conventional process and (b) the flow-through process. Depending on the configuration, the system is carried out using a single module or two modules connected in series.

water (T_1), hard tap water (T_2), cooling tower blowdown (W_1), and wastewater discharge, with good ion selection functions.[75] Zhang *et al.* showed that compared with traditional CDI, membrane participation in the process enhances the adsorption capacity of $F^=$ and DIC species while reducing energy consumption. However, as the voltage increases, the adsorption capacity increases and the energy consumption also increases significantly. Therefore, the voltage is adjusted according to the concentration of ions removed.[76] Bales *et al.* found that MCDI can be operated intermittently using photovoltaics as an electrode power source owing to its low voltage operation and low energy consumption. Consequently, 27% of electricity can be saved. Larger-scale MCDI devices can be synthesized to further improve the desalination efficiency. However, the device's limitations must be considered, and various performance parameters must be balanced.[77]

2.2.4.4 Hybrid capacitive deionization. To overcome the limitations of the traditional CDI deionization efficiency and slow reaction kinetics,[78] a hybrid capacitive deionization (HCDI) system has been developed. The HCDI desalination system is made up of an electrochemical workstation, an HCDI unit, a peristaltic pump, a conductivity meter and a computer. Its

structure is based on hybrid capacitors, and hybrid capacitors guide the dual-stage quality matching strategy in HCDI. As shown in Fig. 8, the HCDI desalination system consists of an electrochemical workstation, an HCDI unit, a peristaltic pump, a conductivity meter, and a computer.[79] It is made of two electrode materials: one is a CDI electrode, which works based on an EDL mechanism, and the other is a battery material
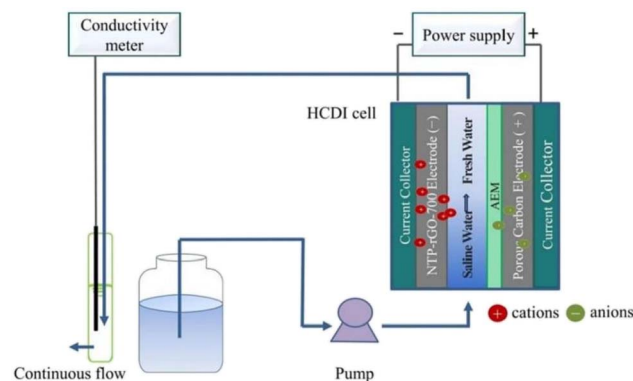

Fig. 8 Schematic of the HCDI composition and process.[79]

electrode, which works through a Faraday reaction.[80] Faraday materials are used to replace traditional carbon electrode materials, which have high desalination ability and ion selectivity.[81] Xing *et al.* found that echinoid $W_{18}O_{49}$@C (UWC) as an HCDI electrode material could achieve excellent desalination from 32.25 ± 0.70 mg g^{-1} to 1000 mg L^{-1}.[82]

2.2.4.5 Inverted capacitive deionization. During traditional CDI charging, the carbon anode oxidizes and co-ions are repelled.[83] Gao *et al.* developed a new seawater desalination system, the inverted capacitive deionization (i-CDI) system, which significantly improves the salt separation performance of the i-CDI system by enhancing the net surface charge of the carbon material, salt desorption during battery charging, and salt adsorption during short circuits. The test potential is shown in Fig. 7, which forms the counter electrode of CDI by assembling two asymmetrical electrodes and then completing the desorption process between the two EPZCs. Fig. 9a shows that this potential window is an innovative modification of the traditional EPZC potential window and that its i-CDI window position is exactly the opposite of the traditional one. This helps to screen the utilization of all estimated voltages, thus improving the limitation that the anode is susceptible to oxidation during operation. In addition, as shown in Fig. 9b, at an operating voltage of 0.8 V, we calculated a potential value of -0.62 V for the Si-CX anode (E) and -0.17 V for the CX cathode (E$^-$) compared to the SCE. Similarly, the short-circuit voltage is -0.19 V. By comparing Fig. 7a and b, we find that the maximum applied voltage of the i-CDI cell should be 0.8 ± 0.1 V, which is slightly higher than the estimate for the EPZC position but still conforms to the value of the EPZC.[84]
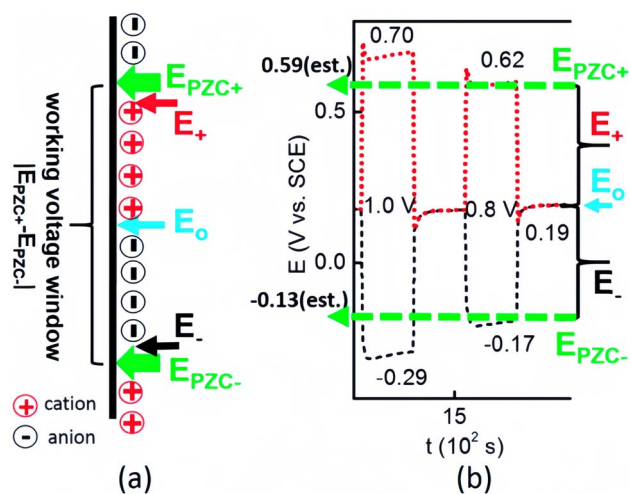

Fig. 9 Electrode potential distribution and desalination characteristics in the reverse capacitive deionization (i-CDI) system.[84] (a) A novel CDI system is proposed called inverted capacitive deionization (i-CDI). When the EPZCs for both electrodes are dissimilarly located with respect to the short-circuit voltage (E_o), the potential window between the EPZCs at the anode and cathode can be used for the desalination process, but the adsorption–desorption behavior is totally inverted. (b) Potentials distributed at the anode (E$^+$) and cathode (E$^-$) at a total cell potential of 0.8 and 1 V in 4.3 mM deaerated NaCl solution when a Si-CX anode and pristine CX cathode were used in a four-electrode cell.

Nie *et al.* produced PAN/PMMA-based porous carbon nanofibers (N-CNFs) *via* electrospinning, which exhibited a negative surface charge. Positively charged carbon nanofibers (P-CNF) were then obtained after chemical modification with ZnCl$_2$. Then, the self-supporting P-CNF cathode and N-CNF anode were obtained to construct an asymmetric capacitive deionization device. Based on the electrostatic synergy between the cathode and anode, an excellent ion adsorption capacity of 30.4 mg g^{-1} and a high ion adsorption rate of 1.0 mg^{-1} g^{-1} min were achieved. In the long-term cycling tests, the asymmetric electrodes showed high charging efficiency, stability, and reusability. Gao *et al.* composed an i-CDI battery using an amine-modified microporous carbon cathode, which positively enhanced the surface charge of the electrode, thereby achieving a desalination capacity of ~ 5.3 mg g^{-1}.[85]

2.2.4.6 Dual-ion capacitive deionization. Owing to the charge/mass imbalance of HCDI, the cathode or anode is underutilized, and there is a kinetic mismatch between the redox and capacitive electrodes.[86] Therefore, scholars have explored the DICD system, which is developed based on the HCDI. By coupling the material to the carbon-based cathode to form an electric double layer, cations and anions can be removed simultaneously *via* Faraday redox reactions.[87] At high voltages, cation insertion occurs at the negative electrode and is offset by the water oxidation of the carbon-based cathode, resulting in a lower voltage. However, if Faraday material is used to replace the carbon-based anode, although the ion adsorption capacity can be enhanced, the operating voltage of the system can also be significantly increased.[88] It has been reported that Wei has developed an advanced pseudocapacitive behavior-induced double-ion selective deionization (Di-CDI) system based on MoS_2/PPy//Ag@PANI/AC to remove Na$^+$ and Cl$^-$ by introducing a Faraday reaction on both electrodes. A high adsorption capacity of 25.1 mg g^{-1} and an ultrafast maximum deionization rate of 5.88 mg g^{-1} min^{-1} are exhibited.[89] Yue *et al.* proposed that $Na_{1.1}V_3O_{7.9}$@reduced graphene oxide (NVO@rGO) was used as the sodium ion intercalated cathode electrode and Ag@rGO chloride ion intercalated anode electrode, and the two electrodes formed a new two-ion hybrid CDI system, with strong sodium ion adsorption capacity owing to its NVO ribbon structure. By coupling with rGO and adding an ion conductor network, it provides a migration platform for high sodium ions and significantly improves their migration rate. The rGO-based flexibility further improves structural stability. To validate the desalination capability of the Di-HCDI system, we tested the desalination capability of Ag@rGO∥ NVO-250@rGO and rGO∥NVO-250@rGO HCDI units. Fig. 10a illustrates the working principle of desalination (1.2 V) and salinization (0.7 V). Then, we introduce an electric field of 1.2 V DC voltage so that a large number of sodium ions move instantaneously under the action of electrostatic force and are inserted into the NVO-250@rGO electrode, and when the Cl ions are easily adsorbed in the Ag@rGO electrode through the corresponding equation below, the initial conductivity generated is 500 μS cm^{-1} (~ 250 mg L^{-1}). The corresponding conductivity and current transients generated are shown in Fig. 10b and c.[90]
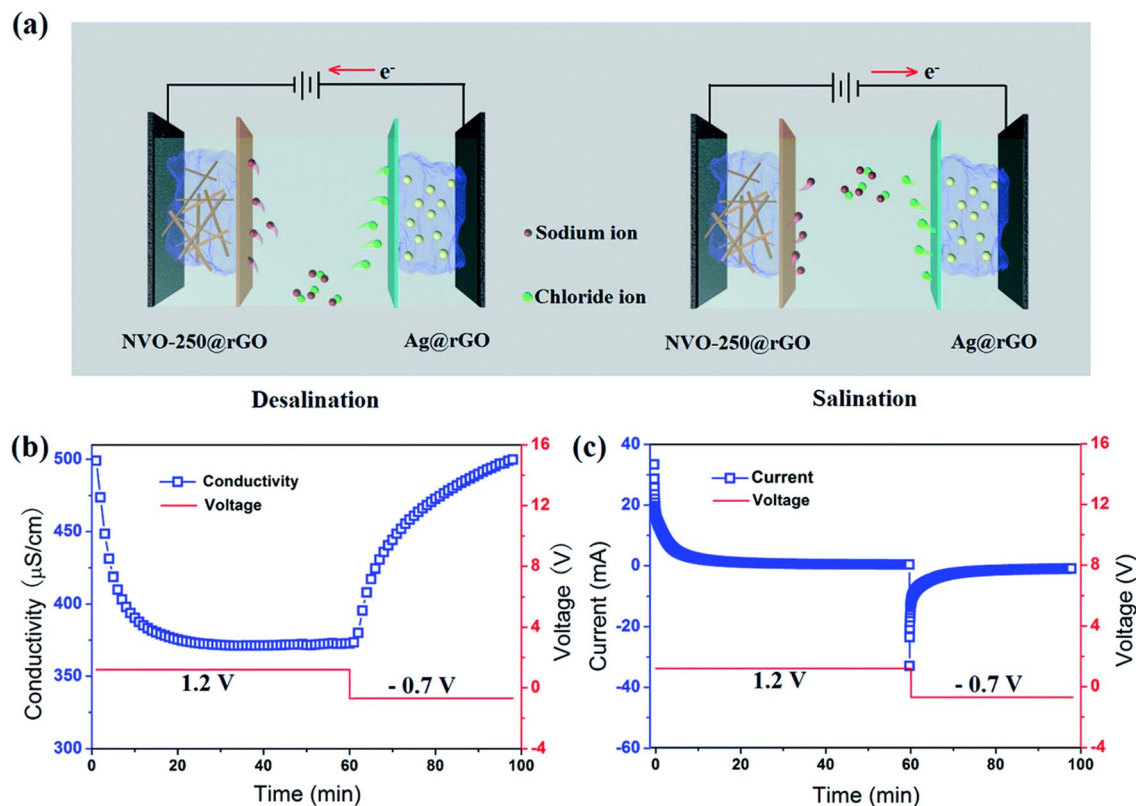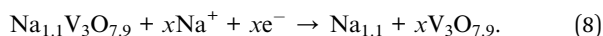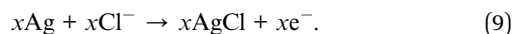
Negative electrode:

Fig. 10 Working mechanism, conductivity characterization, and current transient response of the binary high-capacity electrochemical system Ag@rGO∥NVO-250@rGO in the 1.2 V/500 μS cm^{-1} NaCl system.[90] (a) Working mechanism of Ag@rGO∥NVO-250@rGO Di-HCDI system, (b) conductivity and (c) current transient of the Ag@rGO∥NVO-250@rGO Di-HCDI system in 500 μS cm^{-1} NaCl solution at 1.2 V.

$$Na_{1.1}V_3O_{7.9} + xNa^+ + xe^- \rightarrow Na_{1.1} + xV_3O_{7.9}. \tag{8}$$

Positive electrode:

$$xAg + xCl^- \rightarrow xAgCl + xe^-. \tag{9}$$

To intuitively present the characteristics, advantages, disadvantages and desalination efficiency of the six capacitive deionization types (traditional CDI, MCDI, FCDI, HCDI, i-CDI and DCID), the following table is compiled, which summarizes their structural features, pros and cons, and desalination efficiency (Table 1).

3 Raw materials and structure of biocarbon electrode materials

Electrode materials are critical to CDI operation; their performance directly affects adsorption and desorption efficiency.[94] Carbon materials, such as activated carbon, porous carbon, carbon nanotubes, graphene, templated carbon, metal–organic framework-derived carbon, and hybrids, are the most studied in CDI and electrochemistry. Their large surface area, good conductivity, and high stability meet basic high-performance CDI electrode needs.[95,96] However, traditional carbon materials have drawbacks: expensive precursors and complex, time-consuming synthesis limit large-scale production.[14] Thus,

sustainable, low-cost, eco-friendly carbon materials are vital for CDI.[14] Biomass-derived carbon materials solve these issues. From abundant biomass, they are cheap, green, and renewable. Controlled preparation tunes their chemical structures and morphologies to meet high-performance CDI electrode requirements.[95,97] The following sections detail these materials and their preparation.

The animal and plant components in nature have evolved over hundreds of millions of years to form a relatively complete, multi-scale conforming structure and build a complete and superior biomass material system. In addition, it has attracted the attention of most scholars because of its functional diversity.[98] Biomass is mainly composed of cellulose, hemicellulose, and lignin, with a small amount of extract.[99,100] The above is a narrow definition, and a broader definition is that biomass is a complex bio-organic or non-organic solid product that can be derived from the natural environment, industrial waste, and so on.[101] Biomass in the narrow sense is organic matter formed through photosynthesis, including plant-based materials (such as agricultural and forestry biomass, and forestry biomass) and animal-based materials (such as insects, shrimp and other components). There are also microbial-based materials, such as bacteria and prokaryotes. Biomass in a broad sense can also be derived from industrial waste.[101] In summary, biomass-derived charcoal is derived from organic products, forestry, agricultural, industrial and household wastes or residues, as well as

Table 1 Comparison of structural composition, performance and references of six capacitive deionization units

Unit structure	Structural composition	Advantages	Disadvantages	Desalination efficiency	References
Traditional CDI	It comprises graphite current collectors and carbon-based electrode sheets (fixed on titanium or graphite foil, which also functions as current collectors). The electrode sheets are separated by organic membranes, featuring a parallel electrode arrangement and an intermediate solution chamber	Simple operation, low resistance, low cost	It operates intermittently, accompanied by the co-ion repulsion effect, although it has reduced energy consumption. However, it is only suitable for low-concentration brine and exhibits no ion selectivity, and its electrodes are non-renewable	Treating 2000 mg L^{-1} NaCl solution yields a 50% water recovery rate, 75% desalination rate, and a specific energy consumption (SEC) of 0.85 kW h m^{-3}	91
MCDI	Selective cation and anion exchange membranes are incorporated into the electrodes of traditional CDI systems	It operates at low voltage, entails low energy consumption, and achieves electricity savings	It cannot operate continuously; solid electrodes have limited pores, and the regeneration process is complex. Additionally, it is only suitable for medium and low concentration salt solutions	At an initial conductivity of 110 μs cm^{-1} and a voltage of 1.2 V, a 97% salt removal efficiency is achieved, which is higher than that of membrane-free CDI.	92
FCDI	Flow electrodes are composed of a carbon suspension (carbon slurry). Two flow electrode chambers and one desalination chamber are formed *via* ion exchange membranes	It enables continuous desalination, featuring high production efficiency and strong ion adsorption capacity. Additionally, desorption and adsorption can be performed separately, which reduces co-ion repulsion and makes it suitable for high-concentration brine	It has a limited inflow rate, difficulty in scaling up, and restricted module applications. Additionally, its long-term desalination efficiency stability needs to be studied further. Moreover, carbon slurry viscosity causes reduced conductivity, high resistance, low energy recovery, and clogging tendency	Desalinating 1000 mg L^{-1} brackish water to 150 mg L^{-1} achieves an 85% desalination efficiency	93
HCDI	It is assembled from a faraday electrode and a capacitive carbon electrode	Faraday materials replace traditional carbon electrodes, exhibiting high desalination capacity, high ion selectivity, and more robust salt adsorption/desorption reactions	It requires a high operating voltage. Its desalination capacity and stability are limited by capacitive carbon electrodes, with electrode materials featuring complex preparation, high cost, and sensitivity to impurities	Using urchin-like W$_{18}$O$_{49}$@C as the electrode yields a desalination capacity of 32.25 ± 0.70 mg g^{-1} for 1000 mg L^{-1} (brackish water)	82
i-CDI	It employs carbon electrode materials with entirely distinct surface charge states. This design enhances the net surface charge of carbon materials, resulting in salt desorption during charging and adsorption during short circuits	It improves ion separation capability, reduces anode oxidation, mitigates carbon cathode oxidation, and enhances the cycling stability of CDI devices	High precision is required for regulating the surface charge of electrode materials, and the preparation process is complex. Additionally, asymmetric electrodes may suffer from a charge imbalance	Asymmetric device: ion adsorption capacity 30.4 mg g^{-1}, adsorption rate 1.0 mg g^{-1}min^{-1}	83
DCID	The materials are coupled with a carbon-based cathode to form an electric double layer, and simultaneously remove cations and anions *via* faraday redox reactions	It features rapid adsorption and desorption, high desalination rate, low energy consumption, stable performance, and low operating voltage	The utilization rate of the cathode and anode is low, accompanied by charge/ mass imbalance	The system based on MoS$_2$/PPy//Ag@PANI/AC exhibits an adsorption capacity of 25.1 mg g^{-1} and a maximum deionization rate of 5.88 mg g^{-1} min^{-1}	89

livestock production or livestock waste, and is a renewable resource that can be produced in a relatively short cycle.[102]

3.1 Raw materials for biomass-derived carbon materials

Wood, orange peel, grass, mangosteen peel, apricot shell, coconut shell and other such materials are widely recognized as biomass resources.[103] Additionally, various biological materials, including poplar catkin, lignin, corn stover, bagasse, switchgrass, rice husk, wood chip, animal manure and even sewage sludge, have been used to produce biomass-derived carbon.[104,105]

Biochar is a carbon-rich porous material produced through the thermochemical conversion of biomass. It exhibits high aromaticity and gas-generating properties during formation, with feedstock sources divided into two categories: (1) lignocellulosic biomass includes agricultural/forestry residues and wood waste, and (2) non-lignocellulosic materials are mainly from municipal solid waste.[106] Lignocellulosic is the most abundant renewable biomass, with low moisture, low ash content, high calorific value, high bulk density, and fewer voids.[107] Compared to other feedstock options, wood biochar typically contains a more specific surface area (SSA) and pore volume (PV). SSA and PV are functions that reduce relatively large wood-based cell structures to smaller pores. Wood biochar contains more C, but this is only due to the lack of other elements (*e.g.*, N, S, P, K, Ca, and P), resulting in a low trend of C loss in wood biochar.[108] One of the main characteristics of non-lignocellulosic biomass is its high inorganic ash and carbon content compared to other materials, such as wood or agricultural wood fiber qualities. It also has an abundant element content, which facilitates self-doping and structural regulation.[109] However, non-lignocellulosic biochar(NLBM) waste, which is widely distributed, has a complex and diverse composition owing to its wide range of sources. Its composition mainly includes proteins, lipids, sugars, inorganic substances, and a small part of lignin and cellulose. The threat to the ecological environment is greater because it has a high content of heavy metals and heteroatoms (such as nitrogen, phosphorus, and sulfur) and faces difficulties and challenges in the pretreatment stage. Therefore, it is important to understand the physicochemical properties and select the appropriate pretreatment to achieve efficient preparation, which is discussed in detail in the subsequent sections.[110]

3.1.1 Lignocellulosic biomass. Lignocellulose is composed of cellulose, hemicellulose and lignin with extremely high overall abundance. Among them, lignin comprises 15–30 wt% of the biomass wall. Studies have shown a direct positive correlation between lignin content and biochar yield; higher lignin biomass consistently produces greater biochar quantities.[111] Therefore, the degradation of lignocellulose can be a promising source of aromatic compounds and chemicals.[112] Cellulose is an elongated, linear polysaccharide with a crystalline structure consisting of glucose units linked by β-1,4-glycosidic bonds. Simultaneously, hemicellulose is a branched-chain polysaccharide that comprises various monosaccharides, including pentoses and hexoses. Lignin is a complex three-

dimensional macromolecule composed mainly of aromatic compounds and is a binder between hemicellulose and cellulose. Together, these components form a tightly connected complex supramolecular network structure held together by hydrogen, ester, and ether bonds.[113] The above describes the composition of lignocellulose. Simultaneously, commonly used lignocellulosic biomass can be divided into agricultural waste, forestry waste, energy crops, and human-derived waste. More typical examples within each category are introduced to provide a deeper understanding.

3.1.1.1 Agricultural waste. Straw is a common source of agricultural waste within lignocellulosic biomass. Straw biochar is formed by carbonization under completely anaerobic or partially anoxic conditions. It has an abundant pore structure and a large specific surface area, which has attracted the attention of researchers.[114] Zhang *et al.*'s research indicates that microporous-derived carbon synthesised from corn stalk waste is activated using a potassium hydroxide solution. The analysis shows that SEM and TEM images reveal the formation of abundant micro-mesopores, as illustrated in Fig. 11 and 12, while nitrogen adsorption analysis validates the types of pore diameters, as demonstrated in Fig. 13[115] Gou *et al.* developed an innovative approach to preparing porous carbon materials using agricultural straw as the feedstock. Through KOH-activated carbonization of lignocellulosic foam, they successfully obtained carbon materials exhibiting a high specific surface area of 772 m^2 g^{-1}. The optimized micropore size (1.05–1.74 nm) shows perfect compatibility with 6 M KOH electrolyte, demonstrating excellent electrochemical matching.[116]

3.1.1.2 Forestry waste. Forestry waste primarily refers to forest-derived residues, including leaves, bark, and wood shavings. Patel's study noted that pine sawdust was used as a precursor. A physicochemical activation synthesis scheme using both KOH and CO_2 as activators is proposed. Activated porous carbons were prepared using three methods: physicochemical activation, chemical activation (KOH only), and physical activation (CO_2 only). Their effectiveness was compared, with the maximum BET surface area reaching 2216 m^2 g^{-1}.[117] Prasankumar *et al.* demonstrated that Tasmanian eucalyptus globulus bark (TBG) can serve as a precursor for porous carbon, prepared *via* simple carbonization, followed by KOH activation. The resulting carbon material exhibits a high specific surface area of 971 m^2 g^{-1} and an average pore size of 2.2 nm, with its carbon framework featuring an excellent layered mesoporous structure.[118] Since the carbon content of the carbonaceous residue of eucalyptus leaves is the highest in biomass, the content can reach 75%. It is a good choice for biochar raw materials. Therefore, Bejjanki *et al.* used bio-oil extracted from eucalyptus leaves as a carbon precursor. With $ZnCl_2$ as a chemical activator, they synthesized activated carbon at temperatures ranging from 400 °C to 800 °C. The results showed that at 700 °C, the biocarbon's surface area increased significantly to 1027 m^2 g^{-1}, and its specific capacitance reached 196 F g^{-1}, which was attributed to the expansion of cellulose structures in lignin induced by activation.[119]

3.1.1.3 Municipal waste. Municipal waste includes urban green waste (*e.g.*, leaves, branches, and yard waste), waste wood
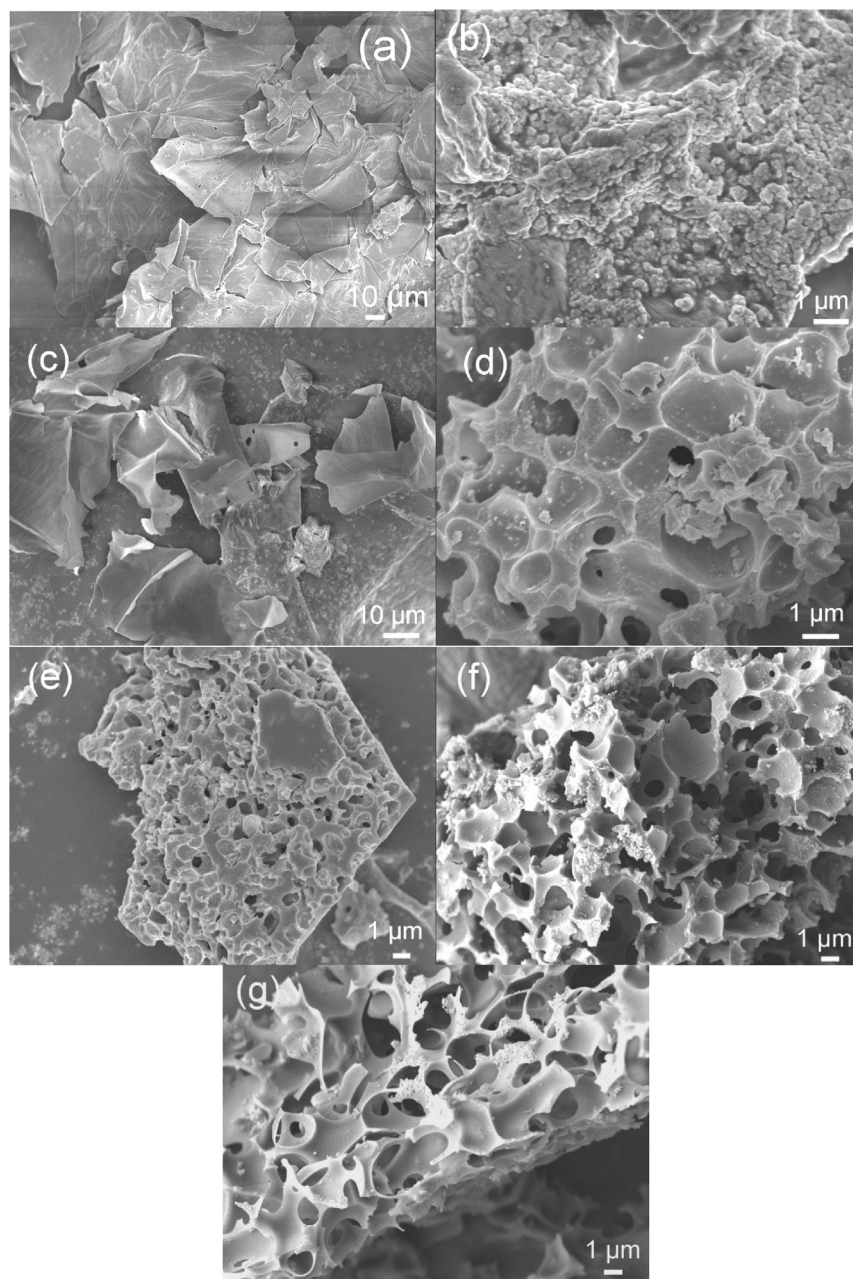
Fig. 11　SEM images[115] of (a) corn stalks, (b) AS-KOH(3), (c) AC-KOH(0), (d) AC-KOH(2), (e) AC-KOH(3), (f) AC-KOH(4) and (g) AC-KOH(5).

products (*e.g.*, sawdust and wooden furniture from manufacturing processes), and waste paper. Treating municipal waste as an alternative to energy crops or agricultural residues can effectively protect the environment and promote sustainable resource development.[120] Menon *et al.* indicated that yard waste—with its high lignin content, abundant natural aromatic carbon rings, and active functional groups—can be converted into biochar materials *via* carbonization (Fig. 14). This process yields a micro-mesoporous structure with a surface area of up to 381 m^2 g^{-1}. Therefore, it is a better raw material selection strategy to effectively reduce energy and environmental pressure by treating it.[121]

3.1.2 Non-lignocellulosic biomass. Compared with ligno-cellulosic biomass, non-lignocellulosic biomass (NLBM) contains more diverse elements, including N, P, S, and metallic elements. NLBM can typically arrange the atoms of these elements in an orderly manner, forming a well-structured framework by embedding the atoms into its building blocks. In the preparation process, it can be used as an activator or catalyst for the thermal decomposition of biomass, which is conducive to the formation of a biochar framework with more pores and structural frameworks. Therefore, it has excellent electrochemical, catalytic and adsorption properties.[122] In non-lignocellulosic biomass, the sources are abundant and the
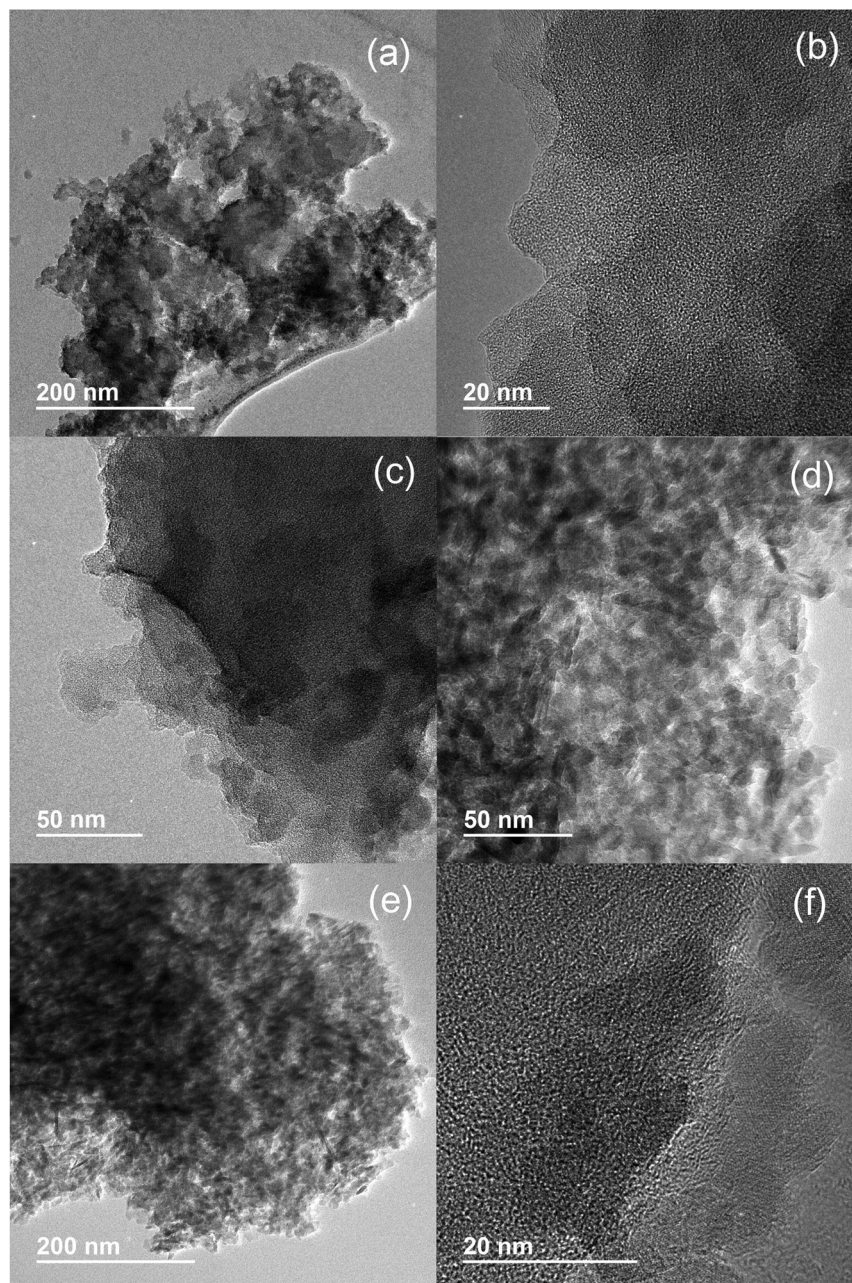
Fig. 12 TEM images[115] of (a) and (b) AC-KOH(2), (c) AC-KOH(3), (d) AC-KOH(4), and (e) and (f) AC-KOH(5).

compositions complex, meaning that it does not fall into a single category. Therefore, we introduce it by giving an example of a representative NLBM.

3.1.2.1 Sewage sludge. Sewage sludge (SS) from urban wastewater treatment is a highly viable biomass resource. It typically contains non-toxic organic compounds and inorganic substances, along with some toxic components and a high moisture content (approximately 55–80%). This is a very feasible biomass generation resource for urban sewage treatment.[123] Zhang *et al.* prepared efficient, layered porous biochar by carbonizing and activating aerobic granular sludge (AGS) from a biological wastewater treatment plant as a precursor. It is

a green and sustainable preparation strategy. As shown in Fig. 15, we can observe that the source of the sludge is extracted from the sludge discharged from the wastewater treatment system. As shown in Fig. 13b and c, the morphology of biochar after drying and carbonization can be observed. The results show that the specific surface area was 1822.07 m^2 g^{-1}, the micropore area ratio was 58.65%, and the micropore volume was 0.576 cm^3 g^{-1}. Biochar has good desalination performance as an electrode in MCDI.[124]

3.1.2.2 Algae. Seaweed is a promising algal resource due to its high content of nutrients, such as N and P, and other nutrients.[125] Compared with lignocellulosic biochar, carbon
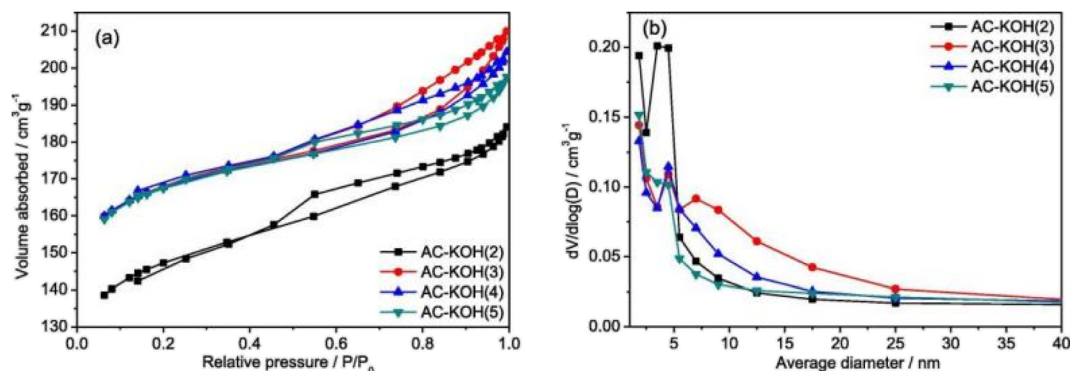
Fig. 13 N$_2$ adsorption and desorption isotherms[115] (a) of the activated carbon samples and the corresponding pore size distribution (b) calculated by the BJH method using the desorption branch of the isotherms.
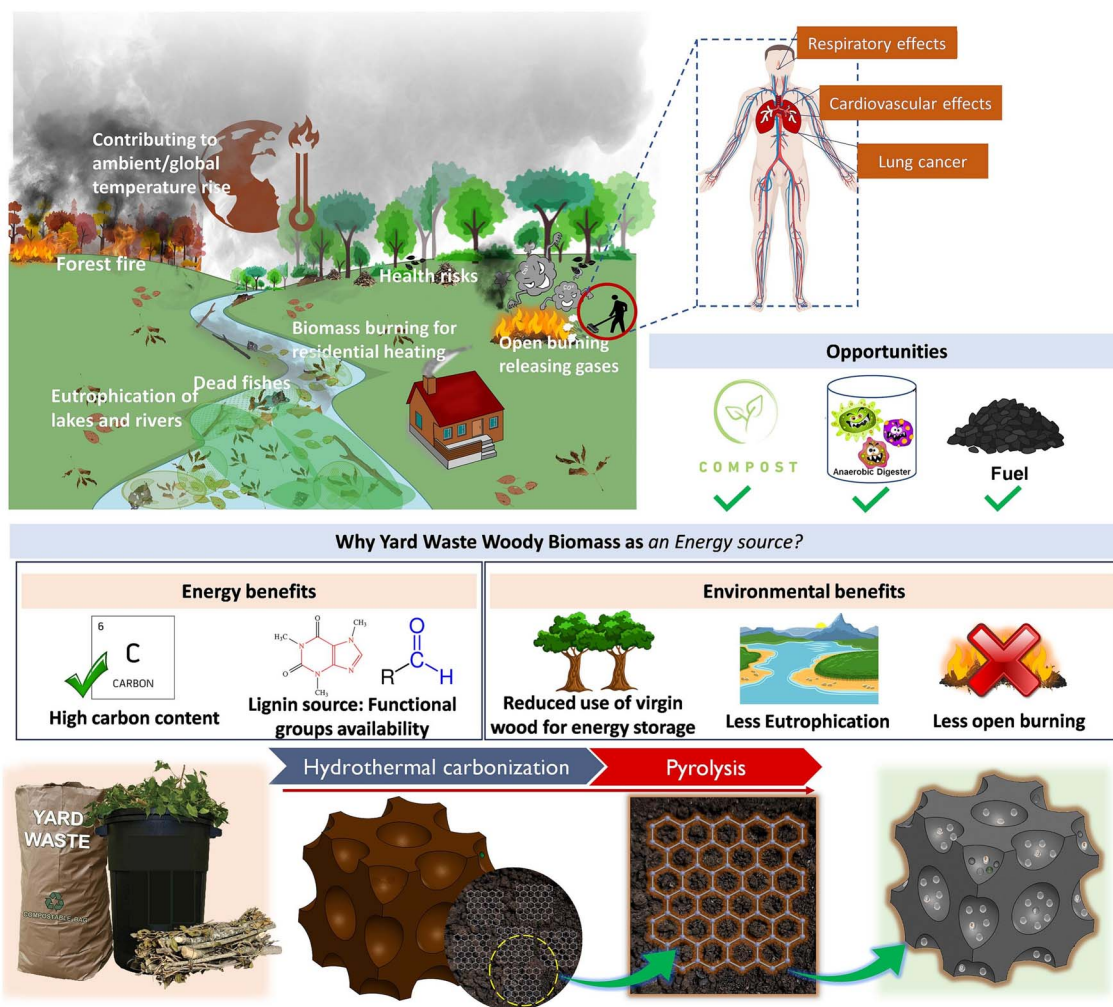

Fig. 14 Representation of the environmental impacts of yard waste woody biomass on the environment and how it can act as a good energy source.[121]

materials derived from algal feedstocks have a lower carbon content, surface area, and cation exchange capacity. Their raw materials contain nitrogen, ash, and other inorganic elements and minerals. Therefore, it can be used as an agricultural soil conditioner to improve soil fertility and nutrient supply

capacity. Additionally, biochar can be used as an adsorbent for wastewater treatment and desalination.[126] Zhang *et al.* synthesised nanoporous microalgal biochar (NP-MBC) using microalgae as the raw material *via* formaldehyde-stabilised hydrothermal treatment, KOH activation, and high-
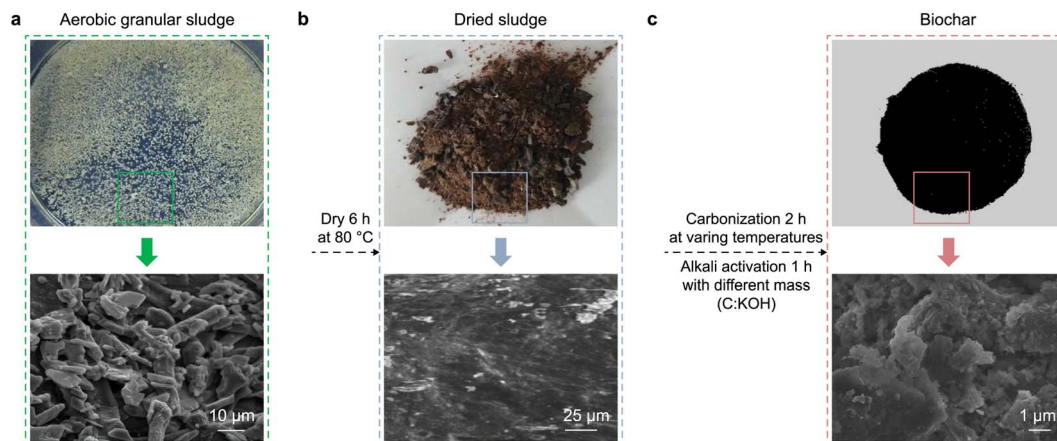
Fig. 15 Preparation process and sample characterization of biochar derived from the AGS wastewater treatment system emissions.[124] (a) AGS was collected from the effluent of the AGS wastewater treatment system. (b) The sludge was obtained after drying at 80 °C for 6 h. (c) Biochar was obtained by carbonization and activation.

temperature pyrolysis. The pyrolysis temperature helped to improve the pore structure and surface chemistry of NP-MBC and increased the specific surface area to 1137 m^2 g^{-1}.

3.1.2.3 Manure. In addition, in the lignocellulosic biochar prepared in the laboratory, the biochar produced from wood biomass has a relatively high C content. Biochar from cow dung and algae showed relatively low elemental carbon levels of 11.55% and 24.62%, respectively. Studies have shown that biochars derived from animal manure have lower carbon, oxygen, and hydrogen contents than those derived from lignocellulosic biomass. This is due to the higher content of volatile compounds in manure, which are lost during the drying and carbonization stages of pyrolysis. In addition, the low carbon content is a typical feature of the microalgae production of biochar compared to lignocellulosic biochar-derived biochar.[127] For example, Tsai *et al.* reported that the first series of biochars derived from dried pig manure fertiliser *via* slow pyrolysis; their pore structure increased significantly with an increase in temperature, and their structure was good.[128]

3.1.2.4 Other. Animal bones and hair are widely available, so using them as precursors for biochar production makes sense for promoting sustainable development. Among them, shrimp shells are the most widely used, containing up to 36.43% chitin—the second most abundant biopolymer on Earth after cellulose. Owing to its strong intermolecular hydrogen bonding, it is conducive to metal ion support and heteroatom doping and activation.[129] Wei *et al.* developed honeycomb-like hierarchical porous carbon (MSHPC) using mantis shrimp shell waste as a precursor *via* a self-template method coupled with hydroxide activation.[130] Hair can be made from bovine hair solid waste, which comes from leather production plants. Song *et al.* prepared biochar (with a specific surface area of up to 1753.075 m^2 g^{-1}) in a N$_2$ atmosphere.[131]

3.2 Structure of biomass-derived carbon materials

Compared with other carbon materials, biomass-derived carbon can inherit the unique structure, defects and chemical

composition of biomass precursors in the preparation process. The electrochemical properties of different carbon species are mainly related to the physicochemical properties of biocarbon-based materials. If the appropriate electrode material can efficiently adsorb the required ions, and the circularity is relatively stable, the desalination efficiency also significantly increases.[132] The macroscopic morphological characteristics of carbon-based materials can be categorised into spherical, fibrous, tubular, and layered shapes.[133] What we want to explore is the multi-dimensional structure of carbon-based materials in different forms, which can be categorised into zero-dimensional, one-dimensional (1D), two-dimensional (2D), and three-dimensional (3D) configurations.[134] These include 0D carbon balls and dots, 1D carbon fibers and tubes, 2D carbon sheets, 3D carbon aerogels, and hierarchical carbon materials.[135] Owing to their sustainability, affordability, and adjustable structure of various forms of carbon materials,[136] zero-dimensional materials feature high-density active sites, one-dimensional materials have porous structures, two-dimensional materials possess tuneable defects, and three-dimensional materials exhibit multi-scale porosity. This enables carbon-based materials to offer potential for a wide range of applications through their multidimensional structures.

3.2.1 Zero-dimensional. Zero-dimensional biomass carbon materials include carbon nanoparticles, carbon dots, carbon nanocages, and carbon nanoonions.[137] They exhibit broad application prospects in rechargeable ionic/metal batteries and supercapacitors. Carbon dots (CDs) are a new type of carbon material consisting of small carbon nanoparticles smaller than 10 nm in size. They are synthesised *via* a bottom-up approach using cross-linking-induced carbonization from various precursors.[138] It has the characteristics of quantum size, abundant surface functional groups, and uniform dispersion, and the ability to adjust the structure and composition of the material.[139] Previously, there were three main types of carbon dot (CD) applications: direct use of CD, CD-based nanohybrid materials, and CD-driven materials. Although there have been

some reports that CD can be used as an electrode material, it is still challenging due to its high cost and relatively low electrochemical performance.[140] Wei *et al.* proposed an innovative strategy to improve cation adsorption capacity by constructing electron-rich regions on the electrode surface, thereby improving electrochemical performance. This method has no adverse effects on carbon materials. A series of multi-level porous carbon materials with controllable surface states (including electron-rich regions) have been successfully fabricated by calcining carbon dot-hydrogel composites.[141]

Li *et al.* pointed out that lignin-derived carbon nanoparticles (LCNPs) constitute a unique class of carbon materials, as shown in Fig. 16c, which have the advantages of high strength, corrosion resistance and heat resistance of traditional carbon materials, and simultaneously, have the characteristics of environmental protection and low energy consumption of lignin. This is because lignin molecules contain 60% carbon and are rich in unsaturated groups, such as aromatic rings and carbon–carbon double bonds, as shown in Fig. 16a. As shown in Fig. 16b, there are six types of LCNPs: spheres, aggregates, hollow spheres, non-spheres, irregular particles, and carbon quantum dots. Therefore, as a nanomaterial, lignin-based carbon nanoparticles (LCNPs) exhibit small particle size effect, surface effect and macroscopic quantum tunneling effect. Compared with traditional carbon materials, LCNP has excellent performance in terms of high specific surface area, tunable permeability, strong mechanical strength and electrical conductivity.[142] In addition, Wu *et al.* showed that a carbon matrix obtained from bamboo fiber (BF) can be used as a support material for immobilized platinum (Pt) nanoparticles. This significantly enhances the performance of the hydrogen evolution reaction (HER). This method takes advantage of the large surface area, excellent conductivity, and environmental protection properties of BF-derived carbons, thereby effectively promoting the dispersion and stability of Pt nanoparticles.[143] Simultaneously, Gaddam *et al.* reported a method for the preparation of carbon nanoparticles (CNPs) from coconut oil by applying the flame deposition method. CNPs were further modified with piranha solution to obtain surface-carboxylated carbon nanoparticles (c-CNPs).[144]

3.2.2 One-dimensional. Bio-carbon nanotubes, carbon nanorods, and carbon nanofibers are common one-dimensional bio-carbon materials with significant application prospects in energy storage and conversion.[145] Hidalgo *et al.* developed carbon nanotubes (CNTs) using biomass as a precursor *via* pyrolysis and microwave-assisted heating, which significantly increased the specific surface area.[146] In addition, carbon nanotubes (CNTs) exhibit excellent chemical stability, flexibility, and excellent electrical properties, making them highly promising candidates for flexible electronic devices. The Seebeck coefficient of carbon nanotubes ranges from 20 to 40 $\mu V\ K^{-1}$ and has good conductivity in the range of 3000–5000 $S\ m^{-1}$.[136]

Owing to the limited aspect ratio of nanorods, it is difficult to establish conductive networks. In addition, their dielectric losses are due to the resulting polarization relaxation of the internal heterogeneous interface. Based on these characteristics, carbon nanorods require a high preparation strategy, usually by *in situ* assembly and synthesis, but self-assembly also faces the challenge of coercivity generated by magnetic metal ions.[147] Therefore, Wu *et al.* converted cellulose nanocrystals (CNCs) into porous nitrogen (N)-doped carbon nanorods for the first time. This is an innovative strategy that allows CNC to be used not only as a carbon source but also as a template to regulate growth. Additionally, by doping melamine formaldehyde (MF) and nitrogen, carbon nanorods (N-MFCNCs) are formed.[148] Fang *et al.* designed a high-strength layered structure with excellent electrochemical properties for the first time—
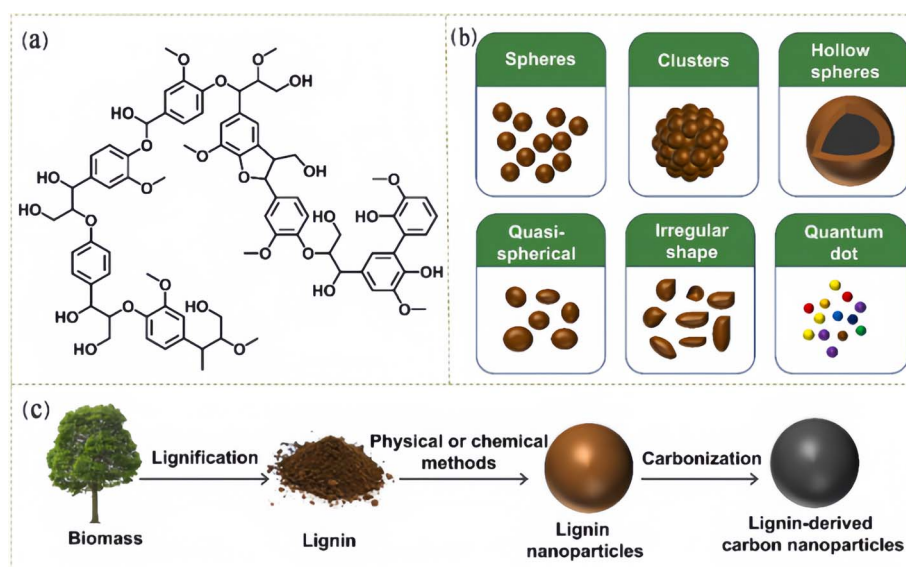

Fig. 16 Schematic of lignin structure, morphological display and manufacturing process diagram of LCNPs.[142] (a) A representative lignin structure (not the actual molecular structure). (b) Common morphologies and (c) fabrication routes of LCNPs.

Fig. 17 Schematic of the synthesis of CNR/HTC/CFs.[151]
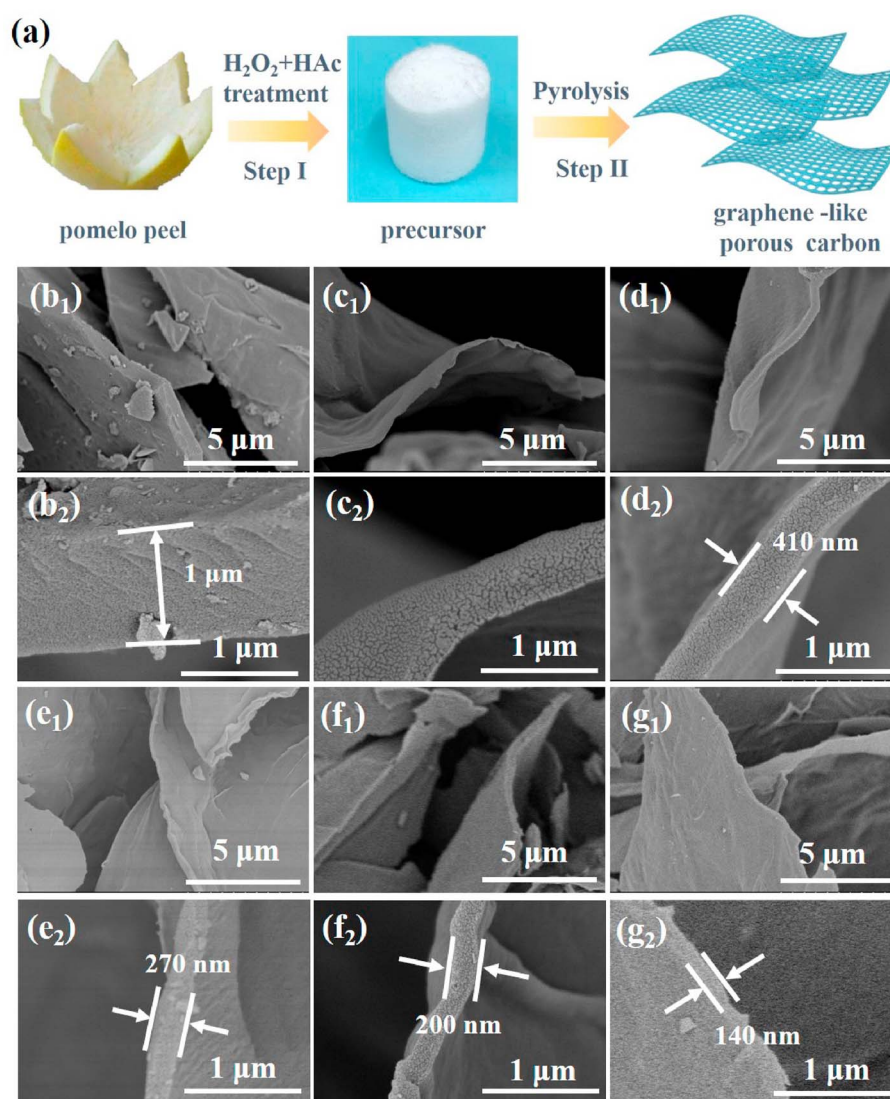

Fig. 18 Comparison of the GPCN preparation process and SEM microstructure of YZP and 10%-A/O series pretreatment samples.[155] (a) Synthetic route of GPCN. SEM images of samples prepared with different pretreatment (b_1 and b_2) YZP, (c_1 and c_2) 10%-A, (d_1 and d_2) 10%-O, (e_1 and e_2) 10%-A/O-1, (f_1 and f_2) 10%-A/O-2, and (g_1 and g_2) 10%-A/O-3.

carbon nanorod-supported hydrothermal carbon and carbon fibers (CNR/HTC/CFs) using waste straw as the carbon source, as shown in Fig. 17. Carbon nanorods with a high specific surface area are formed by purifying the gas after pyrolysis of the straw and then introducing it. The tensile strength of CNR/HTC/CF monofilament could reach 2743 ± 467 MPa.[149] Svinterikos et al. showed that carbon nanofibers (CNFs), as a one-dimensional carbon material, have a wide range of applications in energy storage, catalysis and adsorption with diameters in the sub-micron and nanometer ranges. As a low-cost and renewable biological resource, lignin has become a promising precursor material for the production of CNF.[150]

3.2.3 Two-dimensional. Graphene and its porous derivatives demonstrate exceptional electrochemical properties as advanced electrode materials, combining a high specific surface area with rapid ion/electron transport kinetics. These materials exhibit a remarkable mass loading capacity while maintaining mechanical flexibility and stability during repeated charging or discharging. Compared with conventional carbon-based materials, graphene and its derivatives have demonstrated better

performance in energy storage.[152] Chai et al. highlighted the intrinsic correlation and evolutionary behavior of synergistic interactions between micro/nanostructures, active species, and electrochemical properties.[153] Niu et al. fabricated tunable nitrogen-doped large-scale graphene-like porous carbon nanosheets (LGPCNs) using bagasse pith and chitosan as raw materials via self-template and structural design strategies. Its ingenious design is to use bagasse pith as a carbon source, which also acts as a hard template and nitrogen source, thus providing a platform for regulating nitrogen-doped carbon nanosheets. Therefore, the electronic conductivity and wettability of the surface of the carbon material are enhanced, providing excellent electrochemical properties.[154] Zhao et al. developed graphene-like porous carbon nanosheets (GPCNs) derived from waste pomelo peels, as illustrated in Fig. 18a. Compared with traditional graphene, they prepared GPCNs that have the advantages of low cost, high yield, and ease of production. Fig. 18b$_1$ and b$_2$ show the topography of pomelo peel treated with different amounts of HAc and H_2O_2, which exhibit a brick-like block structure with a smooth surface. The

Fig. 19 Preparation of cellulose-based carbon nanofiber films and multiscale microscopic characterization of CeO$_2$ nanorod composite structures.[157] (a) Optical picture of the size comparison of pristine cellulose-based filter paper (left) and carbon nanofiber film (right) after pyrolysis; (b) SEM image of cross-linked carbon nanofibers derived from cellulose filter paper; (c) SEM image of CeO$_2$ nanorods agglomerates homogeneously decorated on the cellulose-derived carbon structure; (d) higher magnification image of a fiber decorated with CeO$_2$ nanorods. (e and f) TEM images of CeO$_2$ nanorods at various magnifications.

surface of the 10% HAc sample after the hydrothermal reaction showed a rough surface and a sheet-like structure, as shown in Fig. 18c$_1$ and c$_2$. Although another equal amount of H$_2$O$_2$ is carried out under the same reaction, the material retained a brick-like morphology. However, with a 10 wt% HAc/H$_2$O$_2$ mixture, the sample thickness gradually decreased from 270 nm to 140 nm as the HAc/H$_2$O$_2$ molar ratio increased from 1 to 3 (Fig. 18 e$_1$, e$_2$, g$_1$, and g$_2$). This indicates that HAc exerts a more pronounced positive effect on pomelo peel treatment as its content increases.[155]

3.2.4 Three-dimensional. The 3D structures of biocarbon materials exhibit excellent interconnectivity, large specific surface area (SSA) and controllable porous structure, and their structural design has attracted the attention of many researchers. Typical 3D materials include carbon sponges, aerogels, carbon microspheres, and carbon nanofibers, which are mostly composed of 2D materials, such as graphene, carbon nanotubes, or carbon nanofibers. Consequently, they inherit the high electrical conductivity of 2D materials.[156] Azam et al. developed a cost-effective and environmentally friendly method: CeO$_2$ nanorods are used to modify carbon nanofibers on a cellulose paper-based carbon fiber framework, and the composite is then subjected to high-temperature pyrolysis to prepare an intermediate layer for battery cathodes. This layer can alleviate the polysulfide shuttle effect, as shown in Fig. 19a. The morphology and size derived from cellulose fibers are illustrated in Fig. 19b, while the cross-linking state of the pyrolyzed carbon fibers is shown in Fig. 19c and d. These figures also indicate that the CeO$_2$ nanorods are successfully grown on the surface of the carbon nanofibers, forming a strong contact, clearly revealing the 3D structure of the carbon fibers. Fig. 19e and f display the morphology of CeO$_2$ nanorods at different magnifications, with diameters ranging from 5 to 10 nm and from 50 to 150 nm.[157]

In addition, the pore size of three-dimensional porous carbon materials is adjustable, and its pore diameter can be divided into macropores, mesopores, and micropores according to the diameter size. The diameter ranges are >50 nm, 2–50 nm, and <2 nm. Zhao et al. showed that the high reversibility and porosity of microporous-mesoporous-derived carbon materials prepared from mangosteen peel are owing to the micro-mesoporous structure of the materials, electron or ion diffusion.[158] Wu et al. developed bifunctional electrocatalysts for oxygen evolution reaction (OER) and oxygen reduction reaction (ORR) using single and zirconium flux spray drying techniques. Owing to the characteristics of the protein biomass, carbon microspheres have a large specific surface area and high pore volume.[159] However, there are currently no hollow-structured carbon nanospheres that can be derived directly from biomass without using a template method. Qu et al. reported a particle evolving from an aerosol-assisted process, with glucose and glucosamine as precursors, featuring a spherical morphology and falling within the nanoscale range. It also has a high specific capacitance of 266 F g^{-1} at 0.2 A g^{-1}, long-cycle stability of 96.8% capacitance after 3000 cycles, and a fast charge–discharge process. This conclusion can be used to guide the design and synthesis of various hollow materials using biomass as feedstock.[160]

4 Pretreatment and preparation of biomass-derived charcoal

4.1 Pretreatment

Biomass is widely available, has irregular shapes, and is mostly composed of cellulose, hemicellulose, and lignin, of which cellulose is composed of chains of 10 000–15,000 cellobiose units, hemicellulose is a heteropolymer composed of C5 and C6 sugars, with a branched chain structure, forming a sheath-like coating on cellulose fibrils,[161] and the purpose of pretreatment is mainly to treat cellulose and lignin in biomass, achieving a high specific surface area and porosity during biomass carbonization.[162] Untreated biomass-derived carbon, especially lignocellulosic biomass, is not suitable for direct use as an electrode material that contains a large number of electrochemically inert impurities and their native structural resistance. In addition, these impurities and resistance can hinder biomass carbonization.[163] In addition, the carbon yield of bio-derived carbon is determined by its precursor. If the carbon yield rate is very low, even if the electrode material has excellent performance, it limits its large-scale production, and the solution to this issue is to pretreat biomass precursors to facilitate their carbonization, thereby increasing the yield.[164] Second, some biomass residual pollutants lead to secondary pollution if not treated well. For example, sewage sludge produced from wastewater contains a large number of contaminants, and the usual simple cleaning cannot meet the needs of the sample, so it is necessary to select the corresponding pretreatment according to the characteristics of the biomass.[165] Carbohydrate conversion efficiency can be achieved through biological pretreatment solvents, which are commonly used biomass-derived solvents, carbohydrate-derived solvents, and lignin-derived solvents.[166] Pretreatment techniques can generally be categorised into physical, physicochemical, chemical, and biological techniques. The physical method mainly helps to increase the surface area of bio-derived charcoal, while physicochemical methods mainly use chemicals and solvents to facilitate the hydrolysis of cellulose and hemicellulose. The chemical method is mainly used to reduce lignin content, and the biological method is used to change the internal structure of biomass-derived charcoal by producing enzymes.[167] Excess water in the precursor reduces heat transfer rates during biomass carbonization, lowering biocarbonisation efficiency.[168] The second is to make the biomass more evenly heated and have better porosity during the carbonization process through grinding. The third is deashing, which refers to the removal of inorganic substances, such as elements (including K, Na, Ca, Mg, Al, Fe, P, S, Cl, and Si) as well as trace elements (including Mn and Ti) from biomass via pretreatment, thereby reducing adverse effects on the pyrolysis process, such as scaling, slagging, and hot corrosion.[169]

There are many forms of pretreatment, and many researchers have modified the structure of carbon materials

using different pretreatment methods. Qin *et al.* prepared activated carbon (SMAC) using pig manure (SM) as a carbon source by combining the *in situ* template method, KOH activation method, and pyrolysis method. The process of pretreatment and preparation of SMAC is illustrated in Fig. 20. The prepared SMB and SMACs are expressed as SMB*x–y* and SMAC*x–y*, respectively, where *x* represents hydrochloric acid (HCl) pretreatment, *y* represents HF treatment, and SMACNON and SMACPHF represent no pickling and HF pickling after pyrolysis, respectively. The precursor SM is dried at 500 °C and then pickled with KOH solution and hydrofluoric acid HF. After heating, the residual acid in SMACs was removed by repeated washing and pickling processes; finally, activated carbon SMACs were obtained.[170]

Wang *et al.* investigated and indicated that after freeze treatment, the specific surface area (SBET) and total pore volume of carbon materials derived from low-cost coconut shells (CSs) sourced from biological precursors increased significantly by 92.8% and 44.4%, respectively.[171] Wang *et al.* used beehives – a natural pretreatment procedure that is formed by bees chewing and reassembling natural plants. Moreover, the beehive has the microstructure of a micro-nano lignocellulose capillary network, which can complete the activation of biomass-derived carbon with fewer chemical reagents, greatly reducing the use of chemical reagents.[172] However, to address the challenge of traditional pretreatment methods for non-glycogen-derived lignin streams, Meng *et al.* proposed increasing the lignin yield ratio using biomass-derived pretreatment solvents.[173]

4.2 Preparation of biomass-derived carbon materials

There are three approaches to preparing biomass-derived carbon materials (BCMs): carbonization, activation, and templating. Typical carbonization techniques include pyrolytic carbonization, laser-induced carbonization, Joule thermal carbonization, hydrothermal conversion, and salt encapsulation carbonization.[174] Among them, hydrothermal carbonization (HTC) and pyrolysis are the most common methods. There were differences in the morphology and structure of the BCMs prepared by applying different methods. However, porosity is greatly affected by additives such as activation reagents and templates, which can lead to the formation of porous BCMs.[175] In addition, in recent years, there have been novel preparation strategies, such as laser-induced carbonization,[138] pyrolysis carbonization, and pyrolysis.[176]

4.2.1 Carbonization

4.2.1.1 Pyrolysis. Pyrolysis is one of the most efficient and environmentally appealing thermochemical processes[177] that can convert biomass into high-value products, such as biochar, bio-oil, and syngas, at temperatures in the range of 300 °C-900 °C under oxygen-free conditions.[178,179] In the pyrolysis process, a large number of reactions occur in parallel or series. Biomass pyrolysis comprises three main stages: (i) initial evaporation of free water, (ii) primary decomposition, and (iii) secondary reactions (petroleum cracking and repolymerization). These phases do not occur sequentially but in a mixed manner.[180] Fig. 21 illustrates the process of the deoxidation catalytic cracking of structural components during the pyrolysis of lignocellulosic biomass. Pyrolysis is characterised by a significant increase in aromaticity and energy density, while at temperatures above 400 °C, the internal surface area of the solid material increases substantially, while oxygen-containing functional groups decrease, and the material becomes hydrophobic.[181]

Depending on the heating rate, the pyrolysis process can be divided into three types: slow (0.1–1 °C s^{-1}), medium (1–200 °C
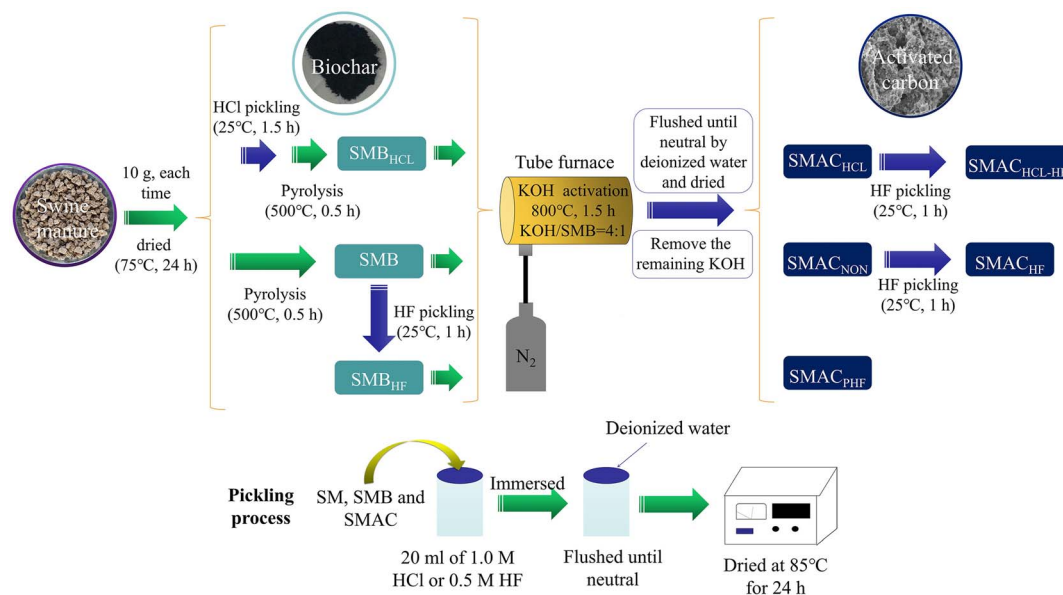

Fig. 20 Schematic of SMAC preparation.[170] The prepared SMBs and SMACs were denoted by SMB*x–y* and SMAC*x–y*, where *x* represents hydrochloric acid (HCl) pretreatment, *y* represents hydrofluoric acid (HF) treatment, and SMACNON and SMACPHF represent no pickling and HF pickling after pyrolysis, respectively.

s^{-1}), and fast pyrolysis (200–1000 °C s^{-1} or flash pyrolysis).[185] We mainly introduce the principles of slow pyrolysis and fast pyrolysis. Medium speed pyrolysis is similar to the first two, but it can be launched in the same way, and it is not elaborated in detail. Slow pyrolysis is a technique that enhances the yield of high-quality carbonised products by combining low heating rates, low temperatures, and long residence times, also known as a continuous system of "charcoal". The minimum heating rate is 5–7 °C min^{-1}, and the maximum heating rate is 20–100 °C min^{-1}. In an anaerobic environment, the organics are slowly heated at temperatures greater than 400 °C for 5–30 minutes or several days, after which the volatile organic compounds begin to crack and recombine to produce coking and other distillate liquids.[186] In rapid pyrolysis, biomass is a liquid product obtained by immediate quenching of the pyrolysis vapour, i.e., bio-oil. Bio-oil is composed of various condensable chemicals produced by many simultaneous and sequential reactions during the pyrolysis of lignocellulosic biomass.[187] Additionally, the pyrolysis rate corresponding to the particle size is different. For small particles, a higher heating rate should be used to accelerate bond cleavage reactions, thereby promoting volatile formation and increasing the yield of bio-oil. When the particles are larger, a relatively slow heating rate may drive the recombination reaction, which may further lead to carbonization rather than volatile formation, thus reducing the yield of bio-oil.[188]

Wang et al. prepared pine source porous carbon (PBC) by mixing KOH and pine powder evenly in proportion and then subjecting the mixture to thermal decomposition in a tube furnace (a nitrogen flow rate of 100 mL min^{-1}, heating rate of 5 °C min^{-1}, and holding time of 2 h) after homogeneous mixing of KOH and pine powder in a proportional and uniform manner.[189] Aspergillus niger mycelia are used as raw materials and are sustainably cultured with food waste hydrolysate as the nutrient substrate. During preparation, mycelial fibers are first filtered and compressed into thick sheets, transforming the dispersed mycelia into dense, thick sheets. Then, carbonization is performed following the method by Chen et al.: the temperature is increased from room temperature to 800 °C at a rate of 5 °C min^{-1}, maintained for 2 hours under an argon atmosphere, and then activated. In this process, the original interwoven and layered porous structure of the mycelial mat is retained, transforming into a porous, flexible, and self-supporting fungal mycelium-derived carbon pad (FhACPad). Meanwhile, an approximate weight loss of 83.2% is observed, with the carbon sheet shrinking to 1 cm × 5 cm in area, about 300 μm in thickness, and having a bulk density of 0.20 g cm^{-3}. This carbon pad can be directly used as a CDI electrode, achieving the conversion of biomass into high-performance electrode materials.[190]

4.2.1.2 Hydrothermal carbonization. Conventional pyrolysis (using tube furnaces or muffle furnaces) exhibits limitations, such as slow heating rates, high energy consumption, and poor efficiency, when processing high-moisture biomass (e.g., algae and sludge). In contrast, hydrothermal carbonization employs water as the reaction medium to efficiently convert biomass into hydrochar at relatively low temperatures, demonstrating
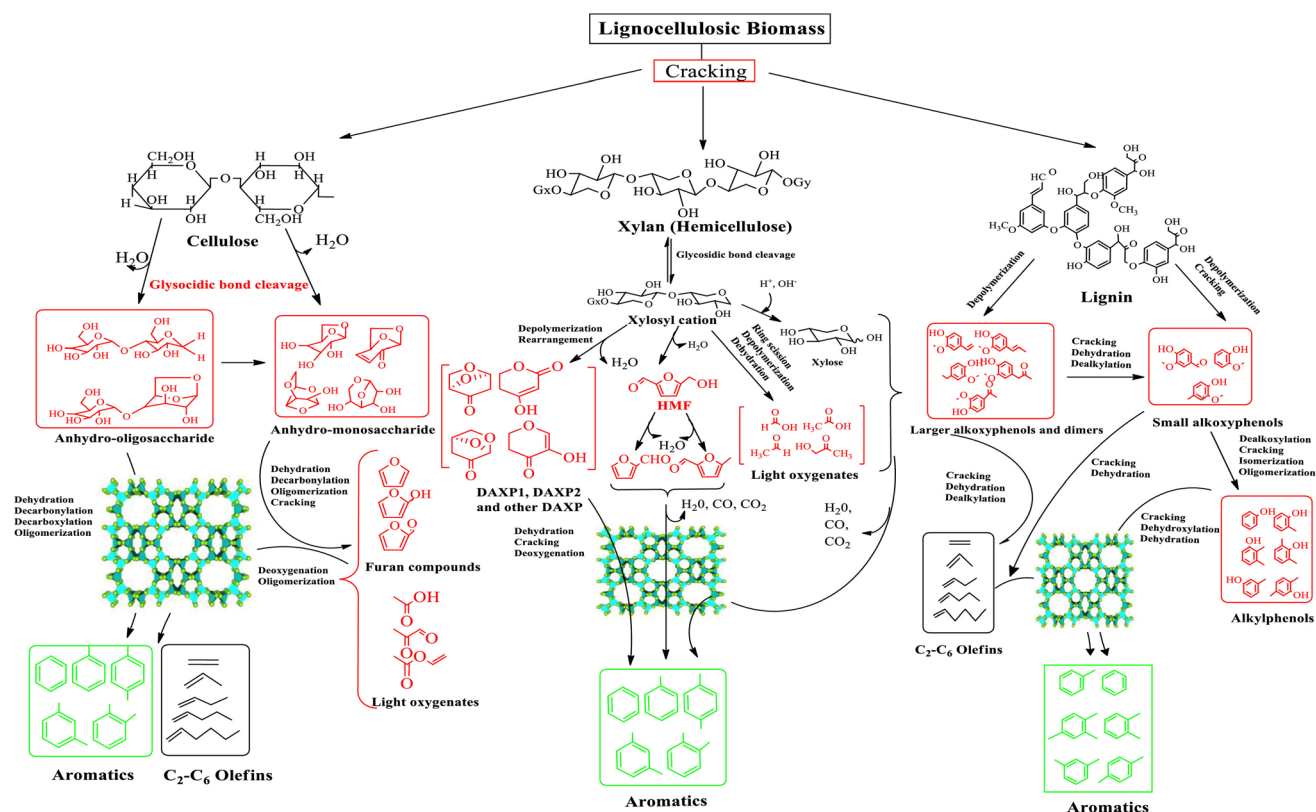

Fig. 21 Catalytic cracking of structural components during rapid pyrolysis of acid catalysts.[182–184]

particular suitability for direct processing of high-moisture feedstocks.[191] This approach not only overcomes the drawbacks of traditional methods but also yields hydrochar with lower ash content and higher calorific value,[192] showing promising potential for energy applications.[193]

When biomass undergoes a hydrothermal reaction, it undergoes a series of reactions, such as condensation, polymerization, hydrolysis, decarboxylation, dehydration, and aromatization. These reactions do not represent sequential reaction steps; they may show different/parallel reaction paths, and the reactions depend primarily on the type of feedstock.[194] As shown in Fig. 22, lignocellulose is mainly composed of carbohydrate polymers (i.e., cellulose and hemicellulose), aromatic polymers (i.e., lignin), extracts (resins, tannins, and fatty acids), and inorganic components (ICs).[195] However, owing to the high ionisation constant of water at elevated temperatures, hydrothermal carbonization can hydrolyze organic compounds; various organic acids are then further catalysed by acids and bases, thereby reducing the pH value.[196] The resulting hydronium ions act as catalysts for the degradation of oligosaccharides into the corresponding monosaccharides, which then undergo cyclic C–C bond cleavage and dehydration

reactions to form furfurals. These compounds are further broken down into aldehydes, acids, and phenols. After a series of reactions, the monomers and decomposed molecules undergo condensation and polymerization into polymers. This polymerization reaction is enhanced by aldol condensation or intermolecular dehydration. It is accompanied by the aromatization of polymers.[197,198] Through this series of processes, after the complete disintegration of the biomass's physical structure, most organic matter in the biomass is converted into solids.[194]

In the HTC process, the longer the reaction time, the greater the structural porosity, pore volume, and BET surface area.[203] However, compared with other methods, carbon materials produced via hydrothermal carbonization have limitations, including a lower specific surface area and poorly developed porosity. Therefore, hydrothermal carbonization is often combined with the activation process to improve the physicochemical properties of carbon materials.[204] Baig et al. synthesised nickel-cobalt sulfide/wheat husk activated carbon (NiCo$_2$S$_4$/WHAC) on nickel foam through an external synthesis process. Its growth was formed through hydrothermal carbonization, with the synthesis mechanism, as illustrated in Fig. 23. The NiCo precursor is synthesized by applying a hydrothermal
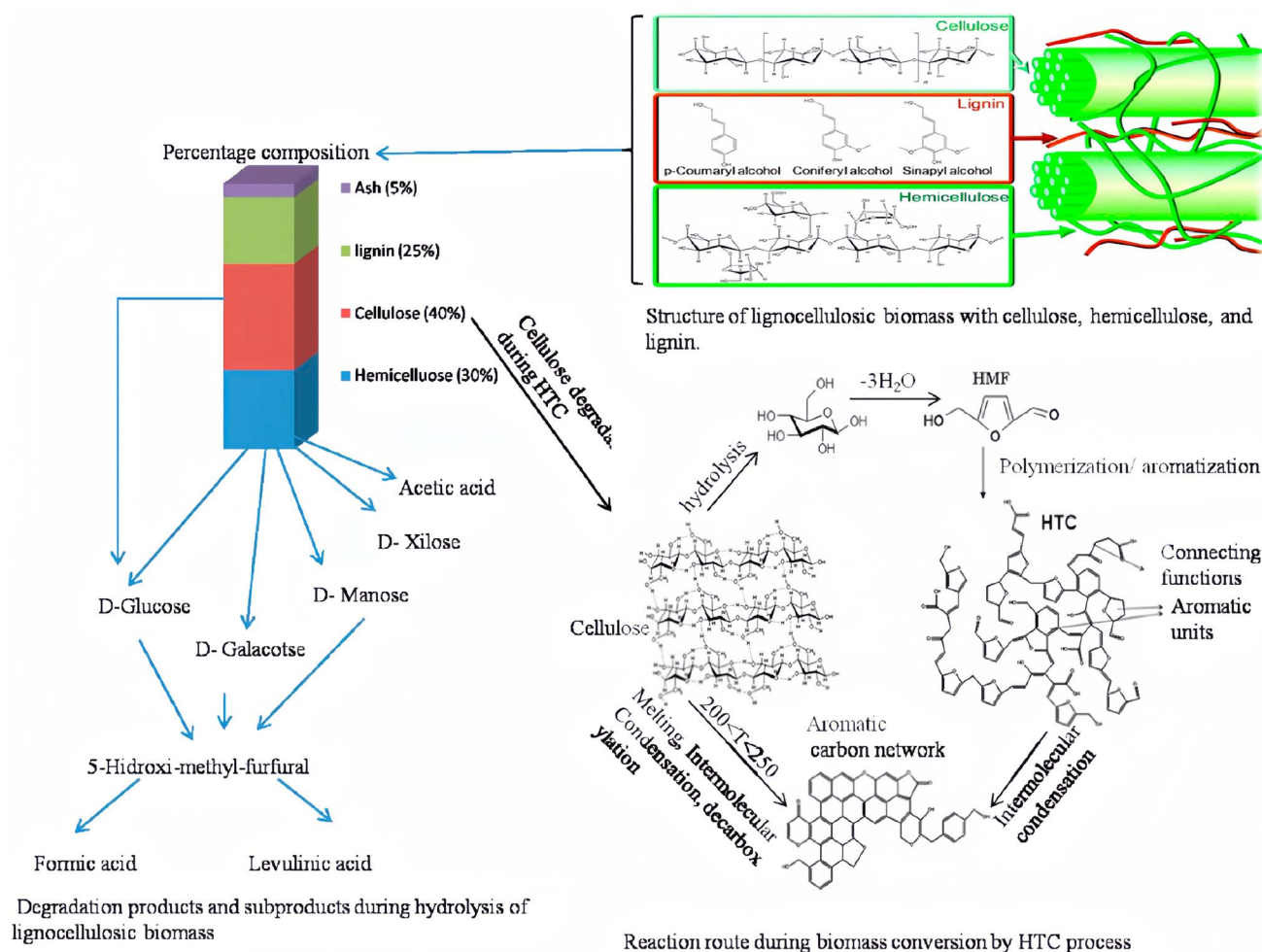

Fig. 22 Detailed structure of biomass, showing lignin, cellulose, and hemicellulose and their conversion routes during HTC.[199–202]
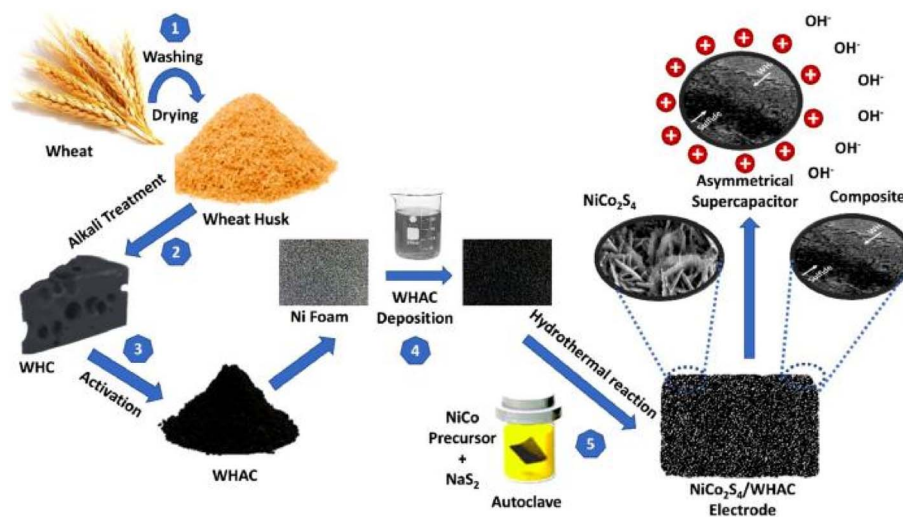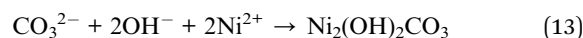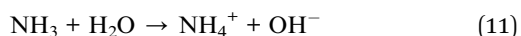
Fig. 23 Schematic of the synthesis of the electrode materials.[207]

method, and its growth mechanism is shown in eqn (10)–(14).[205,206] The reaction starts with the hydrolysis of urea: urea first hydrolyzes to generate hydroxide ions and carbonate ions. Subsequently, in the reaction system, nickel ions and cobalt ions react with the above-mentioned ions, respectively, transforming into nickel hydroxycarbonate and cobalt hydroxycarbonate, and finally forming the NiCo precursor.

$$CO(NH_2)_2 + H_2O \rightarrow 2NH_3 + CO_2 \tag{10}$$

$$NH_3 + H_2O \rightarrow NH_4^+ + OH^- \tag{11}$$

$$CO_2 + H_2O \rightarrow 2H^+ + CO_3^{2-} \tag{12}$$

$$CO_3^{2-} + 2OH^- + 2Ni^{2+} \rightarrow Ni_2(OH)_2CO_3 \tag{13}$$

$$CO_3^{2-} + 2OH^- \rightarrow CO_2(CO_3)(OH)_2 \tag{14}$$

After the hydrothermal reaction, the total mass loading of the material before and after the hydrothermal reaction was measured using an electronic weighing difference method. The mass loading of $NiCo_2S_4$ on the nickel foam was approximately 2.13 milligrams. The morphology of the prepared $NiCo_2S_4$/WHAC electrode can be observed in Fig. 24 *via* scanning electron microscopy (SEM), revealing a floret-like spherical structure composed of nanosheets and small cross-linked
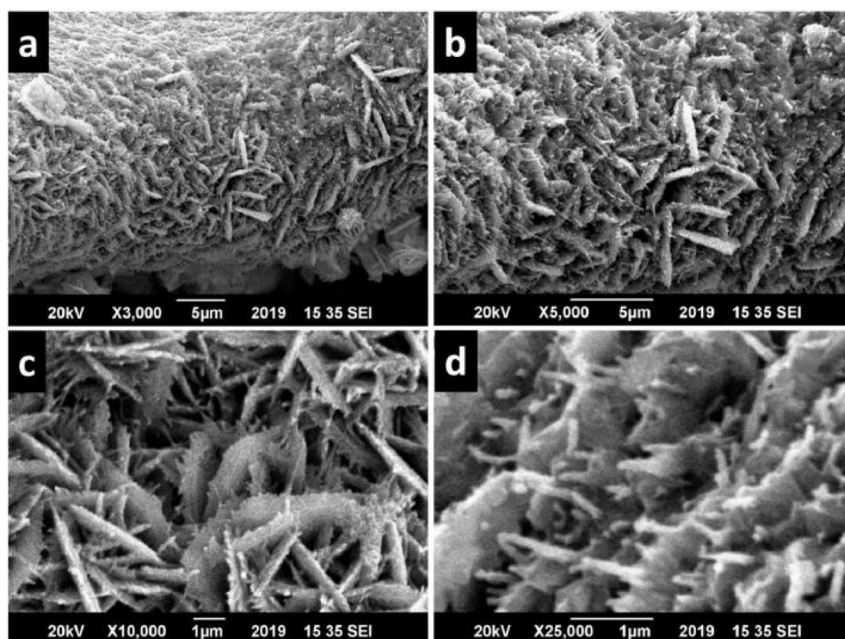

Fig. 24 SEM images of $NiCo_2S_4$/WHAC on Ni foam at different magnifications. (a and b) 5 μm, (c and d) 1 μm.[207]
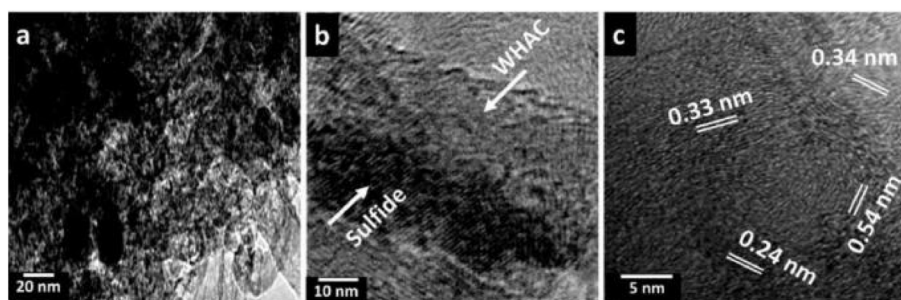
Fig. 25 TEM images of NiCo$_2$S$_4$/WHAC on Ni foam at different magnifications. (a) 20 nm, (b) 10 nm, (c) 5 nm.[207]
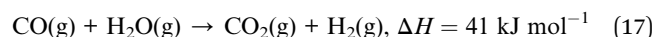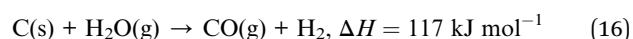
microneedles. However, the lattice fringes observed through transmission electron microscopy (TEM) depicted in Fig. 25 are consistent with the XRD pattern, indicating the polycrystalline nature of NiCo$_2$S$_4$, and the WHAC matrix formed during carbonization offers low resistance[207].

4.2.1.3 Other methods. Altwala *et al.* used date palm seeds as a suitable starting biomass and employed another carbonization process known as flash carbonization, which uses a shorter time (5–10 minutes) and lower temperature (400 °C) in the presence of air to convert the biomass into carbonaceous material, and the carbonaceous substance obtained is resistant to activation, so it produces highly microporous-activated carbon (surface area of 995–2609 m^2 g^{-1} and pore volume of 0.43–1.10 cm^3 g^{-1}). It has a high bulk density even at high activation levels.[208]

4.2.2 Activation. To synthesize activated carbon with a high carbon content and a large specific surface area and pore volume, the biomass material is usually activated in the preparation process. There are usually two types of activation processes: physical activation and chemical activation. Physical activation involves the mild gasification of carbonaceous materials using steam, nitrogen, or carbon dioxide, while chemical activation refers to the activation of biomass using chemical dehydrating agents.[209] The primary goal of the activation process is to fine-tune porosity and eventually form a highly porous material. During activation, pore development takes place in three steps: (a) opening inaccessible pores, (b) forming new pores, and (c) increasing the size of existing pores. Different activation parameters (temperature, time, and water flow rate) have different effects on the pore structure of carbon synthesized from coconut shell biomass.[210]

4.2.2.1 Physical activation. Physical activation is a two-step process: the first step is used to carbonize the raw materials in an inert atmosphere (N$_2$ or Ar) to eliminate volatile substances at low temperatures, and the second step is used to activate the carbonized substances at higher temperatures.[211] CO$_2$ is the most widely used and effective physical activator. This is because CO$_2$ has better pore uniformity compared to steam. The typical reactions associated with CO$_2$ and steam activation are described by eqn (15)–(17).[212] The activation of CO$_2$ occurs mainly through the Budouard reaction (eqn (15)), which is triggered above 700 °C. In addition, physical activation is more environmentally friendly than chemical activation

because it uses naturally occurring activators. However, physical activation occurs at relatively high temperatures and lasts for a long time, and the activation energy of physical activators is higher than that of chemical activation.[213] CO$_2$-based physical activation has been extensively studied, and it is preferred over steam owing to its ease of handling, low activation temperature requirements, and carbon recovery methods. However, the use of purified CO$_2$ streams can increase process expenditures. Therefore, it is recommended that the flue gas produced after post-combustion, containing a binary mixture of N and CO$_2$, is commonly used, and the use of nitrogen helps to control the activation phase, which is easy to handle and inexpensive.[214]

$$C(s) + CO_2(g) \rightarrow 2CO(g), \Delta H = 159 \text{ kJ mol}^{-1} \quad (15)$$

$$C(s) + H_2O(g) \rightarrow CO(g) + H_2, \Delta H = 117 \text{ kJ mol}^{-1} \quad (16)$$

$$CO(g) + H_2O(g) \rightarrow CO_2(g) + H_2(g), \Delta H = 41 \text{ kJ mol}^{-1} \quad (17)$$

4.2.2.2 Chemical activation. Chemical activation is called wet oxidation and is commonly used in raw materials containing cellulose, such as wood, sawdust, or fruit pits. These materials are also known as biomass resources. In the preparation of the activated carbon *via* chemical activation, organic precursors are activated in the presence of chemicals at high temperatures. Compared with the physical activation of carbon gasification, chemical activation is carried out at a relatively low temperature and is completed in a single step, while the prepared carbon material has a higher yield and a very high specific surface area.[215] The precursor material is mixed with activators, such as KOH, ZnCl$_2$, NaOH, K$_2$CO$_3$, H$_3$PO$_4$, and FeCl$_3$, which act as dehydrating and oxidising agents.[216] In chemical activation, H$_3$PO$_4$ and ZnCl$_2$ are often used to activate uncarbonized lignocellulosic materials, while metal compounds, such as KOH, are used to activate the precursors of charcoal and coke. Compared with ZnCl$_2$, H$_3$PO$_4$ has less impact on environmental and toxicological contamination and requires a lower activation temperature than potassium hydroxide.[217]

Most reagents used for chemical activation are KOH, which can be used to prepare highly porous carbon materials with a large surface area (>2000 m^2 g^{-1}). Compared with most chemical reagents,[218] KOH can react with species containing

active O in biomass at a lower chemical-to-biomass ratio (1 : 8–1 : 2) and temperature (400–600 °C). After KOH is completely converted to K_2CO_3, a large amount of gaseous products and 75% phenolic substances are generated. As phenolic substances and O species decrease significantly, hydrocarbons become the dominant component (reaching 57.43%), and O-containing groups are further converted into more stable OH, CO and COOH groups. During the activation process, potassium is embedded into the carbon network, promoting the formation of mesopores and micropores.[219] However, owing to the corrosive and toxic nature of its reagents, its use poses environmental problems. Therefore, the development of a non-hazardous chemical agent is needed to solve this problem.[218] In addition, to remove residues from precursors or reactants, as well as inorganic residues (ash) introduced during activation, post-activation washing of activated carbon is required, which makes the process cumbersome, time-consuming, energy-intensive, and costly. Li *et al.* used a new strategy of Fenton chemical activation to obtain a layered porous biomass carbon material with a very high specific surface area of 3440 $m^2\ g^{-1}$. Compared with the traditional activation process, the activation efficiency doubled. The optimized carbon electrode exhibited an excellent specific capacitance of 425.2 F g^{-1} at a current density of 0.1 A g^{-1} and excellent rate performance in a 6 M KOH electrolyte (286.1 F g^{-1} at 100 A g^{-1}).[220]

4.2.2.3 Microwave-assisted activation. Microwave-assisted activation (MW) is a promising chemical treatment and activation technique for AC heat. The carbon bed converts microwave energy through dipole rotation and ion conduction inside the particle, directly providing energy to the carbon bed. Microwave-induced/assisted activation was developed to avoid the obvious problems of traditional heating processes during physical and chemical activation.[221] MW heating has many advantages, such as uniform and internal heating, fast and selective heating, easy control, simple setup, insensitivity to particle size and shape, and low pretreatment requirements for raw materials.[222] This is based on the fact that the large thermal gradient from the inside of the coke particles to their cooling surface enables microwave-induced reactions to proceed faster and more efficiently at lower overall temperatures, saving energy and reducing processing time.[223] Under microwave, the reaction rate of steam is faster than that of CO_2, resulting in a shorter activation time. However, the use of CO_2 as an activator under microwave can improve the carbon yield, but the resulting AC exhibits porosity characteristics similar to those obtained with conventional heating.[224] Microwave-assisted methods provide highly porous materials with high specific surface area (SSA), such as activated carbon with SSA ≈ 3100 $m^2\ g^{-1}$, a metal–organic framework with SSA ≈ 4200 $m^2\ g^{-1}$, a covalent organic framework with SSA ≈ 2900 $m^2\ g^{-1}$, and a metal oxide with a relatively small SSA ≈ 300 $m^2\ g^{-1}$.[225] As reported by Tsai *et al.*, biochar was prepared from cow manure (CD) by microwave pyrolysis, and the biochar product kept for 5 min at 800 W had a maximum BET surface area of 127 $m^2\ g^{-1}$ and a total pore volume of 0.104 $cm^3\ g^{-1}$.[226] Furthermore, when a microwave (MW) acts on biomass-derived carbon materials, stronger MW absorption occurs at the glass transition temperature of the biomass components. Specifically, when acting on cellulose, microwaves can relax or even significantly activate hydrogen bonds at the O site, enabling the relevant groups to rotate freely and align with the MW field. This makes protons related to the CH_2OH group more accessible. These groups can transfer MW energy to the chemical structure; thus, the interaction between biomass and MW is achieved by promoting hydrolysis or regulating pyrolysis mechanisms.[227]

4.2.3 Template method. Template strategies can be divided into hard templates, soft templates, and dual template methods. The carbon material obtained by applying the template method can have a controlled pore structure. However, the disadvantages of this approach are also obvious; for example, the fact that the template is expensive and the process is relatively time-consuming.[228]

4.2.3.1 Hard formwork method. The hard template method is an inorganic template method, also known as the nano casting method, which uses inorganic materials as templates to prepare the corresponding mesoporous carbon materials, as shown in Fig. 26a.[229,230] Given that metals, inorganic substances, and various mixtures can maintain their microstructure during processing (*e.g.*, high temperatures), they are often used in templating methods.[231] For a solid material to be suitable as a template, it must meet two criteria: it must possess a certain rigidity and have a porous structure. The biomass is melted into a liquid carbon precursor and poured into the pores of the template, and the pore structure of the template is replicated by heat treatment.[232] Commonly used template agents are silica gel, medium-pore molecular sieves, *etc.* Among them, silica-based porous template agents, such as zeolite and mesoporous molecular sieves, have the characteristics of pore structure, narrow pore size distribution and high specific surface area.[233,234] The preparation process involves the penetration of a carbon precursor into the template in the form of a liquid or gas, followed by the carbonization of the biomass precursor at high temperatures; the extraction of the template with acid or alkaline solutions, such as NaOH and HF; and the stimulation of mesopore formation.[229,230]

Li *et al.* synthesized hierarchical porous carbon (HPC) using non-myelinated corn stalks as a carbon source and calcium carbonate ($CaCO_3$) as a hard template through a sustainable one-pot method. $CaCO_3$ can interact with an activator (potassium oxalate) to produce etching effects and vaporization, resulting in a honeycomb structure with many interconnected channels that adjust porosity.[237] The disadvantage of the hard template method is that the template needs to be removed after the preparation is completed, which usually adds difficulty to the preparation process. Therefore, scholars have developed a special hard template method called the self-template method. It uses endogenous minerals in raw materials (such as CaO, MgO, and SiO_2) as hard templates for the production of porous carbon materials, provides a skeleton structure for biochar carbonization, and interacts with organic components during the pyrolysis process without the use of activators, reducing costs. However, the process of mutual reaction may affect the pore structure and functional groups of the biochar.[238]
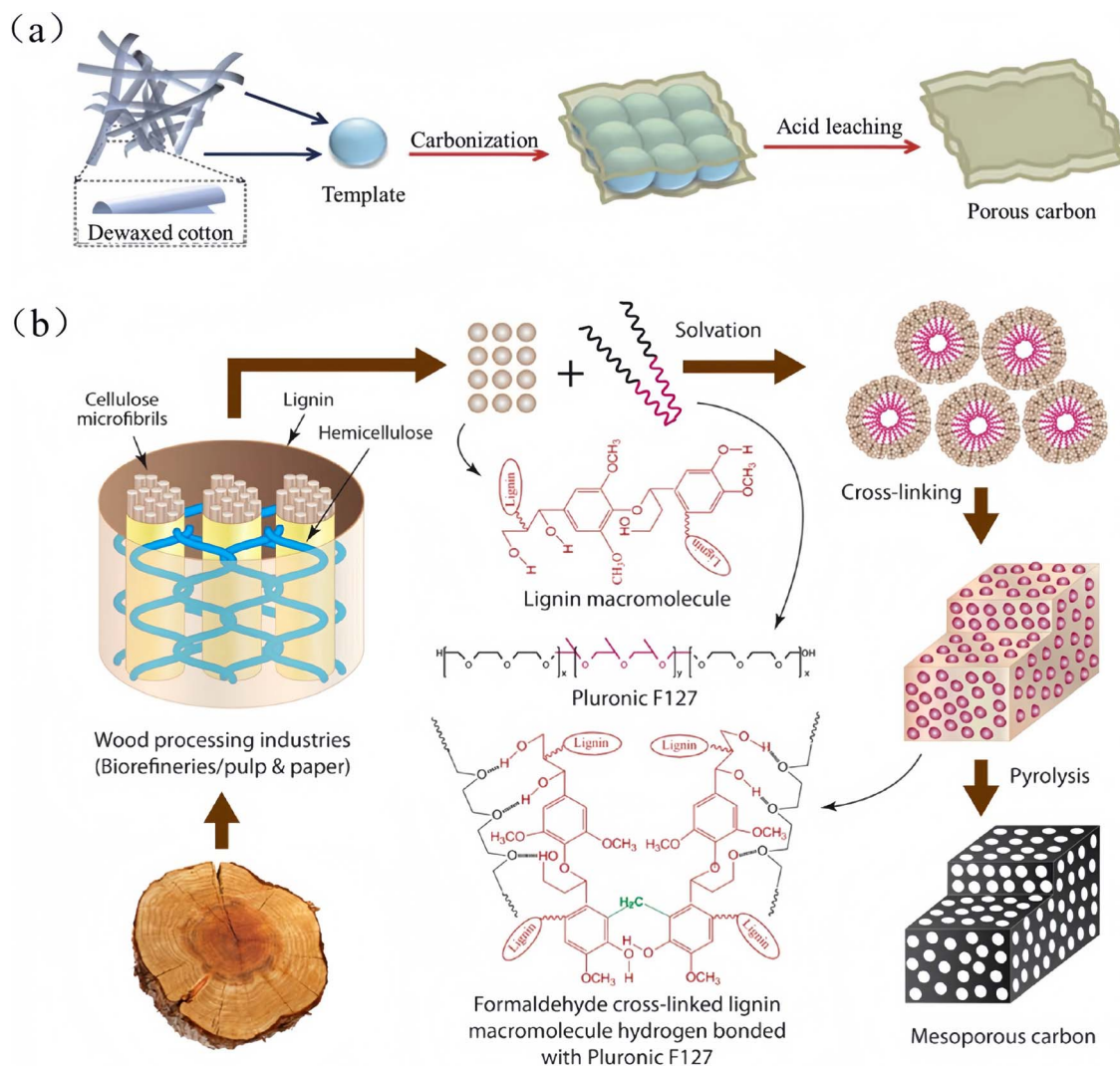
Fig. 26 Schematic of biochar using the template method:[235,236] (a) hard template method and (b) soft formwork method.

Wu *et al.* developed a new strategy for preparing porous biochar (HPBC) through the co-pyrolysis of biomass and zinc salt composites, as shown in Fig. 27a. The *in situ* formation of the mesoporous ZnO template with zinc salt ions effectively addresses the step of removing templates when using hard template methods, thereby saving process time and associated costs. Fig. 27b shows a significant difference between BC and HPBC, and it is found that HPBC is porous owing to the evaporation of $ZnCl_2$ during pyrolysis and thawing owing to the ZnO template. Fig. 27c and d show the morphologies of HPBC-1, HPBC-2, and HPBC-3 by nitrogen adsorption and desorption, which are type I and mixed types I and IV, respectively, indicating that the pore sizes formed are mainly microporous and micromesoporous, respectively.[239]

4.2.3.2 Soft formwork method. The difference between the hard template method and the soft template method is that the hard template method is relatively easy to control the product owing to its template deconstruction and fixation, while the soft template method needs to rely on the co-assembly between the

surfactant and the inorganic phase. However, the hard stencil method requires the use of corrosive acids or alkaline chemicals to remove the template, which leads to a more complex process, high cost, and the limitation of difficulty in mass production. In contrast, soft templates are simple to apply and inexpensive, and have commercial advantages.[240] In the soft stenciling process, there is a distinctive feature: "self-assembly". This refers to the fact that amphiphilic molecules can not only self-compose a series of different deconstructions in solution, but in the case of templates, amphiphilic molecules can also combine with reaction precursors to form composite structures, such as silica nanoparticles, and mesopores filled with surfactant assemblies. Second, the solution is crucial in the soft template and is the key to the size of the assembled structure, as shown in Fig. 26b.[241]

It is important to ensure the complete development of micelles and/or liquid crystal phases in the soft templating method. This must meet two conditions: first, the micelles do not form at a given temperature, and the active agent does not
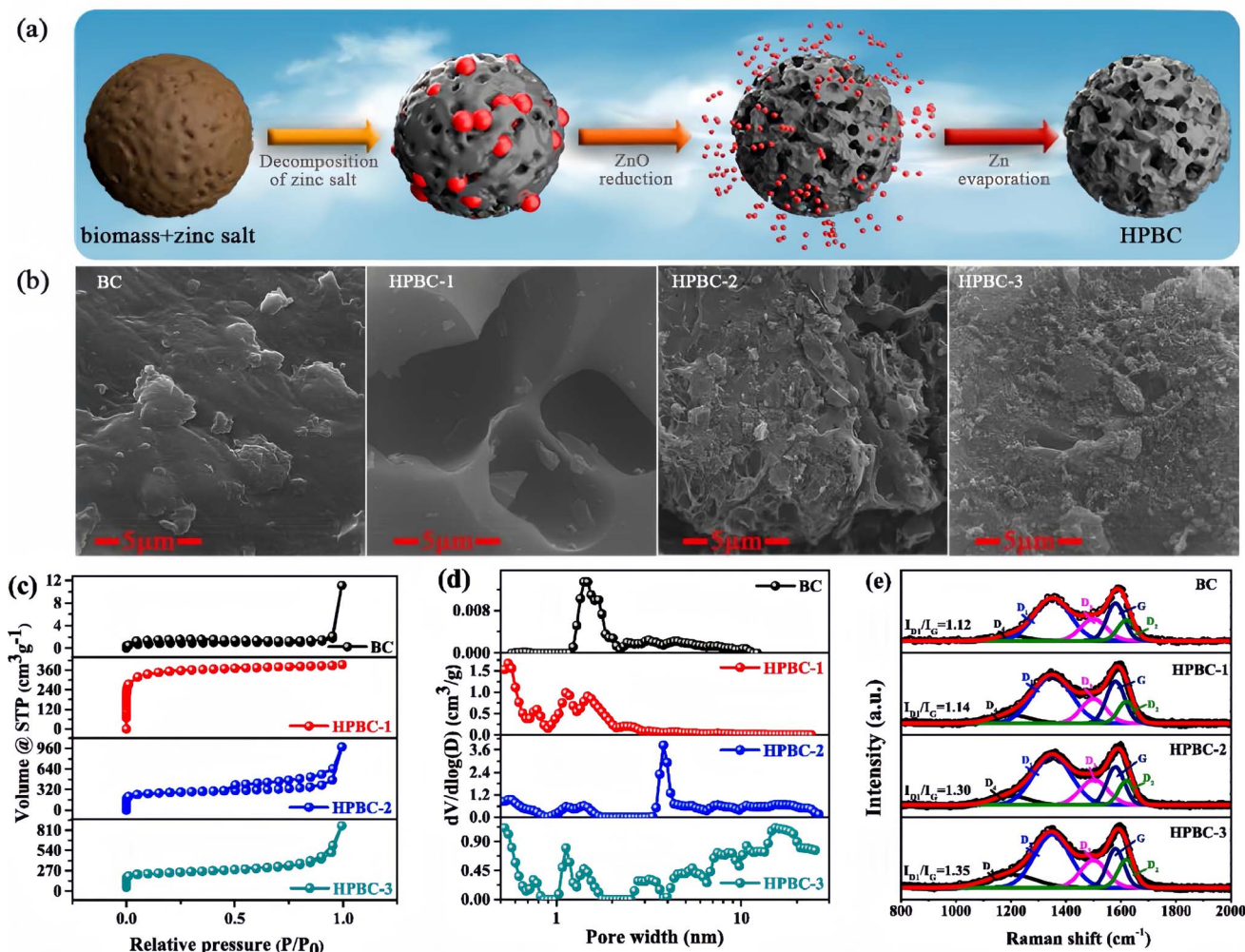
Fig. 27 Characterization diagram of HPBC and adsorbent performance based on biomass/zinc salt composite materials.[239] (a) Schematic of HPBC prepared by biomass/zinc salts composites; (b) SEM images of the adsorbents; (c) N_2 adsorption/desorption isotherms, (d) pore size distribution curve of adsorbents; (e) Raman spectra of the adsorbents.

dissolve below that temperature and remains in a hydrated solid state. Consequently, to reach the Krafft temperature, the solubility increases dramatically, and the surfactant reaches a narrow concentration range, the critical micelle temperature, forming micelles. Second, the addition of surfactants is subsequently incorporated into micelles.[242] However, the flexible film plate method is time-consuming and energy-intensive, and the activation process is often accompanied by significant carbon loss and chemical composition changes.[243] Therefore, scholars are constantly adjusting and improving the soft film plate method to ensure the best performance of the prepared materials. Wu *et al.* used a soft template-assisted method to prepare yolk/silica shell particles, which can produce hollow silica spheres doped with different particles, regardless of their diameter, geometric shape, and composition.[244] Chen *et al.* reported a novel mechanism of dynamic growth induced by synergistic interactions between soft templates and biomass, in which ribose sugar is used as a biological precursor to form carbonaceous nanoparticles through hydrothermal reactions.

Owing to their interactions, asymmetrical flask-like hollow carbonaceous structures with highly uniform morphology and narrow size distribution are created, thus providing a high specific surface area (2335 m^2 g^{-1}) of carbon nanoparticles.[245]

4.2.3.3 Double-template method. To further precisely adjust the pore structure of carbon materials, combining hard and soft templates is common in preparing materials with higher strength and performance. This is because the hard template method requires toxic reagents (*e.g.*, NaOH or HF) for template removal, while the soft template method tends to be unstable under heating—often being accidently removed during carbonization. The dual template method, however, can effectively integrate their advantages and mitigate their drawbacks.[246] It leverages the hard template to accurately replicate pore structures and the soft template to enable mesoporous structure adjustment, thereby obtaining porous carbon materials with more controllable pore structures and surface morphologies. These materials provide more adsorption sites and facilitate rapid mass transport through mesopores and

macropores. Such a hierarchical porous structure in biochar is beneficial for enhancing adsorption capacity.[247]

The research by Xia *et al.* indicates that the natural structure of endogenous activators (IHA) and exogenous organic components, including nitrogen-doped additives (OONA) in pig bones, can play a dual role, as natural porous hard templates and endogenous nitrogen-doped soft templates, during the carbonization process and can form a highly active nitrogen-doped hollow carbon framework on biochar derived from pig bones, which is more conducive to PS-induced catalytic degradation. Fig. 28a shows that different pyrolysis temperatures

significantly affect pig bone biochar (PBCs), resulting in structural and crystal phase transitions. Fig. 28b shows various typical peaks owing to the formation of a carbon network structure by the long chain of organic macromolecules on the surface of porcine bones during the pyrolysis process, which acts as a soft template for carbon formation, providing −OH/−NH active sites for PBCs. Fig. 28c shows that the carbon network formed by OONA can produce a domain-restricted carbonization effect during the preparation process, and the synergistic effect of endogenous IHA in the domain can promote the formation of a three-dimensional porous structure
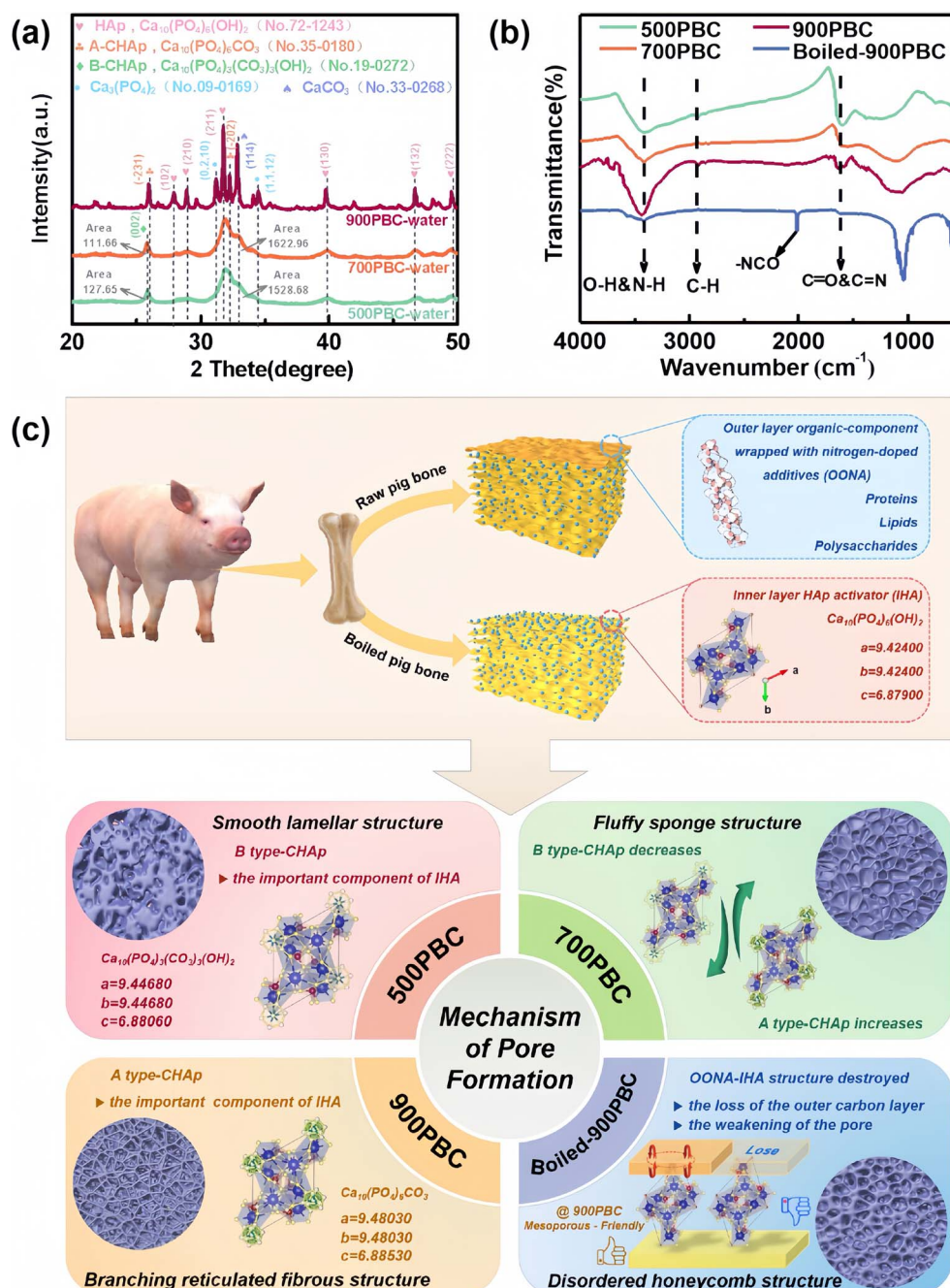

Fig. 28 XRD plots of PBC-water with different carbonization temperatures[248] (a), FTIR plots (b), and the pore formation mechanism of the OONA-IHA structure (c).

of PBCs. In addition, during the pyrolysis process, the collagen in pig bones and the lipid long-chain molecule-fixed carbon skeleton were deformed to cause chemical changes in IHA, which could better exert the hard template effect of IHA.[248]

5 Biomass-derived carbon modification technology for desalination applications

In CDI's desalination applications, electrode materials play a key role. However, traditional energy-intensive electrode materials often cannot fail to meet environmental requirements, and the energy consumption is usually reduced by preparing biomass-derived carbon electrodes. To improve the desalination performance of electrode materials, various preparation strategies are often used, such as embedding agents, surface modification, heteroatom introduction, and compounding of other materials.[249] In this section, we explore various modification technologies for bio-derived charcoal by examining their methodological features and desalination performance.

5.1 Surfactant modification

Surfactant molecules can be anionic, nonionic, and zwitterionic.[250] It goes through various mechanisms, as shown in Fig. 29. These mechanisms include electrostatic interactions, hydrogen bonds, π-π electrons, bilayer formation, and hydrophobic interactions to affect the adsorption capacity of materials. In addition, the formation of multiple layers of surfactants on adsorbents and the formation of micelles further enhance the adsorption capacity of inorganic and organic substances.[251]

Daudi et al. found that KOH-activated coconut shell carbon electrodes acquire positive charges when treated with $(CH_3)_4N^+Br^-$ surfactant. The specific surface area of PAC is 376.29 F g^{-1}, while EAC increases to 628.20 F g^{-1}. The salt adsorption capacities of PAC and EAC are 2.78 and 10.96 mg g^{-1}, respectively.[252] Kosaiyakanon's study showed that coffee shell biochar was prepared by pyrolysis activation and modified with the cationic surfactant cetyltrimethylammonium bromide

(CTAB). In this regard, as the mass of SDBS increases, the adsorption capacity also increases as the modification produces more active sites on the biochar. The maximum adsorption of biochar-SDBS by MB occurs on the adsorbent when the sorbent mass is 15 mg and the optimal pH is 10.[253] Anas et al. modified pyrolysis-derived cassava skin biochar using the anionic surfactant sodium dodecylbenzene sulfonate (SDBS). This modification significantly enhanced the biochar's adsorption performance through two mechanisms: electrostatic interaction and another interaction mechanism.[254]

5.2 Heteroatom doping modification

Heteroatom doping modifies carbon materials by introducing surface functional groups, which generate new active sites while enhancing surface wettability. These modifications lead to edge functionalization, expanded interlayer spacing, and increased adsorption surface area, ultimately resulting in improved adsorption performance.[255,256]

5.2.1 Nitrogen doped. Incorporating nitrogen atoms into the carbon structure induces pseudocapacitive effects through nitrogen-containing functional groups. These effects significantly increase the specific capacitance, as well as the wettability of carbon and electrolyte, and further enhance the conductivity of the material.[257] However, current nitrogen (N) doping requires more complex technical methods. Achieving significant nitrogen doping conveniently remains a challenging area of research. Based on this, Khan et al. pioneered a cost-effective strategy to decorate layered mesoporous carbon with graphene nanospheres and then doped it with N to form a layered mesoporous carbon framework (GNNLMCS). Owing to the high level of N-doping (up to 10.56 at%), the obtained porous carbon exhibits the effects of a layered porous sheet structure with a large surface area. The GNNLMCS-12 CDI electrode, fabricated from a layered mesoporous carbon framework (GNNLMCS), demonstrates concentration-dependent desalination behavior. Under constant voltage conditions, its salt adsorption capacity shows a positive correlation with solution concentration, achieving equilibrium within 40 minutes (Fig. 30a). The Ragone curve shows the
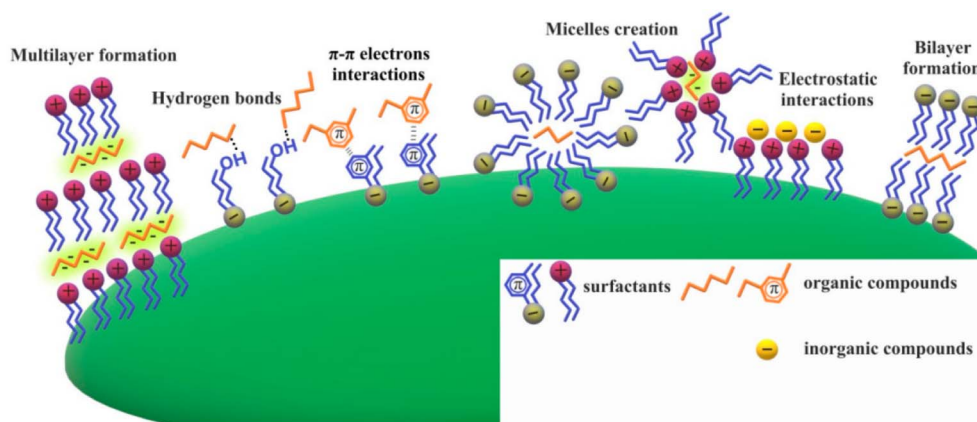

Fig. 29 Possible mechanisms of organic and inorganic compound adsorption on the surfactant-modified biochar surface.[251]

Tutorial Review

RSC Sustainability

fastest SAR and the fastest SAC of the electrode, as shown in Fig. 30b. For the same solution concentration but different voltages, GNNLMCS-12 in 500 mg L^{-1} NaCl solution (flow rate: 25 mL min^{-1}) is shown in Fig. 30c. The results showed that at 1.2 V, the Ragone diagram of the GNNLMCS-12 electrode shifts to the uppermost rightmost region. This indicates that SAR is faster and SAC is faster. At 1.2 V, the charging efficiency of the electrode increases, which improves the SAR of the electrode. Thus, when the applied voltage is increased to 1.2 V, the ions are completely adsorbed from the NaCl solution.[258] However, N doping faces several limitations: (1) excessive nitrogen doping content, (2) demanding preparation requirements, (3) complex processing steps, and (4) high production costs.

5.2.2 Phosphorus-doped. The most widely used N-doping strategies require ammonia gas or more complex processes. In contrast, phosphorus (P)-containing inorganic or organic materials are widely available, making P a better alternative to nitrogen for doping. Owing to P's low electronegativity, it endows P-doped GACs with unique potential properties, aiding charge transfer. Simultaneously, P atoms are larger than carbon atoms, so doping with P increases defect density and interlayer spacing.[259] Among various heteroatoms, such as nitrogen and boron, P doping has attracted significant interest. This is due to P exhibiting lower electronegativity, a larger covalent radius, and a larger atomic size than carbon. P doping introduces more defects and expands interlayer spacing in the carbon structure, thereby promoting charge

redistribution, creating active sites for ion accumulation, and enhancing capacitive performance.[260] Additionally, it endows carbon materials with hydrophilic acidic surfaces while improving their chemical stability. Yi *et al.* found that carbon derived from lignocellulose and produced *via* germanium-assisted pyrolysis exhibits excellent rate performance and retains over 97.9% capacitance after 10 000 cycles.[261] Xing *et al.* developed porous carbon (PPCP) using Pina sinone as the carbon source and H$_3$PO$_4$ as the activator. They demonstrated that this PPCP electrode exhibits desalination capacity. The desalination capacity of the PPCP electrode after desalination testing is shown in Fig. 31a, indicating that the desalination capacity of the PPCP electrode increases significantly with an increase in the concentration of the feed salt solution, suggesting that the initial salt concentration has a positive effect on desalination efficiency. In addition, the PPCP800 electrode showed a high deionization capacity of 14.62 mg g^{-1} at 1.2 V in 1000 mg L^{-1} NaCl solution, with the fastest desalting rate, as shown in Fig. 31b. In addition, cyclic electroadsorption and desorption tests showed good regeneration performance over 200 cycles because the number of ions entering and leaving the electrode before and after charging and discharging remained almost the same. However, by the 100th–200th cycle, the desalination capacity of the electrode decreased possibly owing to oxidation of the carbon electrode[262] (Fig. 31c).

5.2.3 Sulfur-doped. Sulfur(S)-doped carbon exhibits enhanced electrochemical activity owing to its unpaired electrons
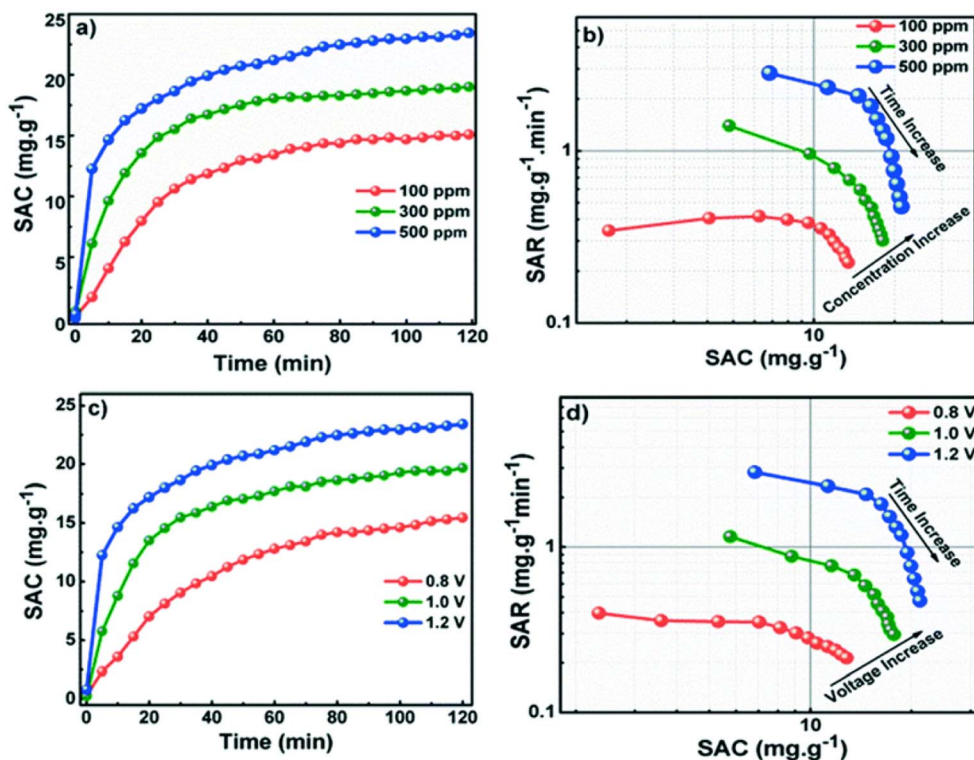

Fig. 30 SAC and Ragone plot of GNNLMCS-12 under different NaCl concentrations and voltages.[258] (a and b) SAC curves and Ragone plots of GNNLMCS-12 at different concentrations of NaCl solution and (c and d) SAC curves and Ragone plots of GNNLMCS-12 at different cell voltages in 500 mg L^{-1} NaCl solution.
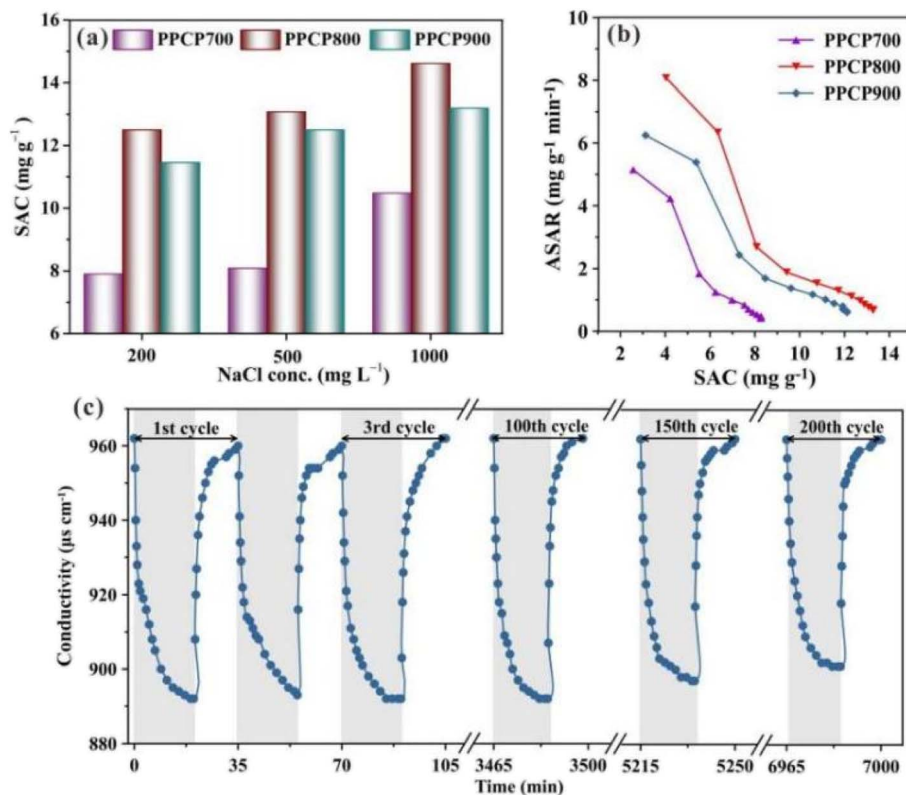
Fig. 31 PPCP electrode performance and cycling stability.[262] (a) Electroadsorption capacity of PPCP electrodes at different initial NaCl concentrations at a charging voltage of 1.2 V; (b) CDI Ragone plot of the PPCP electrode; and (c) cycling stability of the electrode over 200 consecutive adsorption–desorption cycles in 500 mg L^{-1} NaCl solution PPCP800 at a charge voltage of 1.2 V using a short-circuit desorption method.

and high polarizability. These characteristics facilitate the formation of active sites, promote the occurrence of reversible redox reactions, and endow electrode materials with a higher pseudocapacitive effect.[263] Furthermore, S atoms possess a superior atomic size and electrochemical activity compared to nitrogen. When incorporated into carbon matrices, S doping effectively disrupts the electron density equilibrium on the carbon surface through its distinctive functional groups. This structural perturbation induces variations in bond lengths and angles within the carbon framework, ultimately enhancing the material's wettability properties.[264] Zhao et al. fabricated sulfur-rich carbon nanosheets (S-CNSs) via a facile pyrolysis process, utilizing a three-dimensional scaffold framework derived from diverse plant waste sources. The S-CNS demonstrated exceptional electrochemical performance, delivering (1) an ultra-high reversible capacity of 605 mA h g^{-1} at 50 mA g^{-1}, (2) outstanding rate capability with 133 mA h g^{-1} maintained at 10 A g^{-1}, and (3) remarkable cycling stability with ~94% capacity retention after 2000 cycles at 5 A g^{-1}. This further demonstrates that sulfur doping can significantly enhance the performance of electrode materials.[265]

5.2.4 Co-doped. Co-doping is based on the synergistic effect of different atoms.[267] It significantly improves the electrochemical performance of the electrode material. Liu et al. innovatively prepared N,S-codoped porous carbon (HAPCCs) from sewage sludge via hydrothermal carbonization and

chemical activation. The enhanced adsorption capacity stems from its basic functional groups and N/S doping, which impart a positive surface charge, enabling efficient adsorption through strong π-π stacking and electrostatic attraction.[268] Chen et al. synthesized an MOF (metal–organic framework)/biochar composite by carbonizing zirconium-based MOFs and bagasse, achieving in situ nitrogen-zirconium co-doping to form an N@Zr/C electrode material. This material exhibits enhanced adsorption sites, a high specific surface area, and excellent conductivity. Consequently, the N@Zr/C electrode exhibits an optimal electroadsorption capacity of 32.30 mg P g^{-1} at 1.2 V.[269] Huang et al. adopted a one-step method to synthesize three-dimensional carbon nanosheets co-doped with nitrogen and sulfur using mycelium particles as the carbon source. They possess a hierarchical porous structure, and the preparation process is shown in Fig. 32a. SEM reveals that the surface of NSHPC changes before and after doping, from the smooth surface during the original calcination process to the layered structure of interconnected layered pores, along with the abundant microporous structure observed under TEM and HRTEM. This is shown in Fig. 32b and c. The results show that the NSHPC electrode delivers an outstanding electrosorption capacity of 18.71 mg g^{-1} in 500 mg L^{-1} NaCl solution.[266]
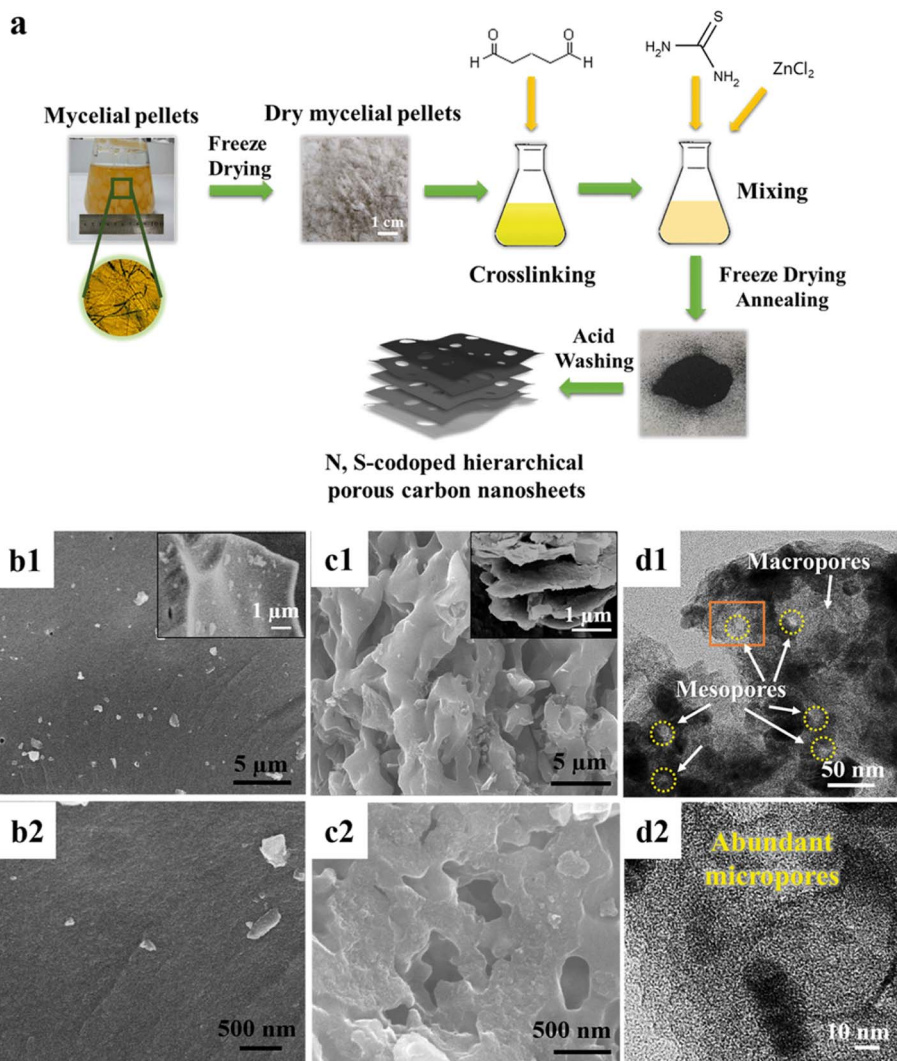
Fig. 32 Preparation process of NSHPC and microstructural characterization of MPC and NSHPC:[266] (a) schematic of the NSHPC preparation procedure, (b1 and b2) SEM images of MPC, (c1 and c2) SEM images of NSHPC, and (d1 and d2)) HRTEM images of NSHPC.

5.3 Acid and alkali treatment modification

5.3.1 Acid treatment. Acid treatment is a typical wet oxidation process. It enhances surface hydrophilicity by introducing oxygen-containing functional groups (*e.g.*, hydroxyl, carbonyl, carboxyl, quinone, lactone, and carboxyanhydride) to the porous carbon surface while eliminating mineral components. Common acids employed for such modifications include HNO_3, H_2SO_4, HCl, H_3PO_4, H_2O_2, and HClO. Among these acids, nitric acid and sulfuric acid are widely utilized by researchers owing to their strong oxidizing properties, while weak acids (*e.g.*, inorganic weak acids) are rarely applied owing to their low ionization degree.[270] Xiao *et al.* prepared O-activated carbon cellulose (O-ACF) with high adsorption activity by 20% nitric acid oxidation as an electrode in the CDI process. Their experiments on Cu(ii) adsorption showed that it had excellent electroadsorption performance. The maximum adsorption capacity was 48.60 mg g^{-1}, which was 1.63 times that of commercially activated carbon. The adsorption regeneration experiment showed that O-ACF retained 95% adsorption

performance for Cu(ii) after 5 adsorption regenerations, which had good practicability.[271] Huang *et al.* showed that activated carbon can be modified with nitric acid as an electrode in the CDI process. The results indicated that the modification greatly improved the desalination efficiency by about 15%. This is because nitric acid modification can enhance the oxygen-containing functional groups on the surface of carbon materials, resulting in an increase in capacitance and a decrease in charge resistance.[272]

5.3.2 Alkali treatment. Alkaline solution modification involves soaking or suspending biochar in various alkaline reagents.[273] This process enhances the material's porosity by introducing alkaline functional groups, thereby increasing the specific surface area of biochar.[274] For example, sodium hydroxide (NaOH), potassium hydroxide (KOH) and calcium hydroxide (Ca(OH)$_2$) are used to enhance the porosity of the material. Compared with acid solution modification, it has higher H/C (stability) and lower O/C (hydrophilicity) compared with acidic solution modification.[273]

Li *et al.* used biogas sludge (BS) as a raw material to produce BS-derived porous carbon materials *via* hydrothermal carbonization and KOH modification. The results showed that with an increase in KOH concentration, the BS-derived porous carbon materials (HA-x, x = 0, 0.5, 1.0, 1.5) showed a trend of first increasing and then decreasing in terms of the specific surface
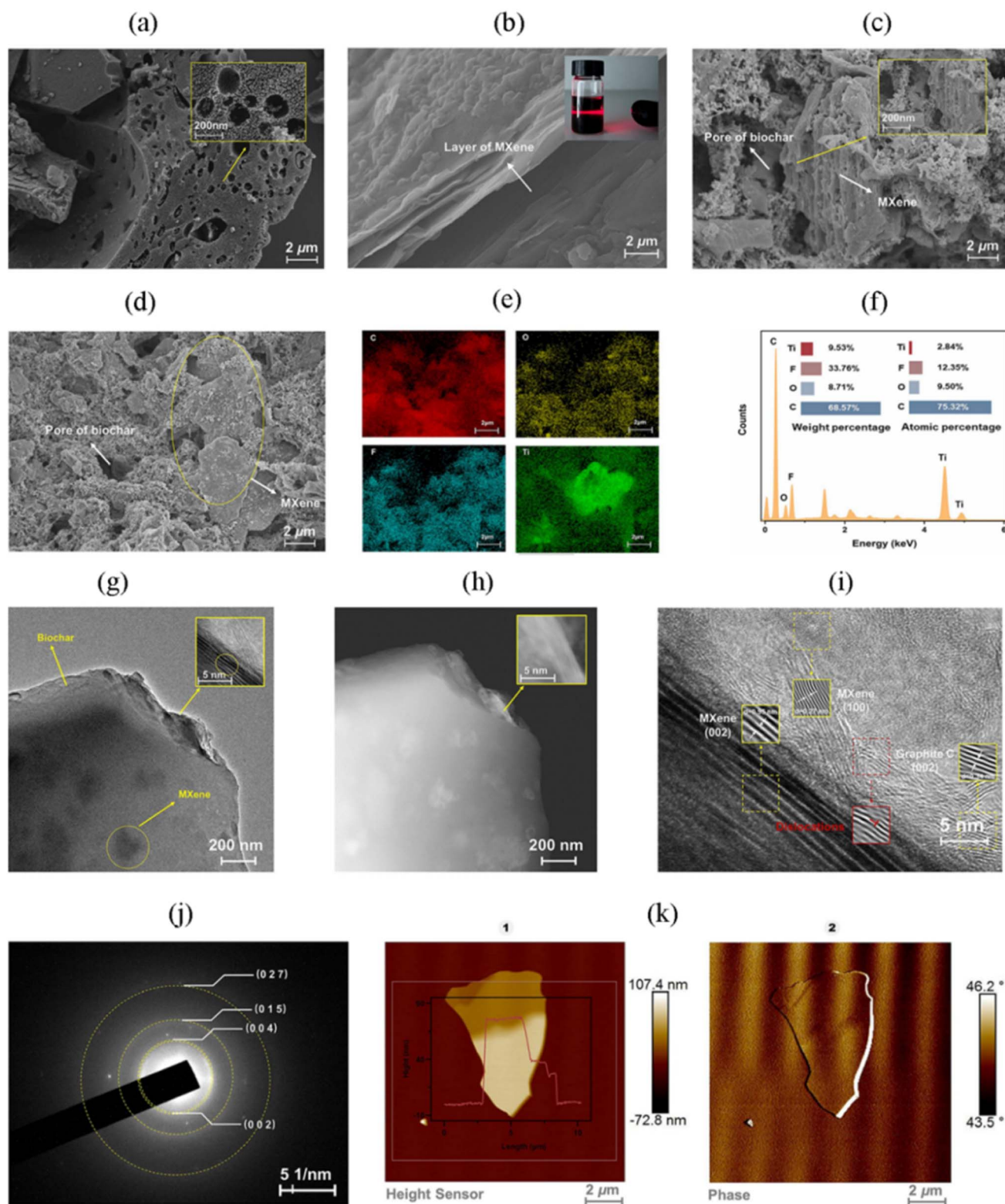

Fig. 33 Microstructure and compositional characterization of biochar, MXene, and BCM-2:[279] (a) SEM image of biochar, (b) SEM image of MXene, (c) cross section of BCM-2, (d) surface of BCM-2, (e and f) EDS mapping images of BCM, (g and h) TEM images of BCM-2, (i) HRTEM images of BCM-2, (j) SAED pattern of BCM-2, and (k1-k2) AFM height image and phase diagram of BCM-2.

area and pore volume. The HA-0.5 sample exhibited the highest specific surface area and largest pore volume of 1040 $m^2 g^{-1}$ and 0.42 $cm^3 g^{-1}$, respectively. The appropriate amount of KOH modification also increased the oxygen content of the HA-0.5 sample (from 6.77% to 10.53%), thereby providing more active sites and enhancing its performance in the electrochemical desalination process. In addition, the HA-0.5 electrode retained more than 80% of its desalination capacity after 50 cycles, exhibiting excellent performance, especially in carbon-based capacitive deionization (CDI) electrodes.[275]

5.4 Composite material modification

In addition, BC-based composites can be modified by combining other materials. Functional materials, magnetic materials, and nanoparticles have been developed and designed for modification, and abundant functional groups have been introduced to effectively play the synergistic effect between different materials and make up for some of the shortcomings of the original BC.[276]

Yu *et al.* prepared MOF-derived porous carbon by applying the solvothermal method, combining it with $Cu@Cu_2O$ to serve as CDI cathode materials. The results showed that HDC-1100 exhibited the best desalination capacity of 30.9 $mg g^{-1}$ under a voltage window of -1.2 V to 1.2 V, a current density of 40 $mA g^{-1}$, and a 5 mmol L^{-1} NaCl solution. HDC-1100 also has good cycling stability. After 20 adsorption and desorption cycles, good adsorption performance was retained.[277] Cheng *et al.* used jute fiber as a precursor and heteroatom doping to form high-value carbon composites. This method significantly improves wettability, and the resulting material has a higher specific surface area, higher microporous/mesoporous properties, higher pore volume, and lower electrical resistance.[278] Ge *et al.* prepared a layered porous MXene-modified biochar material (BCM-2), which serves as an electrode in the mixed process of electrodialysis (EO) and capacitive deionization (CDI). Characterization is shown in Fig. 33a, where activation creates abundant mesopores that facilitate ion adsorption. After modifying biochar with MXene, the layered structure of MXene was observed in the SEM images (Fig. 33b). Furthermore, the elemental mapping images of this area (Fig. 33e and f) indicate that the C, O, and F of polyvinylidene fluoride (PVDF) are uniformly distributed on the surface of BCM-2, while the Ti from MXene is concentrated on the biochar, collectively demonstrating the successful modification of MXene. Additionally, Fig. 33b illustrates the Tyndall effect of the MXene solution. Moreover, the significant enhancement in desalination performance is attributed to the effective combination of the inherent porous structure of biochar and the layered structure of MXene, as depicted in Fig. 33c. This combination effectively increases the specific surface area and significantly reduces the overlapping effects of the electric double layer. We found that MXene also increased the adsorbable sites of the electrode material by forming a membrane over the original biochar, as shown in Fig. 33d. Subsequently, we further illustrated the continuous diffraction rings corresponding to the (027), (015), and (004) planes of MXene, as well as the (002)

plane of graphite, through TEM and HRTEM images, as shown in Fig. 33g–k, further confirming the structure of MXene and indicating good modification. The results indicate that BCM-2 exhibits excellent CDI performance at 1.2 V, achieving desalination capabilities of 15.40–65.97 $mg g^{-1}$ in a 100–1000 $mg L^{-1}$ Na_2SO_4 solution.[279]

5.5 Nanomaterial modification

Nanomaterials are a large class of substances with unique properties. They have structural properties that range from bulk solids to molecules.[280] The doping of nanochar into biochar can perform various functions, enhancing the adsorption performance of BC by altering its functional group profile and active sites on the surface of BC.[281] Wang *et al.* used a 15% concentration of ZnO nanoparticles to modify the biochar material. The results showed that the water contact angle of the ZnO nanoparticle-modified biochar was significantly reduced, and the wettability of the biochar was improved. In addition, the contact area between the modified carbon particles increased, which improved their conductivity. The results showed that the electroadsorption capacity for 20 $mg L^{-1}$ ClO_4^- at 1 V was 28.31 $mg g^{-1}$, which was four times higher than that of an electrode without voltage.[282]

6 Conclusion and outlook

Electrochemical capacitive deionization technology has gradually become one of the most promising desalination technologies, and scholars have spent a lot of energy on the selection and preparation of electrode materials to achieve better desalination performance, adsorption capacity and desalination efficiency. Biomass-derived carbon materials stand out among many electrode materials owing to their wide range of sources, low production cost and environmental friendliness. In this review, the development history and desalination mechanism of capacitive deionization are reviewed, and the advantages and disadvantages of different structures of CDI are demonstrated. Then, different biochar raw materials and preparation methods were introduced, and different modification technologies, such as surfactant treatment and atom-doped composites, were introduced to improve the structure of biomass-based electrode materials and provide better performance. Therefore, we conclude that we can achieve better desalination performance in CDI by modifying biomass-derived carbon materials and that their modification technologies will provide innovative options for seawater desalination.

Biomass-derived carbon materials are characterized by wide sources and controllable structures. Relying on their natural porous structures and abundant surface functional groups, they can achieve the synergistic enhancement of ion adsorption and desorption performance through precise regulation of pore structures and directional doping of atoms, thereby showing unique advantages in the field of seawater desalination. This material also has considerable application potential in various capacitive deionization unit structures. It can be synthesized into electrode materials through processes such as pyrolysis,

physicochemical activation and the template method. By adjusting preparation parameters, such as pyrolysis temperature and activator ratio, biomass-derived carbon with a specific surface area, reasonable pore size distribution and surface charge distribution can be prepared, which can be used as electrode materials to adapt to different CDI structures.

For example, for the traditional CDI structure, it is necessary to prepare biomass-derived carbon electrodes with a higher specific surface area to improve their adsorption capacity for salt ions; for MCDI, surface modification technology can be used to endow the electrodes with specific ion selectivity, combined with ion exchange membranes to enhance the desalination effect. In FCDI, biomass-derived carbon can be made into carbon slurry, which can optimize the conductivity and stability of the flow electrode and reduce the problem of clogging.

However, when biomass-derived carbon materials are adapted to different capacitive deionization structures, there are problems such as significant differences in preparation processes and procedures, temporary inability to achieve large-scale production, and difficulty in accurately matching the needs of capacitive deionization. Simultaneously, it still faces many difficulties in the capacitive deionization stage. First, the phenomenon of ion competitive adsorption is prominent in high-salt concentration environments, and the selective adsorption capacity of the material is insufficient, making it difficult to distinguish efficiently between different types of ions. Second, the cycle stability of the material needs to be improved. After multiple adsorption–desorption cycles, the pore structure is easily blocked by residual ions, resulting in a significant decrease in adsorption capacity. Third, adaptability to different CDI structures needs to be further optimized. For example, in HCDI, the synergistic effect between biomass-derived carbon and Faraday electrodes is weak, which cannot give full play to the performance advantages of composite electrodes. Fourth, during the preparation process, impurities in biomass raw materials are difficult to completely remove, which affects the conductivity and chemical stability of electrode materials.

Therefore, it is urgent to break through the bottleneck of low-cost large-scale production in the future, which requires putting forward innovative ideas. First, *in situ* characterization combined with theoretical calculations can be used to reveal the mechanism of ion adsorption and desorption, providing theoretical support for the precise development of materials suitable for different capacitive deionization structures. For example, by constructing differentiated pore structures and adjusting the pore parameters of electrode materials according to different ion characteristics, ion transport capacity can be improved. Second, using the abundant surface functional groups of biomass-derived carbon materials, a stable surface modification layer can be designed to reduce pore clogging during the cycle and improve the stability of desalination performance. Third, electron transfer efficiency can be optimized through interface engineering to improve the desalination efficiency of composite materials. Finally, aiming at the difficult removal of impurities from raw materials, multiple process means can be coupled to strengthen the treatment of raw material impurities and to fully improve the performance of the prepared materials.

Conflicts of interest

There are no conflicts to declare.

Data availability

All data supporting this article have been included as part of the main text or SI.

References

1 B. A. Samejo, K. Naseer, S. Samejo, F. A. Janjhi, N. Memon, R. Castro-Muñoz and G. Boczkaj, MXene-based composites for capacitive deionization – the advantages, progress, and their role in desalination - a review, *Water Resour. Ind.*, 2024, **31**, 100230.
2 H. Younes, F. Ravaux, N. El Hadri and L. Zou, Nanostructuring of pseudocapacitive MnFe2O4/porous rGO electrodes in capacitive deionization, *Electrochim. Acta*, 2019, **306**, 1–8.
3 A. Shabib, B. Tatan, Y. Elbaz, A. Aly Hassan, M. A. Hamouda and M. A. Maraqa, Advancements in reverse osmosis desalination: technology, environment, economy, and bibliometric insights, *Desalination*, 2025, **598**, 118413.
4 J. Choi, P. Dorji, H. K. Shon and S. Hong, Applications of capacitive deionization: desalination, softening, selective removal, and energy efficiency, *Desalination*, 2019, **449**, 118–130.
5 E. T. Sayed, A. G. Olabi, N. Shehata, M. Al Radi, O. Majdy Muhaisen, C. Rodriguez, M. Ali Atieh and M. A. Abdelkareem, Application of bio-based electrodes in emerging capacitive deionization technology for desalination and wastewater treatment, *Ain Shams Eng. J.*, 2023, **14**, 102030.
6 Z.-H. Zeng, L.-L. Yan, G.-H. Li, P.-H. Rao, Y.-R. Sun and Z.-Y. Zhao, Development of biochar electrode materials for capacitive deionization: preparation, performance, regeneration and other challenges, *New Carbon Mater.*, 2023, **38**, 837–860.
7 M. Askari, E. Salehi and M. Velashjerdi, Intelligent data-based modeling and optimization approach for intensification of capacitive deionization system featuring low-cost carbon electrodes, *Electrochim. Acta*, 2025, **517**, 145786.
8 Y. Li, J. Ma, M. Yu, J. Niu, J. Gu, M. Chen, P. Zhang, J. Zhang and C. Liu, Carbon felt (CF) acted as an "ionic capacitor" to enhance flow electrode capacitive deionization (FCDI) desalination performance, *Desalination*, 2024, **575**, 117341.
9 F. Cheng, J. Liu, Y. Ji, Y. Sun, J. Duan, C. Cai and Y. Fu, Unveiling potential of capacitive deionization: memory-electrostatic synergy for enhanced ion removal and electrode regeneration, *Desalination*, 2025, **601**, 118607.
10 T. M. Subrahmanya, L.-Y. Gua, H. F. M. Austria, T.-H. Huang, S. H. Abebe, W.-S. Hung, C.-F. Wang,

C.-C. Hu, K.-R. Lee and J.-Y. Lai, Organic solvents tuned polymer derived-sulfonated microporous carbon structures enable resource regeneration and recovery in flow electrode capacitive deionization, *Desalination*, 2025, **600**, 118513.

11 K. Zhang, X. Liu, L. Tan, K. Xu, W. Pei, F. Tang, T. Wei, J. Jia, B. Xu, J. Li, X. Zhu and F. Ge, Selective electrosorption of trace Pb(II) from drinking water by a novel energy-recovery & adsorption-enhanced capacitive deionization system, *Desalination*, 2025, **600**, 118518.

12 Y. Oren, Capacitive deionization (CDI) for desalination and water treatment—past, present and future (a review), *Desalination*, 2008, **228**, 10–29.

13 Q. Huang, F. Du, X. Liu, L. Sun, C. Tan, A. Wang, K. Sun, B. Li and D. Yao, Capacitive deionization technology with multi-stage treatment as an efficient desalination process for agricultural irrigation, *Desalination*, 2024, **586**, 117789.

14 Z. Qian, Y. Tao, Y. Peng, Y. Li, L. Ke and M. Shi, Capacitive deionization: an emerging electrosorption technology for efficient radioactive wastewater treatment, *J. Environ. Chem. Eng.*, 2025, **13**, 115104.

15 K. Yang, W.-B. Zhang, J. Zhou, H. Gou, A. Batol, F. Yang, B. Chen, X.-Y. Liu and X.-J. Ma, Construction of 2D-2D heterojunctions of VN nanosheets within Ti₃C₂ nanosheets for improved flow-electrode capacitive deionization performance, *Desalination*, 2025, **606**, 118791.

16 X. Yang, J. Li, W. Qu, W. Wang, P. Wang and J. Ma, Bibliometrics and systematic reviews: recent development and prospects of electrode materials for capacitive deionization, *Desalination*, 2025, **599**, 118450.

17 L. Kant Pandey, M. S. Gaikwad and P. K. Chaudhari, Biowaste materials derived activated carbon (BMDAC) electrodes for removal of pollutant ions using capacitive deionization: a mini review, *Mater. Lett.*, 2023, **340**, 134165.

18 W. Deng, M. Jing, M. Gao, W. Chen, Y. Chen, F. Chen, Y. Tang and Y. Jin, The effect and mechanism of different pore structure distribution on electrosorption selectivity of anions during capacitive deionization, *Desalin. Water Treat.*, 2024, **317**, 100162–100170.

19 H. Wang, X. Xu, X. Gao, Y. Li, T. Lu and L. Pan, Design of three-dimensional faradic electrode materials for high-performance capacitive deionization, *Coord. Chem. Rev.*, 2024, **510**, 215835.

20 X.-L. Zhang, W.-B. Zhang, X.-W. Han, L. Zhang, X. Bao, Y.-W. Guo, S.-S. Chai, S.-B. Guo, X. Zhou and X.-J. Ma, Review—pseudocapacitive energy storage materials from hägg-phase compounds to high-entropy ceramics, *J. Electrochem. Soc.*, 2021, **168**, 120521–120549.

21 *Faradaic electrodes open a new era for capacitive deionization - Li - 2020 - advanced science - wiley online library*, https://advanced.onlinelibrary.wiley.com/doi/full/10.1002/advs.202002213, accessed 16 July 2025.

22 K. Lu, H. Jing, H. Jia, H. Qiang, F. Wang, M. Shi and M. Xia, Defect-rich N, S Co-doped porous carbon with hierarchical channel network for ultrafast capacitive deionization, *J. Colloid Interface Sci.*, 2025, **679**, 262–272.

23 Y. Guo, F. Cheng and X. Li, Research on faradic capacitive deionization regeneration method for absorption air conditioning system, *Appl. Therm. Eng.*, 2025, **258**, 124561.

24 X. Zhang, H. Yang, S. Liu and J. Li, Laser-induced nitrogen and phosphorus-doped spongy carbon with graphene wings derived from lignin for significantly enhanced capacitance deionization performance, *Sep. Purif. Technol.*, 2024, **351**, 128072.

25 Y. Cheng, X. Zhang, S. Qin, J. Li, L. Zhang, Y. Zhang, N. Du, Z. Zhu, X. Li and Y. Zhang, Renewable resources from nature: biomass-derived carbon for composite materials in electrochemical energy storage devices, *J. Energy Storage*, 2025, **106**, 114692.

26 C. Li, M. Yun, X. Zhu, J. Ma, Z. Zhang, W. Kong, B. Shen and Z. Zhao, High-value conversion of bio-dried products derived from municipal organic wastes: activated carbon preparation and electrochemical assessment, *Fuel*, 2025, **387**, 134323.

27 R. Haider, S. Sagadevan, N. R. Cameron and M. R. Johan, Biomass-derived activated carbon for high-performance energy storage devices, *J. Power Sources*, 2025, **633**, 236404.

28 K. Sharma, P. Kadyan, R. K. Sharma and S. Grover, Heteroatom doping in bio-waste derived activated carbon for enhanced supercapacitor performance: a review, *J. Energy Storage*, 2024, **100**, 113679.

29 F. Xu, D. Neshumayev and A. Konist, Synthesis strategies and hydrogen storage performance of porous carbon materials derived from bio-oil, *Chem. Eng. J.*, 2025, **505**, 159381.

30 Q. Lv, Z. Tian, W. Li, G. Duan, X. Han, C. Zhang, S. He, H. Mao, C. Ma and S. Jiang, Porous carbon derived from biomass-based polymers: innovative applications in supercapacitors, *Chin. Chem. Lett.*, 2025, 110860.

31 C. He, B. Li, G. Yang, S. He, S. Jiang, H. Yang, J. Han, X. Li, F. Wu and Q. Zhang, Progress of 0D biomass-derived porous carbon materials produced by hydrothermal assisted synthesis for advanced supercapacitors, *J. Colloid Interface Sci.*, 2025, **685**, 487–508.

32 B. Yan, C. Han, Y. Dai, M. Li, Z. Wu and X. Gao, Biomass derived hard carbon materials for sodium ion battery anodes: exploring the influence of carbon source on structure and sodium storage performance, *Fuel*, 2024, **371**, 132141.

33 G. Bharath, A. Hai, K. Rambabu, F. Ahmed, A. S. Haidyrah, N. Ahmad, S. W. Hasan and F. Banat, Hybrid capacitive deionization of NaCl and toxic heavy metal ions using faradic electrodes of silver nanospheres decorated pomegranate peel-derived activated carbon, *Environ. Res.*, 2021, **197**, 111110.

34 H. Jiang, K. Li, Y. Qiao, W. Zeng, H. Huang, C. Zhang, Z. Fan and H. Hu, Efficient capacitive deionization of N-doped g-C₃N₄ quantum dots modified carbon cloth electrode under alkaline conditions, *Desalination*, 2025, **601**, 118588.

35 K. Rambabu, G. Bharath, A. Hai, S. Luo, K. Liao, M. A. Haija, F. Banat and Mu. Naushad, Development of watermelon rind derived activated carbon/manganese ferrite

nanocomposite for cleaner desalination by capacitive deionization, *J. Cleaner Prod.*, 2020, **272**, 122626.

36 J. W. Blair and G. W. Murphy, in *Saline Water Conversion*, American Chemical Society, 1960, vol. 27, pp. 206–223.

37 G. W. Murphy and D. D. Caudle, Mathematical theory of electrochemical demineralization in flowing systems, *Electrochim. Acta*, 1967, **12**, 1655–1664.

38 S. Evans and W. S. Hamilton, The mechanism of demineralization at carbon electrodes, *J. Electrochem. Soc.*, 1966, **113**, 1314.

39 A. M. Johnson, W. Venolia, *The Electrosorb Process for Desalting Water*, 1970.

40 G. W. Reid, *Field Operation of a 20 Gallons Per Day Pilot Plant Unit for Electrochemical Desalination of Brackish Water*, US Department of the Interior, 1968.

41 M. E. Suss, S. Porada, X. Sun, P. M. Biesheuvel, J. Yoon and V. Presser, Water desalination *via* capacitive deionization: what is it and what can we expect from it?, *Energy Environ. Sci.*, 2015, **8**, 2296–2319.

42 S. Porada, R. Zhao, A. van der Wal, V. Presser and P. M. Biesheuvel, Review on the science and technology of water desalination by capacitive deionization, *Prog. Mater. Sci.*, 2013, **58**, 1388–1442.

43 J. Ma, C. Zhai and F. Yu, Review of flow electrode capacitive deionization technology: research progress and future challenges, *Desalination*, 2023, **564**, 116701.

44 M. Tauk, G. Folaranmi, M. Cretin, M. Bechelany, P. Sistat, C. Zhang and F. Zaviska, Recent advances in capacitive deionization: a comprehensive review on electrode materials, *J. Environ. Chem. Eng.*, 2023, **11**, 111368.

45 K. Sun, M. Tebyetekerwa, C. Wang, X. Wang, X. Zhang and X. S. Zhao, Electrocapacitive deionization: mechanisms, electrodes, and cell designs, *Adv. Funct. Mater.*, 2023, **33**, 2213578.

46 J. G. Gamaethiralalage, K. Singh, S. Sahin, J. Yoon, M. Elimelech, M. E. Suss, P. Liang, P. M. Biesheuvel, R. L. Zornitta and L. C. P. M. de Smet, Recent advances in ion selectivity with capacitive deionization, *Energy Environ. Sci.*, 2021, **14**, 1095–1120.

47 G. Folaranmi, M. Bechelany, P. Sistat, M. Cretin and F. Zaviska, Towards electrochemical water desalination techniques: a review on capacitive deionization, membrane capacitive deionization and flow capacitive deionization, *Membranes*, 2020, **10**, 96.

48 C. Zhang, D. He, J. Ma, W. Tang and T. D. Waite, Faradaic reactions in capacitive deionization (CDI) – problems and possibilities: a review, *Water Res.*, 2018, **128**, 314–330.

49 Y. Bai, Z. Tang, K. Jiang, H. Xu, C. Xu, T. Wei, Y. Zhao, J. Xiong, L. Jiang and G. Zhu, Gorgeous multistage channel heteroatom doped carbon tubes facilely obtained from PoPD carbon fibers by carbonization accompany with faraday pseudo-capacitors to electrical double-layer capacitors behavior, *J. Energy Storage*, 2024, **84**, 110953.

50 D. He, C. E. Wong, W. Tang, P. Kovalsky and T. D. Waite, Faradaic reactions in water desalination by batch-mode capacitive deionization, *Environ. Sci. Technol. Lett.*, 2016, **3**, 222–226.

51 L. Guan, L. Yu and G. Z. Chen, Capacitive and non-capacitive faradaic charge storage, *Electrochim. Acta*, 2016, **206**, 464–478.

52 Y. Liu, S. P. Jiang and Z. Shao, Intercalation pseudocapacitance in electrochemical energy storage: recent advances in fundamental understanding and materials development, *Mater. Today Adv.*, 2020, **7**, 100072.

53 C. Zhang, D. He, J. Ma, W. Tang and T. D. Waite, Faradaic reactions in capacitive deionization (CDI) – problems and possibilities: a review, *Water Res.*, 2018, **128**, 314–330.

54 F. Xu, L. Yuan, R. Zhao, B. Qin, F. Zhang, L. Ren, H. Yang and M. Yuan, Selective ion separation by capacitive deionization: a comprehensive review, *Materials*, 2025, **18**, 1107.

55 M. Chu, W. Tian, J. Zhao, M. Zou, Z. Lu, D. Zhang and J. Jiang, A comprehensive review of capacitive deionization technology with biochar-based electrodes: biochar-based electrode preparation, deionization mechanism and applications, *Chemosphere*, 2022, **307**, 136024.

56 A. Zhu, Y. Li, M. Xue, H. Chu and H. Wei, The research progress on the removal of heavy metals using carbon electrodes in capacitive deionization technology, *Rev. Inorg. Chem.*, 2025, DOI: **10.1515/revic-2024-0028**.

57 X. Ma, Y.-A. Chen, K. Zhou, P.-C. Wu and C.-H. Hou, Enhanced desalination performance *via* mixed capacitive-faradaic ion storage using RuO_2-activated carbon composite electrodes, *Electrochim. Acta*, 2019, **295**, 769–777.

58 F. Yu, L. Wang, Y. Wang, X. Shen, Y. Cheng and J. Ma, Faradaic reactions in capacitive deionization for desalination and ion separation, *J. Mater. Chem. A*, 2019, **7**, 15999–16027.

59 S. Kocaman, Evaluation of adsorption characteristics of new-generation CNT-based adsorbents: characterization, modeling, mechanism, and equilibrium study, *Carbon Lett.*, 2023, **33**, 883–897.

60 Z.-Q. Yang, W.-B. Zhang, K. Yang, B. Chen, Y. Yin, J.-J. Li, J.-L. Yang, Y. Gao and X.-J. Ma, Switchable NaCl cages *via* a MWCNTs/Ni[Fe(CN)$_6$]$_2$ nanocomposite for high performance desalination, *Nanoscale*, 2023, **15**, 19330–19338.

61 T. N. Baroud and E. P. Giannelis, High salt capacity and high removal rate capacitive deionization enabled by hierarchical porous carbons, *Carbon*, 2018, **139**, 614–625.

62 Y. Liu, Z. Li, X. Liu, Z. Chen, D. Fu, F. Fan, H. Xu and X. Wang, Capacitive deionization technology in efficiently removing heavy metal ions and radionuclides from aqueous solutions, *Sep. Purif. Technol.*, 2025, **364**, 132343.

63 M. A. Hassan, M. M. Taha, G. Hamdy, F. A. Taher and N. K. Allam, Sustainable capacitive deionization with recycled zinc–carbon battery electrodes, *Desalination*, 2025, 118804.

64 M. Chu, W. Tian, J. Zhao, D. Zhang, M. Zou, Z. Lu and J. Jiang, Dual-activated biochar with a multichannel structure enhanced electrosorption capacity of capacitive deionization for sulfate removal from mining wastewater, *Desalination*, 2023, **556**, 116588.

65 J.-H. Lee, W.-S. Bae and J.-H. Choi, Electrode reactions and adsorption/desorption performance related to the applied potential in a capacitive deionization process, *Desalination*, 2010, **258**, 159–163.

66 M. Tauk, P. Sistat, R. Habchi, M. Cretin, F. Zaviska and M. Bechelany, Exploring flow-electrode capacitive deionization: an overview and new insights, *Desalination*, 2025, **597**, 118392.

67 S. Jeon, H. Park, J. Yeo, S. Yang, C. H. Cho, M. H. Han and D. K. Kim, Desalination *via* a new membrane capacitive deionization process utilizing flow-electrodes, *Energy Environ. Sci.*, 2013, **6**, 1471.

68 H. Chand, Z. Liu, Q. Wei, M. S. Gaballah, W. Li, O. Osmolovskaya, A. Podurets, M. Voznesenskiy, N. Pismenskaya, L. P. Padhye and C. Zhang, Performance and mechanism of chromium removal using flow electrode capacitive deionization (FCDI): validation and optimization, *Sep. Purif. Technol.*, 2024, **340**, 126696.

69 J. Ma, L. Chen and F. Yu, Environmental applications and perspectives of flow electrode capacitive deionization (FCDI), *Sep. Purif. Technol.*, 2024, **335**, 126095.

70 B. Lee, J. An, S. Yeon, C. Oh and H. J. Oh, Enhanced desalination performance of pilot-scale membrane capacitive deionization (MCDI) system with circulation process, *Desalination*, 2025, **604**, 118686.

71 C. Oh, B. Lee, J. An, S. Yeon and H. Je Oh, Performance optimization of a pilot-scale membrane capacitive deionization (MCDI) system operating with circulation process, *Sep. Purif. Technol.*, 2024, **343**, 126937.

72 M.-C. Wu, Y.-H. Kao and C.-H. Hou, Evaluating boron removal from aqueous solutions using membrane capacitive deionization (MCDI): efficacy and limitations, *J. Environ. Chem. Eng.*, 2024, **12**, 113104.

73 Z. He, C. J. Miller, Y. Zhu, Y. Wang, J. Fletcher and T. D. Waite, Membrane capacitive deionization (MCDI): a flexible and tunable technology for customized water softening, *Water Res.*, 2024, **259**, 121871.

74 Q. Xiao, J. Ma, L. Xu, K. Zuo, H. Guo and C. Y. Tang, Membrane capacitive deionization (MCDI) for selective ion separation and recovery: fundamentals, challenges, and opportunities, *J. Membr. Sci.*, 2024, **699**, 122650.

75 T.-H. Chen, K.-H. Yeh, C.-F. Lin, M. Lee and C.-H. Hou, Technological and economic perspectives of membrane capacitive deionization (MCDI) systems in high-tech industries: from tap water purification to wastewater reclamation for water sustainability, *Resour. Conserv. Recycl.*, 2022, **177**, 106012.

76 H. Zhang, T. Pang and M. Xie, Fluoride removal using membrane capacitive deionization: the role of pH-dependent dissolved inorganic carbon, *Sep. Purif. Technol.*, 2025, **359**, 130411.

77 C. Bales, B. Lian, Y. Zhu, H. Zhou, Y. Wang, J. Fletcher and T. D. Waite, Photovoltaic powered operational scale membrane capacitive deionization (MCDI) desalination with energy recovery for treated domestic wastewater reuse, *Desalination*, 2023, **559**, 116647.

78 M. Liu, M. He, Y. Lu, X. Li, Z. Li, Y. Yao, H. Zhang, B. Wang and W. Wang, Enhanced cation storage capacity in MXene electrode through the incorporation of polypyrrole for hybrid capacitive deionization, *Desalination*, 2025, **606**, 118763.

79 X. Bu, Y. Zhang, H. Guo, S. Wang and X. Du, Enhanced hybrid capacitive deionization performance by the mass balance of electrodes, *Desalination*, 2023, **567**, 116982.

80 M. R. Vengatesan, I. F. Fahmi Darawsheh, B. Govindan, E. Alhseinat and F. Banat, Ag-Cu bimetallic nanoparticle decorated graphene nanocomposite as an effective anode material for hybrid capacitive deionization (HCDI) system, *Electrochim. Acta*, 2019, **297**, 1052–1062.

81 M. Xu, Z. Tan, Y. Tian, F. Gong, K. Yi, Z. He and X. Ji, Binder-free Bi@MXene film with 3D sandwich structure for highly hybrid capacitive deionization, *Sep. Purif. Technol.*, 2025, **363**, 132263.

82 W. Xing, K. Luo, J. Liang, C. Su and W. Tang, Urchin-like core–shell tungsten oxide@carbon composite electrode for highly efficient and stable water desalination *via* hybrid capacitive deionization (HCDI), *Chem. Eng. J.*, 2023, **477**, 147268.

83 P. Nie, S. Wang, X. Shang, B. Hu, M. Huang, J. Yang and J. Liu, Self-supporting porous carbon nanofibers with opposite surface charges for high-performance inverted capacitive deionization, *Desalination*, 2021, **520**, 115340.

84 X. Gao, A. Omosebi, J. Landon and K. Liu, Surface charge enhanced carbon electrodes for stable and efficient capacitive deionization using inverted adsorption–desorption behavior, *Energy Environ. Sci.*, 2015, **8**, 897–909.

85 X. Gao, A. Omosebi, J. Landon and K. Liu, Enhanced salt removal in an inverted capacitive deionization cell using amine modified microporous carbon cathodes, *Environ. Sci. Technol.*, 2015, **49**, 10920–10926.

86 D.-C. Han, S.-Y. Wang, C.-M. Zhang, R.-Y. Yue, S.-G. Wang and X.-F. Sun, Efficient dual-ions hybrid capacitive system for superior deionization with enhanced kinetics match, *Electrochim. Acta*, 2022, **436**, 141380.

87 Y. Li, J. He, H. Liu and C. Yan, Next-generation brackish water treatment: exploring dual-ion capacitive deionization, *J. Environ. Chem. Eng.*, 2025, **13**, 116037.

88 Y. Li, J. He, H. Liu and C. Yan, Next-generation brackish water treatment: exploring dual-ion capacitive deionization, *J. Environ. Chem. Eng.*, 2025, **13**, 116037.

89 B. Wei and Z. Liu, Pseudo-capacitive behaviors induced dual-ion selective deionization system based on MoS_2/PPy//Ag@PANI/AC, *Sep. Purif. Technol.*, 2025, **362**, 131906.

90 Z. Yue, Y. Ma, J. Zhang and H. Li, Pseudo-capacitive behavior induced dual-ion hybrid deionization system based on Ag@rGO‖$Na_{1.1}V_3O_{7.9}$@rGO, *J. Mater. Chem. A*, 2019, **7**, 16892–16901.

91 G. Folaranmi, M. Bechelany, P. Sistat, M. Cretin and F. Zaviska, Towards Electrochemical Water Desalination Techniques: A Review on Capacitive Deionization, Membrane Capacitive Deionization and Flow Capacitive Deionization, *Membranes*, 2020, **10**, 96.

92 H. Li and L. Zou, Ion-exchange membrane capacitive deionization: a new strategy for brackish water desalination, *Desalination*, 2011, **275**, 62–66.

93 J. Ma, J. Ma, C. Zhang, J. Song, W. Dong and T. D. Waite, Flow-electrode capacitive deionization (FCDI) scale-up using a membrane stack configuration, *Water Res.*, 2020, **168**, 115186.

94 J. Elisadiki, T. E. Kibona, R. L. Machunda, M. W. Saleem, W.-S. Kim and Y. A. C. Jande, Biomass-based carbon electrode materials for capacitive deionization: a review, *Biomass Convers. Biorefin.*, 2020, **10**, 1327–1356.

95 C. Zhao, G. Liu, N. Sun, X. Zhang, G. Wang, Y. Zhang, H. Zhang and H. Zhao, Biomass-derived N-doped porous carbon as electrode materials for Zn-air battery powered capacitive deionization, *Chem. Eng. J.*, 2018, **334**, 1270–1280.

96 T. Lu, Y. Liu, X. Xu, L. Pan, A. A. Alothman, J. Shapter, Y. Wang and Y. Yamauchi, Highly efficient water desalination by capacitive deionization on biomass-derived porous carbon nanoflakes, *Sep. Purif. Technol.*, 2021, **256**, 117771.

97 Z. Xie, X. Shang, J. Yan, T. Hussain, P. Nie and J. Liu, Biomass-derived porous carbon anode for high-performance capacitive deionization, *Electrochim. Acta*, 2018, **290**, 666–675.

98 J. Sun, Z. Wu, C. Ma, M. Xu, S. Luo, W. Li and S. Liu, Biomass-derived tubular carbon materials: progress in synthesis and applications, *J. Mater. Chem. A*, 2021, **9**, 13822–13850.

99 W.-J. Liu, W.-W. Li, H. Jiang and H.-Q. Yu, Fates of chemical elements in biomass during its pyrolysis, *Chem. Rev.*, 2017, **117**, 6367–6398.

100 M. Li, G. Luo, R. Zou, W. Qiu, Y. Xiao, G. Xu and H. Yao, Combustion kinetics and ash particles structure analysis of biomass *in situ* and cooling char, *Energy*, 2025, **318**, 134883.

101 M. Tripathi, J. N. Sahu and P. Ganesan, Effect of process parameters on production of biochar from biomass waste through pyrolysis: a review, *Renewable Sustainable Energy Rev.*, 2016, **55**, 467–481.

102 H. He, R. Zhang, P. Zhang, P. Wang, N. Chen, B. Qian, L. Zhang, J. Yu and B. Dai, Functional carbon from nature: biomass-derived carbon materials and the recent progress of their applications, *Adv. Sci.*, 2023, **10**, 2205557.

103 Y. Sun, X.-L. Shi, Y.-L. Yang, G. Suo, L. Zhang, S. Lu and Z.-G. Chen, Biomass-derived carbon for high-performance batteries: from structure to properties, *Adv. Funct. Mater.*, 2022, **32**, 2201584.

104 K. Kalus, J. A. Koziel and S. Opaliński, A review of biochar properties and their utilization in crop agriculture and livestock production, *Appl. Sci.*, 2019, **9**, 3494.

105 Y. Liu, J. Chen, B. Cui, P. Yin and C. Zhang, Design and preparation of biomass-derived carbon materials for supercapacitors: a review, *C*, 2018, **4**, 53.

106 V. Kumar, P. Sharma, R. Pasrija, P. Chakraborty, T. Basheer, J. Thomas, S. S. Sehgal, M. Gupta and K. Muzammil, Engineered lignocellulosic based biochar to remove endocrine-disrupting chemicals: assessment of binding mechanism, *Chemosphere*, 2024, **362**, 142584.

107 A. Tomczyk, Z. Sokołowska and P. Boguta, Biochar physicochemical properties: pyrolysis temperature and feedstock kind effects, *Rev. Environ. Sci. Bio/Technol.*, 2020, **19**, 191–215.

108 J. A. Ippolito, L. Cui, C. Kammann, N. Wrage-Mönnig, J. M. Estavillo, T. Fuertes-Mendizabal, M. L. Cayuela, G. Sigua, J. Novak, K. Spokas and N. Borchard, Feedstock choice, pyrolysis temperature and type influence biochar characteristics: a comprehensive meta-data analysis review, *Biochar*, 2020, **2**, 421–438.

109 X. Liu, Y. Wen, X. Chen, T. Tang and E. Mijowska, Co-etching effect to convert waste polyethylene terephthalate into hierarchical porous carbon toward excellent capacitive energy storage, *Sci. Total Environ.*, 2020, **723**, 138055.

110 D.-C. Li and H. Jiang, The thermochemical conversion of non-lignocellulosic biomass to form biochar: a review on characterizations and mechanism elucidation, *Bioresour. Technol.*, 2017, **246**, 57–68.

111 D. Pandey, A. Daverey and K. Arunachalam, Biochar: Production, properties and emerging role as a support for enzyme immobilization, *J. Cleaner Prod.*, 2020, **255**, 120267.

112 N. Nwabunwanne, T. Vuyokazi, A. Olagoke, O. Mike, M. Patrick and O. Anthony, Improving the solid fuel properties of non-lignocellulose and lignocellulose materials through torrefaction, *Materials*, 2021, **14**, 2072.

113 P. Bajpai, in *Pretreatment of Lignocellulosic Biomass for Biofuel Production*, ed. P. Bajpai, Springer, Singapore, 2016, pp. 7–12.

114 R. Xie, Y. Zhu, H. Zhang, P. Zhang and L. Han, Effects and mechanism of pyrolysis temperature on physicochemical properties of corn stalk pellet biochar based on combined characterization approach of microcomputed tomography and chemical analysis, *Bioresour. Technol.*, 2021, **329**, 124907.

115 J. Zhao, L. Yu, H. Ma, F. Zhou, K. Yang and G. Wu, Corn stalk-based activated carbon synthesized by a novel activation method for high-performance adsorption of hexavalent chromium in aqueous solutions, *J. Colloid Interface Sci.*, 2020, **578**, 650–659.

116 G. Gou, F. Huang, M. Jiang, J. Li and Z. Zhou, Hierarchical porous carbon electrode materials for supercapacitor developed from wheat straw cellulosic foam, *Renewable Energy*, 2020, **149**, 208–216.

117 H. Patel, H. Weldekidan, A. Mohanty and M. Misra, Effect of physicochemical activation on CO_2 adsorption of activated porous carbon derived from pine sawdust, *Carbon Capture Sci. Technol.*, 2023, **8**, 100128.

118 T. Prasankumar, D. Salpekar, S. Bhattacharyya, K. Manoharan, R. M. Yadav, M. A. Campos Mata, K. A. Miller, R. Vajtai, S. Jose, S. Roy and P. M. Ajayan, Biomass derived hierarchical porous carbon for supercapacitor application and dilute stream CO_2 capture, *Carbon*, 2022, **199**, 249–257.

119 D. Bejjanki, P. Banothu, V. B. Kumar and P. S. Kumar, Biomass-derived N-doped activated carbon from eucalyptus leaves as an efficient supercapacitor electrode material, *C*, 2023, **9**, 24.

120 Y. Li, L. W. Zhou and R. Z. Wang, Urban biomass and methods of estimating municipal biomass resources, *Renewable Sustainable Energy Rev.*, 2017, **80**, 1017–1030.

121 U. Menon, D. Mandal, S. Anshu, A. Mondal, R. Bhar, A. Chandra, A. Kumar and B. K. Dubey, From garden to grid: harnessing yard waste into carbon electrode with an insight into life cycle assessment, *Sci. Total Environ.*, 2025, **978**, 179442.

122 D.-C. Li and H. Jiang, The thermochemical conversion of non-lignocellulosic biomass to form biochar: a review on characterizations and mechanism elucidation, *Bioresour. Technol.*, 2017, **246**, 57–68.

123 N. Nwabunwanne, T. Vuyokazi, A. Olagoke, O. Mike, M. Patrick and O. Anthony, Improving the Solid Fuel Properties of Non-Lignocellulose and Lignocellulose Materials through Torrefaction, *Materials*, 2021, **14**, 2072.

124 Y. Zhang, X. Bu, Y. Wang, Z. Hang and Z. Chen, Hierarchically porous biochar derived from aerobic granular sludge for high-performance membrane capacitive deionization, *Environ. Sci. Ecotechnol.*, 2024, **17**, 100297.

125 F. Suo, X. You, S. Yin, H. Wu, C. Zhang, X. Yu, R. Sun and Y. Li, Preparation and characterization of biochar derived from co-pyrolysis of *enteromorpha prolifera* and corn straw and its potential as a soil amendment, *Sci. Total Environ.*, 2021, **798**, 149167.

126 K. L. Yu, P. L. Show, H. C. Ong, T. C. Ling, J. Chi-Wei Lan, W.-H. Chen and J.-S. Chang, Microalgae from wastewater treatment to biochar – feedstock preparation and conversion technologies, *Energy Convers. Manage.*, 2017, **150**, 1–13.

127 S. Gupta, K. N. Palansooriya, P. D. Dissanayake, Y. S. Ok and H. W. Kua, Carbonaceous inserts from lignocellulosic and non-lignocellulosic sources in cement mortar: preparation conditions and its effect on hydration kinetics and physical properties, *Constr. Build. Mater.*, 2020, **264**, 120214.

128 W.-T. Tsai, S.-C. Liu, H.-R. Chen, Y.-M. Chang and Y.-L. Tsai, Textural and chemical properties of swine-manure-derived biochar pertinent to its potential use as a soil amendment, *Chemosphere*, 2012, **89**, 198–203.

129 J. Xu, Y. Xie, Q. Yao, L. Lv and H. Chu, Advances in sustainable nano-biochar: precursors, synthesis methods and applications, *Nanoscale*, 2024, **16**, 15009–15032.

130 X. Wei, B. Qiu, L. Xu, Q. Qin, W. Zhang, Z. Liu, F. Wei and Y. Lv, High performance hierarchical porous carbon derived from waste shrimp shell for supercapacitor electrodes, *J. Energy Storage*, 2023, **62**, 106900.

131 J. Song, Y. Li, Y. Wang, L. Zhong, Y. Liu, X. Sun, B. He, Y. Li and S. Cao, Preparing biochars from cow hair waste produced in a tannery for dye wastewater treatment, *Materials*, 2021, **14**, 1690.

132 J. Zhou, S. Zhang, Y.-N. Zhou, W. Tang, J. Yang, C. Peng and Z. Guo, Biomass-derived carbon materials for high-performance supercapacitors: current status and perspective, *Electrochem. Energy Rev.*, 2021, **4**, 219–248.

133 D. Wu, F. Sun, M. Xie, H. Wang, W. Fan, J. Gao, G. Zhao and S. Liu, A review on multi-scale structure engineering of carbon-based electrode materials towards dense energy storage for supercapacitors, *J. Energy Chem.*, 2025, **102**, 768–799.

134 M. Umar, B. O. Yusuf, M. Aliyu, I. Hussain, A. M. Alhassan, M. M. Awad, O. A. Taialla, B. Ali, K. R. Alhooshani and S. A. Ganiyu, Advancing frontiers in CO_2 capture: the renaissance of biomass-derived carbon materials, *Coord. Chem. Rev.*, 2025, **526**, 216380.

135 Y. Wang, M. Zhang, X. Shen, H. Wang, H. Wang, K. Xia, Z. Yin and Y. Zhang, Biomass-derived carbon materials: controllable preparation and versatile applications, *Small*, 2021, **17**, 2008079.

136 Q. Jiang, Z. Yu, X. Zhang, S. Chen, J. Yi and Y. Liu, Flexible polyvinylidene fluoride/multiwall carbon nanotube-based thermoelectric composite films with excellent environmental stability and enhanced power factor from ferroelectric polarization, *Sci. China Mater.*, 2025, **68**(4), 1240–1248.

137 Z. Yang, T. Xu, H. Li, M. She, J. Chen, Z. Wang, S. Zhang and J. Li, Zero-dimensional carbon nanomaterials for fluorescent sensing and imaging, *Chem. Rev.*, 2023, **123**, 11047–11136.

138 N. Jaswal, V. Bharati Jaryal, R. Singh, P. Kumar and N. Gupta, Harnessing biomass derived carbon material with heteroatoms for sensitive and selective detection of Mercury (II) ions in waste water, *Microchem. J.*, 2024, **207**, 111767.

139 R. Guo, L. Li, B. Wang, Y. Xiang, G. Zou, Y. Zhu, H. Hou and X. Ji, Functionalized carbon dots for advanced batteries, *Energy Storage Mater.*, 2021, **37**, 8–39.

140 S. Li, L. Li, H. Tu, H. Zhang, D. S. Silvester, C. E. Banks, G. Zou, H. Hou and X. Ji, The development of carbon dots: from the perspective of materials chemistry, *Mater. Today*, 2021, **51**, 188–207.

141 J.-S. Wei, C. Ding, P. Zhang, H. Ding, X.-Q. Niu, Y.-Y. Ma, C. Li, Y.-G. Wang and H.-M. Xiong, Robust negative electrode materials derived from carbon dots and porous hydrogels for high-performance hybrid supercapacitors, *Adv. Mater.*, 2018, **31**(5), 1806197.

142 C. Li, W. Li, H. Liu, Y. Li, L. Dai, C. Li and C. Si, State-of-the-art on the production and application of lignin-derived carbon nanoparticles, *Ind. Crops Prod.*, 2024, **222**, 120123.

143 N. Wu, W. He, S. Shi, X. Yuan, J. Li, J. Cao, C. Yuan and X. Liu, Bamboo fiber-derived carbon support for the immobilization of Pt nanoparticles to enhance hydrogen evolution reaction, *J. Colloid Interface Sci.*, 2025, **684**, 658–667.

144 R. R. Gaddam, D. Yang, R. Narayan, K. Raju, N. A. Kumar and X. S. Zhao, Biomass derived carbon nanoparticle as anodes for high performance sodium and lithium ion batteries, *Nano Energy*, 2016, **26**, 346–352.

145 V. Georgakilas, J. A. Perman, J. Tucek and R. Zboril, Broad family of carbon nanoallotropes: classification, chemistry, and applications of fullerenes, carbon dots, nanotubes, graphene, nanodiamonds, and combined superstructures, *Chem. Rev.*, 2015, **115**, 4744–4822.

146 P. Hidalgo, R. Navia, R. Hunter, G. Coronado and M. Gonzalez, Synthesis of carbon nanotubes using biochar as precursor material under microwave irradiation, *J. Environ. Manage.*, 2019, **244**, 83–91.

147 C. Ding, C. Shao, S. Wu, Y. Ma, Y. Liu, S. Ma, X. Hu, Z. Cao, X. Ren, B. Zhong, G. Wen and X. Huang, A review of 1D carbon-based materials assembly design for lightweight microwave absorption, *Carbon*, 2023, **213**, 118279.

148 X. Wu, Z. Shi, R. Tjandra, A. Justine Cousins, S. Sy, A. Yu, R. M. Berry and K. C. Tam, Nitrogen-enriched porous carbon nanorods templated by cellulose nanocrystals as high performance supercapacitor electrodes, *J. Mater. Chem. A*, 2015, **3**, 23768–23777.

149 C. Fang, P. Hu, S. Dong, Y. Cheng, D. Zhang and X. Zhang, Construction of carbon nanorods supported hydrothermal carbon and carbon fiber from waste biomass straw for high strength supercapacitor, *J. Colloid Interface Sci.*, 2021, **582**, 552–560.

150 E. Svinterikos, I. Zuburtikudis and M. Al-Marzouqi, Electrospun lignin-derived carbon micro- and nanofibers: a review on precursors, properties, and applications, *ACS Sustainable Chem. Eng.*, 2020, **8**, 13868–13893.

151 C. Fang, P. Hu, S. Dong, Y. Cheng, D. Zhang and X. Zhang, Construction of carbon nanorods supported hydrothermal carbon and carbon fiber from waste biomass straw for high strength supercapacitor, *J. Colloid Interface Sci.*, 2021, **582**, 552–560.

152 R. Kumar, E. Joanni, S. Sahoo, J.-J. Shim, W. K. Tan, A. Matsuda and R. K. Singh, An overview of recent progress in nanostructured carbon-based supercapacitor electrodes: from zero to bi-dimensional materials, *Carbon*, 2022, **193**, 298–338.

153 L. Chai, R. Li, Y. Sun, K. Zhou and J. Pan, MOF-derived carbon-based materials for energy-related applications, *Adv. Mater.*, 2025, DOI: 10.1002/adma.202413658.

154 Q. Niu, K. Gao, Q. Tang, L. Wang, L. Han, H. Fang, Y. Zhang, S. Wang and L. Wang, Large-size graphene-like porous carbon nanosheets with controllable N-doped surface derived from sugarcane bagasse pith/chitosan for high performance supercapacitors, *Carbon*, 2017, **123**, 290–298.

155 H. Zhao, Y. Cheng, Z. Zhang, B. Zhang, C. Pei, F. Fan and G. Ji, Biomass-derived graphene-like porous carbon nanosheets towards ultralight microwave absorption and excellent thermal infrared properties, *Carbon*, 2021, **173**, 501–511.

156 H. He, R. Zhang, P. Zhang, P. Wang, N. Chen, B. Qian, L. Zhang, J. Yu and B. Dai, Functional carbon from nature: biomass-derived carbon materials and the recent progress of their applications, *Adv. Sci.*, 2023, **10**, 2205557.

157 S. Azam, Z. Wei and R. Wang, Cerium oxide nanorods anchored on carbon nanofibers derived from cellulose paper as effective interlayer for lithium sulfur battery, *J. Colloid Interface Sci.*, 2022, **615**, 417–431.

158 S. F. Zhao, C. Li, Z. Cui, J. Zhang, W. Hu, R. Ma and C. M. Li, Biomass-derived micro-mesoporous carbon with oxygen functional groups for high-rate Na–S batteries at room temperature, *Adv. Energy Mater.*, 2023, **13**(45), 2302490.

159 H. Wu, J. Geng, H. Ge, Z. Guo, Y. Wang and G. Zheng, Egg-derived mesoporous carbon microspheres as bifunctional oxygen evolution and oxygen reduction electrocatalysts, *Adv. Energy Mater.*, 2016, **6**(20), 1600794.

160 H. Qu, X. Zhang, J. Zhan, W. Sun, Z. Si and H. Chen, Biomass-based nitrogen-doped hollow carbon nanospheres derived directly from glucose and glucosamine: structural evolution and supercapacitor properties, *ACS Sustainable Chem. Eng.*, 2018, **6**, 7380–7389.

161 M. Belluati, S. Tabasso, E. C. Gaudino, G. Cravotto and M. Manzoli, Biomass-derived carbon-based catalysts for lignocellulosic biomass and waste valorisation: a circular approach, *Green Chem.*, 2024, **26**, 8642–8668.

162 S.-E. Ban, E.-J. Lee, D.-J. Lim, I.-S. Kim and J.-W. Lee, Evaluation of sulfuric acid-pretreated biomass-derived biochar characteristics and its diazinon adsorption mechanism, *Bioresour. Technol.*, 2022, **348**, 126828.

163 C. He, M. Huang, L. Zhao, Y. Lei, J. He, D. Tian, Y. Zeng, F. Shen and J. Zou, Enhanced electrochemical performance of porous carbon from wheat straw as remolded by hydrothermal processing, *Sci. Total Environ.*, 2022, **842**, 156905.

164 Y. Liu, J. Chen, B. Cui, P. Yin and C. Zhang, Design and preparation of biomass-derived carbon materials for supercapacitors: a review, *C*, 2018, **4**, 53.

165 B. A. Mohamed, R. Ruan, M. Bilal, N. A. Khan, M. K. Awasthi, M. A. Amer, L. Leng, M. A. Hamouda, D. N. Vo and J. Li, Co-pyrolysis of sewage sludge and biomass for stabilizing heavy metals and reducing biochar toxicity: a review, *Environ. Chem. Lett.*, 2023, **21**, 1231–1250.

166 X. Meng, Y. Wang, A. J. Conte, S. Zhang, J. Ryu, J. J. Wie, Y. Pu, B. H. Davison, C. G. Yoo and A. J. Ragauskas, Applications of biomass-derived solvents in biomass pretreatment – strategies, challenges, and prospects, *Bioresour. Technol.*, 2023, **368**, 128280.

167 A. Ramos, E. Monteiro and A. Rouboa, Biomass pre-treatment techniques for the production of biofuels using thermal conversion methods – a review, *Energy Convers. Manage.*, 2022, **270**, 116271.

168 H. Zhang, H. Sun, S. Huang, J. Lan, H. Li and H. Yue, Biomass-derived carbon materials for electrochemical sensing: recent advances and future perspectives, *Crit. Rev. Anal. Chem.*, 2024, 1–26.

169 S. Sun, Q. Wang, X. Wang, C. Wu, X. Zhang, J. Bai and B. Sun, Dry torrefaction and continuous thermochemical conversion for upgrading agroforestry waste into eco-friendly energy carriers: current progress and future prospect, *Sci. Total Environ.*, 2023, **905**, 167061.

170 L. Qin, Y. Wu and E. Jiang, In situ template preparation of porous carbon materials that are derived from swine

manure and have ordered hierarchical nanopore structures for energy storage, *Energy*, 2022, **242**, 123040.

171 J. Wang, Q. Zhang and M. Deng, Eco-friendly preparation of biomass-derived porous carbon and its electrochemical properties, *ACS Omega*, 2022, **7**, 22689–22697.

172 C. Wang, H. Wang, C. Yang, B. Dang, C. Li and Q. Sun, A multilevel gradient structural carbon derived from naturally preprocessed biomass, *Carbon*, 2020, **168**, 624–632.

173 X. Meng, Y. Wang, A. J. Conte, S. Zhang, J. Ryu, J. J. Wie, Y. Pu, B. H. Davison, C. G. Yoo and A. J. Ragauskas, Applications of biomass-derived solvents in biomass pretreatment – strategies, challenges, and prospects, *Bioresour. Technol.*, 2023, **368**, 128280.

174 J. Jin, H. Ma, H. Liang and Y. Zhang, Biopolymer-derived carbon materials for wearable electronics, *Adv. Mater.*, 2025, DOI: **10.1002/adma.202414620**.

175 H. He, R. Zhang, P. Zhang, P. Wang, N. Chen, B. Qian, L. Zhang, J. Yu and B. Dai, Functional carbon from nature: biomass-derived carbon materials and the recent progress of their applications, *Adv. Sci.*, 2023, **10**, 2205557.

176 Hydrogen generation from biomass by pyrolysis, *Nat. Rev. Methods Primers*, 2022, **2**, 21.

177 F. Campuzano, R. C. Brown and J. D. Martínez, Auger reactors for pyrolysis of biomass and wastes, *Renewable Sustainable Energy Rev.*, 2019, **102**, 372–409.

178 S. Seraj, R. Azargohar and A. K. Dalai, Dry torrefaction and hydrothermal carbonization of biomass to fuel pellets, *Renewable Sustainable Energy Rev.*, 2025, **210**, 115186.

179 Z. Zhang, Z. Zhu, B. Shen and L. Liu, Insights into biochar and hydrochar production and applications: a review, *Energy*, 2019, **171**, 581–598.

180 M. Chu, W. Tian, J. Zhao, M. Zou, Z. Lu, D. Zhang and J. Jiang, A comprehensive review of capacitive deionization technology with biochar-based electrodes: biochar-based electrode preparation, deionization mechanism and applications, *Chemosphere*, 2022, **307**, 136024.

181 A. Anca-Couce, Reaction mechanisms and multi-scale modelling of lignocellulosic biomass pyrolysis, *Prog. Energy Combust. Sci.*, 2016, **53**, 41–79.

182 J. Liang, G. Shan and Y. Sun, Catalytic fast pyrolysis of lignocellulosic biomass: critical role of zeolite catalysts, *Renewable Sustainable Energy Rev.*, 2021, **139**, 110707.

183 K. Wang, K. H. Kim and R. C. Brown, Catalytic pyrolysis of individual components of lignocellulosic biomass, *Green Chem.*, 2014, **16**, 727–735.

184 W. Wang, Y. Shi, Y. Cui and X. Li, Catalytic fast pyrolysis of cellulose for increasing contents of furans and aromatics in biofuel production, *J. Anal. Appl. Pyrolysis*, 2018, **131**, 93–100.

185 R. Liu, M. Sarker, M. M. Rahman, C. Li, M. Chai, Nishu, R. Cotillon and N. R. Scott, Multi-scale complexities of solid acid catalysts in the catalytic fast pyrolysis of biomass for bio-oil production – a review, *Prog. Energy Combust. Sci.*, 2020, **80**, 100852.

186 A. Al-Rumaihi, M. Shahbaz, G. Mckay, H. Mackey and T. Al-Ansari, A review of pyrolysis technologies and feedstock: a blending approach for plastic and biomass towards optimum biochar yield, *Renewable Sustainable Energy Rev.*, 2022, **167**, 112715.

187 C. Liu, H. Wang, A. M. Karim, J. Sun and Y. Wang, Catalytic fast pyrolysis of lignocellulosic biomass, *Chem. Soc. Rev.*, 2014, **43**, 7594–7623.

188 R. Kumar, V. Strezov, H. Weldekidan, J. He, S. Singh, T. Kan and B. Dastjerdi, Lignocellulose biomass pyrolysis for bio-oil production: a review of biomass pre-treatment methods for production of drop-in fuels, *Renewable Sustainable Energy Rev.*, 2020, **123**, 109763.

189 C. Wang, X. Wu, F. Wang, F. Xie and Y. Yao, Pine-derived porous carbon for efficient capacitive deionization and the role of its hierarchical pore structure, *Sep. Purif. Technol.*, 2024, **342**, 126865.

190 J. Chen, K. Zuo, B. Li, J. Hu, W. Liu, D. Xia, L. Lin, J. Liang and X. Li, Fungal hypha-derived freestanding porous carbon pad as a high-capacity electrode for water desalination in membrane capacitive deionization, *Chem. Eng. J.*, 2022, **433**, 133781.

191 P. Roy, A. Dutta and J. Gallant, Evaluation of the life cycle of hydrothermally carbonized biomass for energy and horticulture application, *Renewable Sustainable Energy Rev.*, 2020, **132**, 110046.

192 S. Yu, J. He, Z. Zhang, Z. Sun, M. Xie, Y. Xu, X. Bie, Q. Li, Y. Zhang, M. Sevilla, M.-M. Titirici and H. Zhou, Towards negative emissions: hydrothermal carbonization of biomass for sustainable carbon materials, *Adv. Mater.*, 2024, **36**(18), 2307412.

193 J. González-Arias, M. E. Sánchez, J. Cara-Jiménez, F. M. Baena-Moreno and Z. Zhang, Hydrothermal carbonization of biomass and waste: a review, *Environ. Chem. Lett.*, 2022, **20**, 211–221.

194 H. B. Sharma, A. K. Sarmah and B. Dubey, Hydrothermal carbonization of renewable waste biomass for solid biofuel production: a discussion on process mechanism, the influence of process parameters, environmental performance and fuel properties of hydrochar, *Renewable Sustainable Energy Rev.*, 2020, **123**, 109761.

195 F. Qin, C. Zhang, G. Zeng, D. Huang, X. Tan and A. Duan, Lignocellulosic biomass carbonization for biochar production and characterization of biochar reactivity, *Renewable Sustainable Energy Rev.*, 2022, **157**, 112056.

196 Y. Wang, Y.-J. Hu, X. Hao, P. Peng, J.-Y. Shi, F. Peng and R.-C. Sun, Hydrothermal synthesis and applications of advanced carbonaceous materials from biomass: a review, *Adv. Compos. Hybrid Mater.*, 2020, **3**, 267–284.

197 M. Kumar, A. Olajire Oyedun and A. Kumar, A review on the current status of various hydrothermal technologies on biomass feedstock, *Renewable Sustainable Energy Rev.*, 2018, **81**, 1742–1770.

198 Ł. Sobol, A. Dyjakon and K. Soukup, Dioxins and furans in biochars, hydrochars and torrefactes produced by thermochemical conversion of biomass: a review, *Environ. Chem. Lett.*, 2023, **21**, 2225–2249.

199 D. M. Alonso, S. G. Wettstein and J. A. Dumesic, Bimetallic catalysts for upgrading of biomass to fuels and chemicals, *Chem. Soc. Rev.*, 2012, **41**, 8075.

200 S. Román, J. M. V. Nabais, C. Laginhas, B. Ledesma and J. F. González, Hydrothermal carbonization as an effective way of densifying the energy content of biomass, *Fuel Process. Technol.*, 2012, **103**, 78–83.

201 A. M. Ruppert, K. Weinberg and R. Palkovits, Hydrogenolysis goes bio: from carbohydrates and sugar alcohols to platform chemicals, *Angew. Chem., Int. Ed.*, 2012, **51**, 2564–2601.

202 M.-M. Titirici, R. J. White, C. Falco and M. Sevilla, Black perspectives for a green future: hydrothermal carbons for environment protection and energy storage, *Energy Environ. Sci.*, 2012, **5**, 6796.

203 S. Nizamuddin, H. A. Baloch, G. J. Griffin, N. M. Mubarak, A. W. Bhutto, R. Abro, S. A. Mazari and B. S. Ali, An overview of effect of process parameters on hydrothermal carbonization of biomass, *Renewable Sustainable Energy Rev.*, 2017, **73**, 1289–1299.

204 X. Yang, H. He, T. Lv and J. Qiu, Fabrication of biomass-based functional carbon materials for energy conversion and storage, *Mater. Sci. Eng., R*, 2023, **154**, 100736.

205 G. Zhu, C. Xi, M. Shen, C. Bao and J. Zhu, Nanosheet-Based Hierarchical $Ni_2(CO_3)(OH)_2$ Microspheres with Weak Crystallinity for High-Performance Supercapacitor, *ACS Appl. Mater. Interfaces*, 2014, **6**, 17208–17214.

206 J. Xia, J. Liu, G. Huang, Q. Liu, H. Zhang, X. Jing, Y. Yuan and J. Wang, Morphology controllable synthesis of $NiCo_2S_4$ and application as gas sensors, *Mater. Lett.*, 2017, **188**, 17–20.

207 M. M. Baig and I. H. Gul, Transformation of wheat husk to 3D activated carbon/$NiCo_2S_4$frameworks for high-rate asymmetrical supercapacitors, *J. Energy Storage*, 2021, **37**, 102477.

208 A. Altwala and R. Mokaya, Predictable and targeted activation of biomass to carbons with high surface area density and enhanced methane storage capacity, *Energy Environ. Sci.*, 2020, **13**, 2967–2978.

209 M. Danish and T. Ahmad, A review on utilization of wood biomass as a sustainable precursor for activated carbon production and application, *Renewable Sustainable Energy Rev.*, 2018, **87**, 1–21.

210 S. S. Sekhon, P. Kaur and J.-S. Park, From coconut shell biomass to oxygen reduction reaction catalyst: tuning porosity and nitrogen doping, *Renewable Sustainable Energy Rev.*, 2021, **147**, 111173.

211 A. Benítez, J. Amaro-Gahete, Y.-C. Chien, Á. Caballero, J. Morales and D. Brandell, Recent advances in lithium-sulfur batteries using biomass-derived carbons as sulfur host, *Renewable Sustainable Energy Rev.*, 2022, **154**, 111783.

212 X. Yuan, J. Wang, S. Deng, M. Suvarna, X. Wang, W. Zhang, S. T. Hamilton, A. Alahmed, A. Jamal, A.-H. A. Park, X. Bi and Y. S. Ok, Recent advancements in sustainable upcycling of solid waste into porous carbons for carbon dioxide capture, *Renewable Sustainable Energy Rev.*, 2022, **162**, 112413.

213 H. Patel, A. Mohanty and M. Misra, Post-combustion CO_2 capture using biomass based activated porous carbon: latest advances in synthesis protocol and economics, *Renewable Sustainable Energy Rev.*, 2024, **199**, 114484.

214 B. R. Patra, A. Mukherjee, S. Nanda and A. K. Dalai, Biochar production, activation and adsorptive applications: a review, *Environ. Chem. Lett.*, 2021, **19**, 2237–2259.

215 J. L. Santos, P. Mäki-Arvela, A. Monzón, D. Y. Murzin and M. Á. Centeno, Metal catalysts supported on biochars: part I synthesis and characterization, *Appl. Catal., B*, 2020, **268**, 118423.

216 A. M. Abioye and F. N. Ani, Recent development in the production of activated carbon electrodes from agricultural waste biomass for supercapacitors: a review, *Renewable Sustainable Energy Rev.*, 2015, **52**, 1282–1293.

217 Z. Heidarinejad, M. H. Dehghani, M. Heidari, G. Javedan, I. Ali and M. Sillanpää, Methods for preparation and activation of activated carbon: a review, *Environ. Chem. Lett.*, 2020, **18**, 393–415.

218 M. Sevilla, N. Diez, G. A. Ferrero and A. B. Fuertes, Sustainable supercapacitor electrodes produced by the activation of biomass with sodium thiosulfate, *Energy Storage Mater.*, 2019, **18**, 356–365.

219 T. W. Chew, P. S. H'Ng, B. C. T. G. Luqman Chuah Abdullah, K. L. Chin, C. L. Lee, B. M. S. Mohd Nor Hafizuddin and L. TaungMai, A review of bio-based activated carbon properties produced from different activating chemicals during chemicals activation process on biomass and its potential for Malaysia, *Materials*, 2023, **16**, 7365.

220 Y. Li, L. Ni, J. Luo, L. Zhu, X. Zhang, H. Li, I. Zada, J. Yu, S. Zhu, K. Lian, Y. Li and D. Zhang, Fenton reaction doubled biomass carbon activation efficiency for high-performance supercapacitors, *Adv. Funct. Mater.*, 2024, DOI: 10.1002/adfm.202403448.

221 Z. Hrdlička, J. Brejcha, J. Otruba, J. Skočilas, J. Štancl, A. Kadeřábková, D. Čadek, J. Krmela and V. Krmelová, Microwave activation of ground tyre rubber and its application in off-road tyre tread formulation, *Adv. Compos. Hybrid Mater.*, 2025, DOI: 10.1007/s42114-024-01179-9.

222 W. Ao, J. Fu, X. Mao, Q. Kang, C. Ran, Y. Liu, H. Zhang, Z. Gao, J. Li, G. Liu and J. Dai, Microwave assisted preparation of activated carbon from biomass: a review, *Renewable Sustainable Energy Rev.*, 2018, **92**, 958–979.

223 F. K. Yuen and B. H. Hameed, Recent developments in the preparation and regeneration of activated carbons by microwaves, *Adv. Colloid Interface Sci.*, 2009, **149**, 19–27.

224 S. K. N, D. Grekov, P. Pré and B. J. Alappat, Microwave mode of heating in the preparation of porous carbon materials for adsorption and energy storage applications – an overview, *Renewable Sustainable Energy Rev.*, 2020, **124**, 109743.

225 S. Głowniak, B. Szczęśniak, J. Choma and M. Jaroniec, Advances in microwave synthesis of nanoporous materials, *Adv. Mater.*, 2021, **33**(48), 2103477.

226 W.-T. Tsai, L.-A. Kuo, C.-H. Tsai, H.-L. Huang, R.-Y. Yang and J.-H. Tsai, Production of porous biochar from cow dung using microwave process, *Materials*, 2023, **16**, 7667.

227 E. C. Gaudino, G. Cravotto, M. Manzoli and S. Tabasso, From waste biomass to chemicals and energy *via* microwave-assisted processes, *Green Chem.*, 2019, **21**, 1202–1235.

228 X. Li, J. Zhang, B. Liu and Z. Su, A critical review on the application and recent developments of post-modified biochar in supercapacitors, *J. Cleaner Prod.*, 2021, **310**, 127428.

229 D. V. Cuong, B. M. Matsagar, M. Lee, Md. S. A. Hossain, Y. Yamauchi, M. Vithanage, B. Sarkar, Y. S. Ok, K. C.-W. Wu and C.-H. Hou, A critical review on biochar-based engineered hierarchical porous carbon for capacitive charge storage, *Renewable Sustainable Energy Rev.*, 2021, **145**, 111029.

230 J. Luo, Z. Fang and R. L. Smith, Ultrasound-enhanced conversion of biomass to biofuels, *Prog. Energy Combust. Sci.*, 2014, **41**, 56–93.

231 S. Zhu, N. Zhao, J. Li, X. Deng, J. Sha and C. He, Hard-template synthesis of three-dimensional interconnected carbon networks: rational design, hybridization and energy-related applications, *Nano Today*, 2019, **29**, 100796.

232 Q. Liang, D. Pan and X. Zhang, Construction and application of biochar-based composite phase change materials, *Chem. Eng. J.*, 2023, **453**, 139441.

233 J. Xi, H. Li, J. Xi, S. Tan, J. Zheng and Z. Tan, Preparation of high porosity biochar materials by template method: a review, *Environ. Sci. Pollut. Res.*, 2020, **27**, 20675–20684.

234 X. Zhang, C. Chen, C. Tang and Y. Wang, Morphological control of biochar with emerging functionalities by thermodynamic and kinetic approaches, *Acc. Mater. Res.*, 2022, **3**, 525–539.

235 D. G. Atinafu, W. Dong, C. Wang and G. Wang, Synthesis of porous carbon from cotton using an $Mg(OH)_2$ template for form-stabilized phase change materials with high encapsulation capacity, transition enthalpy and reliability, *J. Mater. Chem. A*, 2018, **6**, 8969–8977.

236 D. Saha, E. A. Payzant, A. S. Kumbhar and A. K. Naskar, Sustainable mesoporous carbons as storage and controlled-delivery media for functional molecules, *ACS Appl. Mater. Interfaces*, 2013, **5**, 5868–5874.

237 J. Li, Q. Jiang, L. Wei, L. Zhong and X. Wang, Simple and scalable synthesis of hierarchical porous carbon derived from cornstalk without pith for high capacitance and energy density, *J. Mater. Chem. A*, 2020, **8**, 1469–1479.

238 W. Zhang, Y. Zhang, M. Zhao, S. Wang, X. Fan, N. Zhou and S. Fan, Preparation of mesoporous biogas residue biochar *via* a self-template strategy for efficient removal of ciprofloxacin: effect of pyrolysis temperature, *J. Environ. Manage.*, 2024, **360**, 121140.

239 J. Wu, T. Wang, N. Shi and W.-P. Pan, Insight into mass transfer mechanism and equilibrium modeling of heavy metals adsorption on hierarchically porous biochar, *Sep. Purif. Technol.*, 2022, **287**, 120558.

240 Z. Zheng, B. Zhao, Y. Guo, Y. Guo, T. Pak and G. Li, Preparation of mesoporous batatas biochar *via* soft-template method for high efficiency removal of tetracycline, *Sci. Total Environ.*, 2021, **787**, 147397.

241 Z. Yang, Y. Zhang and Z. Schnepp, Soft and hard templating of graphitic carbon nitride, *J. Mater. Chem. A*, 2015, **3**, 14081–14092.

242 N. D. Petkovich and A. Stein, Controlling macro- and mesostructures with hierarchical porosity through combined hard and soft templating, *Chem. Soc. Rev.*, 2013, **42**, 3721–3739.

243 M. Zhang, C. Yu, Z. Ling, J. Yu, S. Li, C. Zhao, H. Huang and J. Qiu, A recyclable route to produce biochar with a tailored structure and surface chemistry for enhanced charge storage, *Green Chem.*, 2019, **21**, 2095–2103.

244 X.-J. Wu and D. Xu, Soft template synthesis of yolk/silica shell particles, *Adv. Mater.*, 2010, **22**, 1516–1520.

245 C. Chen, H. Wang, C. Han, J. Deng, J. Wang, M. Li, M. Tang, H. Jin and Y. Wang, Asymmetric flasklike hollow carbonaceous nanoparticles fabricated by the synergistic interaction between soft template and biomass, *J. Am. Chem. Soc.*, 2017, **139**, 2657–2663.

246 T. Li, R. Ma, J. Lin, Y. Hu, P. Zhang, S. Sun and L. Fang, The synthesis and performance analysis of various biomass-based carbon materials for electric double-layer capacitors: a review, *Int. J. Energy Res.*, 2020, **44**, 2426–2454.

247 X. Zhang, J. Tian, P. Wang, T. Liu, M. Ahmad, T. Zhang, J. Guo, H. Xiao and J. Song, Highly-efficient nitrogen self-doped biochar for versatile dyes' removal prepared from soybean cake *via* a simple dual-templating approach and associated thermodynamics, *J. Cleaner Prod.*, 2022, **332**, 130069.

248 X. Xia, S. Zeng, K. Li, L. Zeng and S. Miao, Unraveling the outstanding catalytic efficiency of unprocessed bone-derived biochar: a deep dive into the mechanisms of native organic encapsulation and defective nitrogen doping in boosting persulfate activation for tetracycline degradation, *Sep. Purif. Technol.*, 2025, **353**, 128571.

249 M.-R. Huang, L. Rao, J. Chen, X. Wang, R. Zhou, F. Yu, X.-G. Li and J. Ma, Advancements in electrode materials: the role of MXenes in capacitive deionization technology, *ACS Mater. Lett.*, 2025, **7**, 1400–1418.

250 M. E. Mahmoud, G. M. Nabil, N. M. El-Mallah, H. I. Bassiouny, S. Kumar and T. M. Abdel-Fattah, Kinetics, isotherm, and thermodynamic studies of the adsorption of reactive red 195 a dye from water by modified switchgrass biochar adsorbent, *J. Ind. Eng. Chem.*, 2016, **37**, 156–167.

251 M. Gęca, A. M. Khalil, M. Tang, A. K. Bhakta, Y. Snoussi, P. Nowicki, M. Wiśniewska and M. M. Chehimi, Surface treatment of biochar—methods, surface analysis and potential applications: a comprehensive review, *Surfaces*, 2023, **6**, 179–213.

252 L. M. Daudi, A. M. Bairo, O. M. Sufiani, J. Elisadiki, M. G. Sahini and S. Vuai, Enhanced coconut shell-based activated carbon for water desalination using an adsorption-capacitive deionization hybrid system, *East*

Afr. J. Sci. Technol. Innovation, 2024, DOI: 10.37425/mmq3gq76.

253 C. Kosaiyakanon and S. Kungsanant, Adsorption of reactive dyes from wastewater using cationic surfactant-modified coffee husk biochar, Environ. Nat. Resour. J., 2020, 18, 21–32.

254 A. K. Anas, S. Y. Pratama, A. Izzah and M. A. Kurniawan, Sodium dodecylbenzene sulfonate-modified biochar as an adsorbent for the removal of methylene blue, Bull. Chem. React. Eng. Catal., 2021, 16, 188–195.

255 Q. Fan, C. Song and P. Fu, Advances in the improvement of the quality and efficiency of biomass-derived porous carbon: a comprehensive review on synthesis strategies and heteroatom doping effects, J. Cleaner Prod., 2024, 452, 142169–142193.

256 W. Zhang, R. Xi, Y. Li, Y. Zhang, P. Wang and D. Hu, Recent development of transition metal doped carbon materials derived from biomass for hydrogen evolution reaction, Int. J. Hydrogen Energy, 2022, 47, 32436–32454.

257 L. Wang, Z. Gao, J. Chang, X. Liu, D. Wu, F. Xu, Y. Guo and K. Jiang, Nitrogen-doped porous carbons As electrode materials for high-performance supercapacitor and dye-sensitized solar cell, ACS Appl. Mater. Interfaces, 2015, 7, 20234–20244.

258 Z. Ullah Khan, T. Yan, J. Han, L. Shi and D. Zhang, Capacitive deionization of saline water using graphene nanosphere decorated N-doped layered mesoporous carbon frameworks, Environ. Sci.: Nano, 2019, 6, 3442–3453.

259 Z. Yin, F. Wu, C. He, L. Tang, Y. Chen, G. Lin, B. Huang, J. Chen and B. Lu, Renewable biomass-derived, P-doped granular activated carbon for efficient oxidation of 5-hydroxymethylfurfural to 2,5-diformylfuran: insights into the crucial role of P and N functionality, Renewable Energy, 2023, 219, 119388.

260 V. Ganesan, K. M. Begum, S. S. Meera and N. Mohammed, Effective chromium mitigation using phosphorous doped bio carbon electrode via capacitive deionisation, Environ. Technol., 2024, 45, 6011–6023.

261 J. Yi, Y. Qing, C. Wu, Y. Zeng, Y. Wu, X. Lu and Y. Tong, Lignocellulose-derived porous phosphorus-doped carbon as advanced electrode for supercapacitors, J. Power Sources, 2017, 351, 130–137.

262 W. Xing, M. Zhang, J. Liang, W. Tang, P. Li, Y. Luo, N. Tang and J. Guo, Facile synthesis of pinecone biomass-derived phosphorus-doping porous carbon electrodes for efficient electrochemical salt removal, Sep. Purif. Technol., 2020, 251, 117357.

263 S. Shaheen Shah, S. M. Abu Nayem, N. Sultana, A. J. Saleh Ahammad and Md. Abdul Aziz, Preparation of sulfur-doped carbon for supercapacitor applications: a review, ChemSusChem, 2022, 15, e202101282.

264 L. Ji, B. Wang, Y. Yu, N. Wang and J. Zhao, N, S co-doped biomass derived carbon with sheet-like microstructures for supercapacitors, Electrochim. Acta, 2020, 331, 135348.

265 G. Zhao, D. Yu, H. Zhang, F. Sun, J. Li, L. Zhu, L. Sun, M. Yu, F. Besenbacher and Y. Sun, Sulphur-doped carbon nanosheets derived from biomass as high-performance anode materials for sodium-ion batteries, Nano Energy, 2020, 67, 104219–104229.

266 Y. Huang, J. Yang, L. Hu, D. Xia, Q. Zhang, Y. Liao, H. Li, W. Yang, C. He and D. Shu, Mycelial pellet-derived heteroatom-doped carbon nanosheets with a three-dimensional hierarchical porous structure for efficient capacitive deionization, Environ. Sci.: Nano, 2019, 6, 1430–1442.

267 H. Wu, Q. Zhao, S. Jiang, W. Liu, H. Xiao and W. Wu, Research advances in doped carbon electrocatalysts derived from biomass, Chem. Eng. J., 2025, 505, 159694–159732.

268 T. Liu, Y. Li, N. Peng, Q. Lang, Y. Xia, C. Gai, Q. Zheng and Z. Liu, Heteroatoms doped porous carbon derived from hydrothermally treated sewage sludge: structural characterization and environmental application, J. Environ. Manage., 2017, 197, 151–158.

269 X. Chen, X. Song, W. Chen, T. Ao, Q. Yang and L. Zhao, MOFs/biomass-derived carbon as a high-performance anode for phosphorus removal, Sep. Purif. Technol., 2025, 354, 129125.

270 M. K. Jha, S. Joshi, R. K. Sharma, A. A. Kim, B. Pant, M. Park and H. R. Pant, Surface modified activated carbons: sustainable bio-based materials for environmental remediation, Nanomaterials, 2021, 11, 3140.

271 Z. Xiao, X. Zhao, J. Gu, Z. Hu, H. Fan and Q. Chen, O-modified activated carbon fiber electrode efficiently adsorption of Cu(II) in wastewater, Sustainability, 2023, 15, 10078.

272 W. Huang, Y. Zhang, S. Bao, R. Cruz and S. Song, Desalination by capacitive deionization process using nitric acid-modified activated carbon as the electrodes, Desalination, 2014, 340, 67–72.

273 A. Kumar, T. Bhattacharya, W. A. Shaikh, S. Chakraborty, D. Sarkar and J. K. Biswas, Biochar modification methods for augmenting sorption of contaminants, Curr. Pollut. Rep., 2022, 8, 519–555.

274 H. Cui, W. Yu, S. Li, S. Zhang, S. Hu and J. Zhou, Alkali-modified biomass ash enhances the adsorption capacities of Cu^{2+}, Cd^{2+}, and Pb^{2+} and their immobilization in soil, J. Environ. Chem. Eng., 2024, 12, 113490.

275 L. Li, X. Zhong, F. Yu, J. Zhao and J. Ma, Concentrated biogas slurry-derived porous carbon activated by KOH for high-performance capacitive deionization, Sep. Purif. Technol., 2025, 364, 132641.

276 L. Liang, F. Xi, W. Tan, X. Meng, B. Hu and X. Wang, Review of organic and inorganic pollutants removal by biochar and biochar-based composites, Biochar, 2021, 3, 255–281.

277 F. Yu, H. Yin, X. Bai, J. Pan, X. Zhang and J. Ma, $Cu@Cu_2O$/carbon for efficient desalination in capacitive deionization, Chin. Chem. Lett., 2023, 34, 108362.

278 M.-C. Cheng, Y.-S. Chang, D.-C. Tsai, Y.-L. Huang and F.-S. Shieu, High content heteroatoms doped and valuable biomass derived activated carbon composited with graphene for high performance supercapacitors, Fuel, 2025, 387, 133790–133801.

279 Y. Ge, X. Li, Z. Zheng, J. Ke, H. Zhao, Y. Liu, R. Guo and J. Chen, Simultaneous removal of sulfamethazine and sulfate *via* electrochemical oxidation and capacitive deionization: mechanisms of *in situ* activation and strategies of the hybrid system, *Sep. Purif. Technol.*, 2024, **344**, 127202.

280 N. A. Nosratabad, Q. Yan, Z. Cai and C. Wan, Exploring nanomaterial-modified biochar for environmental remediation applications, *Heliyon*, 2024, DOI: **10.1016/j.heliyon.2024.e37123**.

281 R. Ahuja, A. Kalia, R. Sikka and C. P, Nano modifications of biochar to enhance heavy metal adsorption from wastewaters: a review, *ACS Omega*, 2022, **7**, 45825–45836.

282 B. Wang, Y. Zhai, T. Hu, Q. Niu, S. Li, X. Liu, X. Liu, Z. Wang, C. Li and M. Xu, Green quaternary ammonium nitrogen functionalized mesoporous biochar for sustainable electro-adsorption of perchlorate, *Chem. Eng. J.*, 2021, **419**, 129585.